Development and Performance Investigation of a Biomass-fired Grain Dryer Coupled with Solar Air Heaters

A Thesis

Submitted in Partial Fulfilment of the Requirements for the

Award of the Degree of

Doctor of Philosophy

by

Dhananjay Kumar

(Reg. No. 156103046)

Department of Mechanical Engineering

Indian Institute of Technology Guwahati

Guwahati – 781039, INDIA

March 2022

CERTIFICATE

This is to certify that the thesis entitled "**Development and Performance Investigation of a Biomass-fired Grain Dryer Coupled with Solar Air Heaters**" is being submitted by **Mr. Dhananjay Kumar (156103046)** to the Indian Institute of Technology Guwahati, India for the award of the degree of **Doctor of Philosophy** in Mechanical Engineering Department is a bonafide research work carried out by him under our supervision. The results presented in this thesis have not been submitted elsewhere either by him or anybody else for the award of any other degree.

In our opinion, this work has reached the standard fulfilling the requirements for the award of the degree of Doctor of Philosophy under the regulations of the University.

Prof. Pinakeswar Mahanta

Professor
Department of Mechanical Engineering, IIT Guwahati

Prof. Pankaj Kalita

Associate Professor
School of Energy Science and Engineering, IIT Guwahati

Date:

DECLARATION

I, **Dhananjay Kumar**, do hereby declare that the thesis entitled "**Development and Performance Investigation of a Biomass-fired Grain Dryer Coupled with Solar Air Heaters**" submitted to the Indian Institute of Technology Guwahati, India for the award of the degree of Doctor of Philosophy in the Mechanical Engineering, is the outcome of my original research work except for various articles, which have been duly acknowledged. I also declare that I have adhered to all principles of academic honesty and integrity and have not misrepresented or fabricated or falsified any idea/data/fact/source in my submission. I know that any violation of the above will be cause for disciplinary action by the Institute and can also evoke penal action from the sources which have thus not been properly cited or from whom proper permission has not been taken when needed.

Place: **(Dhananjay Kumar)**

Date: **Registration No. 156103046**

ACKNOWLEDGEMENT

I would like to express my deepest gratitude to my supervisors Prof. Pinakeswar Mahanta, Department of Mechanical Engineering, IIT Guwahati, and Prof. Pankaj Kalita, Associate Professor, School of Energy Sciences and Engineering, IIT Guwahati for their continuous guidance, encouragement, and sharing valuable time throughout the process of this research work and in the writing this thesis.

I would like to thank my doctoral committee members, Prof. U. K. Saha, Department of Mechanical Engineering, Prof. P.K. Mondal, Department of Mechanical Engineering, and Prof. V. V. Goud Department of Chemical Engineering, IIT Guwahati for their valuable suggestions and encouragement during my research work.

I am thankful to the Dept. of mechanical engineering, IIT Guwahati for the continuous financial support to develop the experimental setup. I thank Prof. S. K. Dwivedi, HOD Dept. of Mechanical Engineering for providing the necessary support from the side of the department. I would like to thank Mr. Nip Borah technical superintendent and Dr. Rituraj Saikiya, Technical officer for providing the necessary support during the time of the experiment. I also thank Mr. Gautam Gogoi, Gokul Das, and Dulumoni Das, Junior Technician in the Mechanical workshop for their support during the experimental setup fabrication. I am thankful to all my colleagues and friends for being with me in good and as well as difficult times throughout these years.

Finally, I express heartfelt gratitude to my family members and relatives for their constant support and love. Last, but not least I praise all mightily for giving me the strength to carry out the research work.

(Dhananjay Kumar)

ABSTRACT

India is one of the leading rice grain-producing countries, and stands second in the world. Due to high nutrition and caloric supply, about 33% of the world's population depend on rice. Hence, the preservation of rice for food security throughout the year is one of the challenges. Drying is an essential post-harvest process for the preservation, storage, and transportation of food/agricultural products. It guarantees the product's shelf life and reduces the handling problem without any deterioration.

Traditional open sun drying is widely used in rural areas despite having many disadvantages. The traditional drying technique is a very slow process and inefficient in terms of product quality. On the other hand, solar drying is a preferred technique over open sun drying. Several types of solar dryers have been developed by researchers in the last few years. However, the solar dryer can only be operated when sufficient solar insolation is available. In the present investigation, a cost-effective and efficient biomass-solar hybrid dryer has been developed for meeting the drying demand of agricultural products suitable for developing countries. The dryer mainly consists of a furnace, rectangular chamber, PCM tray, drying chamber, drying tray, solar air heaters, PVC pipe, sensible thermal storage (pebbles), and latent thermal storage (paraffin wax).

In the present study, thermal analysis of the dryer is done for optimum removal of moisture. Energy and exergy analysis of the biomass-operated dryer, natural convection solar dryer, and forced convection solar dryer has been carried out. The drying characteristics of paddy have also been studied in the dryer. In the biomass-operated dryer, the effect of the sensible heat storage medium in the rectangular chamber was studied and found that the use of a sensible heat storage medium reduces the energy losses from the rectangular chamber (brick wall). It also reduces the exergy destruction in the rectangular chamber and retains a higher temperature for a longer period. Hence, it enhances the performance of the biomass-operated grain dryer. The effect of flue gas energy recovery has also been studied and found that the energy recovery technique reduces the wastage of energy in the flue gas. The use of a regulator valve in the exhaust pipe increases the temperature in the drying chamber.

The energy efficiency of the solar air heater (SAH) and the dryer system under natural convection mode was found in the range of 14.32–22.35% and 10.49–17.66%, respectively. The

exergetic efficiency of the SAH and the dryer system were ranged from 1.16–2.22% and 0.88–1.78%, respectively. The improvement potential, sustainability index, and waste energy ratio were ranged from 2.62–5.59 W, 6.62–16.41, and 6.09–15.1%, respectively. The performance of the SAH was also performed under forced convection mode for the airflow rate range of 0.0166–0.058 kg/s. The optimum value of the energy and exergy efficiency of the SAH was obtained for the air flow rate of 0.05 kg/s. The energy and exergy efficiency of the SAH under forced convection was ranged from 51.54–67.7% and 3.49–7.3%, respectively. The energy and exergy efficiency of the solar dryer was ranged from 40.99–55.39% and 2.73–5.76%, respectively. The improvement potential, sustainability index, and waste energy ratio were ranged from 4.9–27.84 W, 4.09–21.14, and 4.73–24.43%, respectively. In this study, the capacity of the natural convection hybrid dryer was found to be 48 kg/day while the capacity of the forced convection hybrid dryer was found to be 56 kg/day.

Keywords: Biomass; Solar energy; Natural convection; Forced convection; Thermodynamic analysis; Drying kinetics.

CONTENTS

List of Figures

List of Tables

Symbol and Abbreviations

A	Surface area (m^2)
C_p	Specific heat of the air (kJ/kg K)
db	Dry basis
DR	Drying rate (kg/kg h)
ℓ	Enthalpy (kJ/kg)
EMC	Equilibrium moisture content
FC	Forced convection
FCSAH	Forced convection solar air heater
FCSD	Forced convection solar dryer
Fig.	Figure
G	Solar irradiance (W/m^2)
g	Gram
h	Convective heat transfer coefficient of the furnace (W/m^2 K)
h_r	Radiant heat transfer coefficient of the furnace (W/m^2 K)
I	Inventory
IP	Improvement potential (J/s)
k	Thermal conductivity (W/m K)
L	Characteristics dimension (m)
m	Mass (kg)
M	Moisture content (%)
MR	Moisture ratio
NA	Not available
ΔP	Pressure difference
Q	Heat (J)
NC	Natural convection
NCSD	Natural convection solar dryer
PCM	Phase change material
s	Entropy (kJ/kg K)
SI	Sustainability index
SMER	Specific moisture extraction rate (kg/kWh)

SAH-1	First solar air heater
SAH-2	Second solar air heater
STD	Solar tunnel dryer
T	Temperature (°C)
V	Velocity (m/s)
WER	Waste energy ratio
wb	Wet basis
X	The cross-sectional area of PVC pipe (m^2)
Z	Height from the base of the conical furnace (m)

Non-dimensional number

Gr	Grashof number
Nu	Nusselt number
Pr	Prandtl number
Ra	Rayleigh number

Greek letters

α	Absorptivity
β	Coefficient of thermal expansion (1/K)
ρ	Density (kg/m^3)
μ	Dynamic viscosity (kg/m s)
ϑ	Kinematic viscosity (m^2/s)
η	Thermal efficiency (%)
τ	Transmittance

Subscript

0	Reference
a	Air
amb	Ambient
C	Collector

CS	Collector surface
Des	Destruction
d	Dried product
D	Drying chamber
eff.	Efficiency
exp.	Experimental
f	Flue gas
FS	Furnace surface
g	Glass cover
i	Inlet
l	Loss
O	Outlet
P	Paddy
pred.	Predicted
r	Received
req.	Required
RC	Rectangular chamber
SAH	Solar air heater
wvap	Water vapor

Chapter 1

Introduction

1.1 Motivation

Nowadays the major problem faced by humankind is the balance of food production and consumption in the day-by-day increasing population of the world. India and China produce about 50% of total rice production in the world (Muthayya et al., 2014). From the studies, it is found that about 10-30% of food loss occurs due to inappropriate methods of preservation in developing countries (Yaldýz and Ertekýn, 2001). The preservation of agricultural products is essentially required to maintain the safe moisture content (MC) level in the food grains for safe storage without any quality deterioration (Aydin et al., 2019). Water activity (a_w) has great importance on food preservation. It is a criterion for microorganism growth. It is the ratio of partial pressure of water vapour to the partial pressure of pure water. Most bacteria grow at about $a_w = 0.85$, mold and yeast grow at about $a_w = 0.61$, fungi at $a_w < 0.7$ (Belessiotis and Delyannis, 2011). Drying is one of the oldest techniques of food preservation to prolong the life of the grain. Drying not only reduces the weight, storage, and transportation cost of the products (Aghbashlo et al., 2009) but also prevents the growth of microorganisms such as bacteria, yeast, etc. Further, it reduces the wastage of agricultural products which results in the reduction of food scarcity worldwide. Despite many disadvantages like losses of natural colour, losses due to birds and insects, contamination, and high labour cost, etc., traditional drying (open sun) is popular in rural areas (Rabha et al., 2017). Therefore, to overcome these problems many solar dryers have been developed by researchers in the last few years. Solar drying has the advantage over open sun drying (Hao et al., 2018) however, it has a strong dependency on sunshine hours (Hadibi et al., 2021).

1.2 Drying process

Drying is a moisture removal process from food/agricultural products (Murugavelh et al., 2019). It is a heat and mass transfer process that causes physical and biochemical changes such as shrinkage, color, texture, and odors. In this process, the heat transfer takes place between the medium and the product by conduction, convection, and radiation or in combination, depending on the drying methods.

1.2.1 Conductive drying

The transfer of heat from one part of a body to another without appreciable displacement of the particle is referred to as conduction. This mode of heat transfer is called molecular heat transfer, because it involves the transfer of kinetic energy from one molecule to the one adjacent to it, e.g., conduction of heat along the length of a metal rod when one end is heated.

1.2.2 Convective drying

This is the most widely used drying method. In this method, the agricultural product is exposed to hot air. The heat transfer to the product takes place due to temperature differences and the moisture is evaporated from the products. Since the moisture is released from the products to the atmosphere i.e., the mass transfer takes place in addition to heat transfer. The transfer of heat from a body to the fluid or one point to another in a fluid by the mixing process is called convective heat transfer. In most cases, convection involves the transfer of heat from a solid surface to the bulk of the fluid; the change in heat induces a change in the density of the fluid.

1.2.3 Radiation drying

The transfer of heat by radiant energy in the form of electromagnetic waves which travel in straight lines at the speed of light is called radiation heat transfer. As a body is heated, it emits radiant energy, e.g., sun and infrared heat lamps. One of the main properties of radiation drying is that it does not require any medium to transfer heat. When this radiation strikes another body, the portions of the radiation may be absorbed, transmitted, and reflected.

1.3 Drying mechanism

Drying is a process that lowers the moisture content of wet food grain by exposing it to hot air/sunlight. In this process, hot air evaporates the moisture and carries it away from the grain surface. The physical phenomenon that occurs during the drying includes the removal of moisture from the interior of the grains (diffusion) and the loss of water vapour from the product surface. The driving force for the removal of surface moisture is the difference between the vapour pressure of the air and water in the product. Therefore, when the vapour pressure of the air and water are equal, then there is no driving force between the air and water hence moisture transfer does not take place from the grain. The moisture content at which the driving force is zero is called the

equilibrium moisture content (EMC) of the product. In the drying process, hot air passes over the product, which causes an increase in the vapour pressure of moisture within the products. It increases the moisture evaporation from the products and significantly decreases the relative humidity of the drying air to enhance its moisture carrying capacity. To maintain the quality of the products, it should not be dried too fast hence; the drying process should be slow and uniform. The surface moisture of agricultural products evaporates easily and quickly, but the interior moisture of the products lasts longer.

The drying rate is determined by the initial moisture content, temperature, and thickness of the agricultural products. The drying rate is also affected by the drying air temperature, relative humidity, and volume of air passing over the products. The drying method, types of the dryer, and efficiency of the equipment also affect the moisture removal rate of the products. The higher the initial moisture content of the grain, the more time it will take to achieve the safe moisture content. In general, the moisture removal rate is higher for the high temperature of the drying air. The moisture removal rate is lower in the case of the high relative humidity of the drying air because the air having low relative humidity has more capacity to absorb moisture and leading to faster drying. A drying curve, as illustrated in Fig. 1.1 shows how the product moisture content and temperature change over time. It can be seen from the figure that the slope of the moisture content curve changes with time.

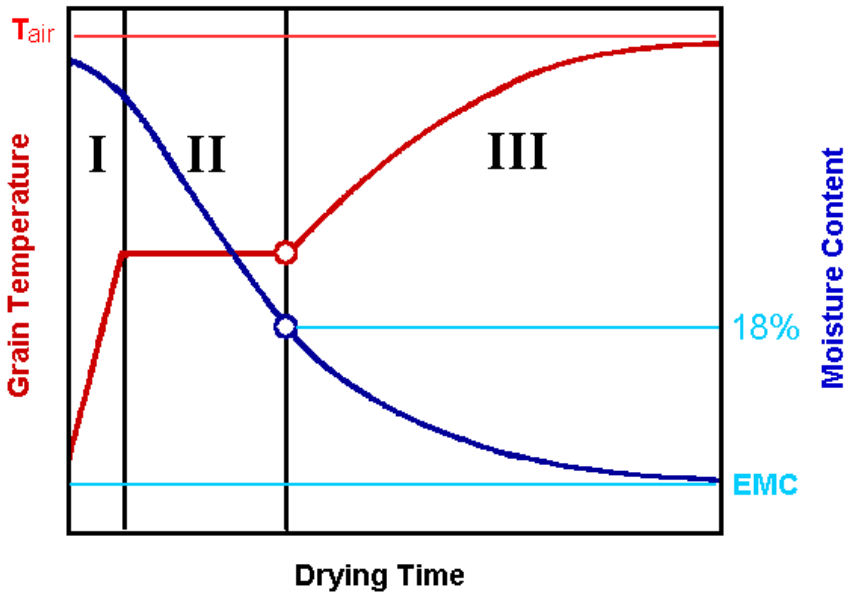

Fig. 1.1 Theoretical drying curve for paddy (grain temperature red and moisture content blue) (IRRI training manual, 2013)

The drying of food grains occurs in the following consecutive periods:

(i) Preheating period: During this period, a very slight change in moisture content is observed. Initially, when hot air passes over the wet grain, most of the energy from the hot air is used to heat the grain.

(ii) Constant-rate period: Once the grain reaches its drying temperature, water starts evaporating from the surface of the grain. The energy from the drying air is used to evaporate the surface moisture and the amount of moisture removed from the grain is constant with time. Hence, it is called the constant-rate period. During this period, grain temperature is constant as well. The primary resistance to heat and mass transfer is at the grain surface. Once the surface appears to develop dry patches, the rate of drying begins to decrease. The moisture removal rate from the product surface can be expressed in equation (1.1) (Zaman and Bala, 2001):

$$\frac{dM}{dt} = -kA(M - M_e) \tag{1.1}$$

where *M, Me, k,* and *t* are moisture content of the grain, equilibrium moisture content (EMC), drying constant, and drying time, respectively.

(iii) Falling-rate period: As the drying progresses, it takes more time for internal moisture to appear at the surface, and the evaporation of water is no longer constant with time. As a result, the drying rate declines. During this period, some amount of drying air heat is used to heat the grain. For paddy grain, the falling rate period typically occurs at around 18% moisture content. In this period, the rate of drying is controlled by the rate of migration of moisture.

The mechanisms of moisture transfer from the interior of the grains are as follows:

(i) Liquid movement due to capillary forces.

(ii) Diffusion of liquid due to the concentration difference.

(iii) Water-vapour diffusion by a partial-pressure difference.

1.4 Thin-layer drying and deep bed drying

The drying rate can be controlled with the help of the thickness of the grain layer. Based on the grain layer thickness, drying is classified as thin-layer drying and deep bed drying.

1.4.1 Thin-layer drying

In this drying, the grain bed depth is up to 0.2 m. The drying rate is proportional to the pressure difference between the vapour pressure of moisture in the grain and in the drying air. All commercial dryers are designed on the principle of thin-layer drying because the drying air volume is much higher than the grain volume (Belessiotis and Delyannis, 2011).

1.4.2 Deep bed drying

When the thickness of the grain layer is more than 0.2m then it is deep bed drying. The moisture removal rate is higher at the bottom layer where hot air enters the drying chamber. A temperature gradient is developed across the bed. Hence, the drying is considered non-uniform. As the drying air flows through the grain bed, its temperature drops. In this process, the drying rate mainly depends on air velocity, temperature, and the depth of the grain bed. Figure 1.2 shows the schematic of the deep bed dryer.

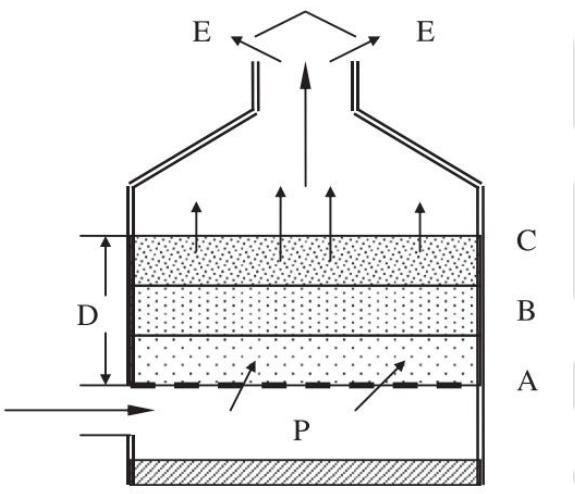

Fig. 1.2 schematic of deep bed dryer (Belessiotis and Delyannis, 2011). D, Bed height; P, Plenum chamber; E, outlet. Adapted with copyright permission 2022, Elsevier

1.5 Different types of dryer and drying methods

Many methods have been devised for drying agricultural products, yet no ideal dryer seems to have been developed. Some of the most commonly used dryer and drying methods are shown in Fig. 1.3.

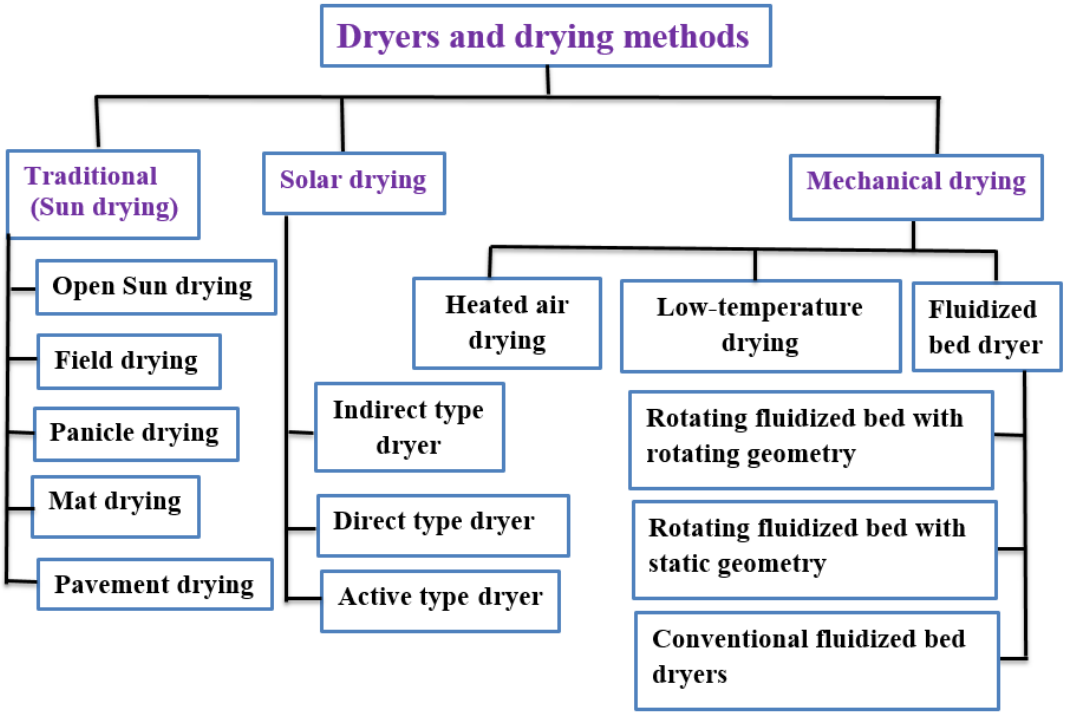

Fig. 1.3 Schematic diagram of dryer classification

1.5.1 Traditional drying

1.5.1.1 Open sun drying

It is the drying of agricultural products under direct sunlight. In this traditional drying process, the products are spread out in a thin layer on the ground/mat/tray. Figure 1.4 shows the photographs of the different paddy drying methods. This is the most widely used drying process in rural areas of developing countries. However, open sun drying has many limitations such as:

(i) Contamination of products due to dust, bird droppings, etc.

(ii) Longer drying time due to slow drying rates.

(iii) Large drying area requirement.

(iv) Loss of products due to insects, birds, and adverse weather conditions.

Panicle drying

Field drying

Open sun drying

Fig. 1.4 Photographs of the paddy drying methods (IRRI training manual, 2013)

1.5.1.2 Field drying

This is a method for pre-drying hand-harvested crops where farmers cut rice panicles in the field and stacked them in small piles on top of the crop stubble. In this traditional harvesting process, farmers leave their harvested rice in the field for an extended time because either they are waiting for the thresher or want to pre-dry the paddy. The rice plants are either left lying in the field or stacked in piles with the panicles inside to protect them from rain, birds, and rodents. This can lead to massive heat buildup inside the stacks. As a result, molds grow quickly and infest the grains leading to discoloration within the first few days of field drying. Another unwanted effect is that grains that are already dry often absorb water from the wetter straw, which leads to fissuring of the grains and thus reduces the potential head rice recovery.

1.5.2 Mechanical Solar drying

It is a form of convective drying. The main objective of solar drying is to supply more heat to the products than the traditional open sun drying. In a solar dryer, we can extend the drying period of the food/agricultural products for about 4−5 hours by using a thermal storage medium. In this drying, products can be dried even at a higher temperature than the traditional (open sun) drying. This is an efficient way of utilizing solar energy. Mainly three types of solar dryers are used, viz. direct, indirect, and active type solar dryers.

1.5.2.1 Direct type solar dryer

The direct type of solar crop dryer is also known as a solar cabinet dryer. The moisture of the product is evaporated by the air entering into the cabinet and exiting at the outlet of the drying chamber. In the cabinet dryer, a part of the solar radiation that falls on the glass cover is reflected in the atmosphere and the remaining is transmitted in the cabinet. A part of the transmitted radiation is reflected from the crop surface and the remaining is absorbed by the crop which increases the temperature of the crop. The glass cover does not allow the emitted long-wavelength radiations in the ambient. This phenomenon causes the temperature of the crop inside the cabinet to be higher. Hence, the glass cover reduces the convective losses to the ambient, which plays an important role in increasing the crop and cabinet temperature.

1.5.2.2 Indirect type dryer

The crops in the indirect solar dryers are located in trays or shelves inside a drying cabinet and a separate unit termed as a solar air heater is used for heating the air entering the cabinet. The heated air is allowed to flow over the wet crop leading to moisture evaporation by convective heat transfer. Drying takes place due to the difference in moisture concentration between the drying air and the crop surface. In some of the dryers, in addition to the heated air from solar heaters, the grains also receive direct solar radiation for drying. Figure 1.5 shows the indirect type solar dryer.

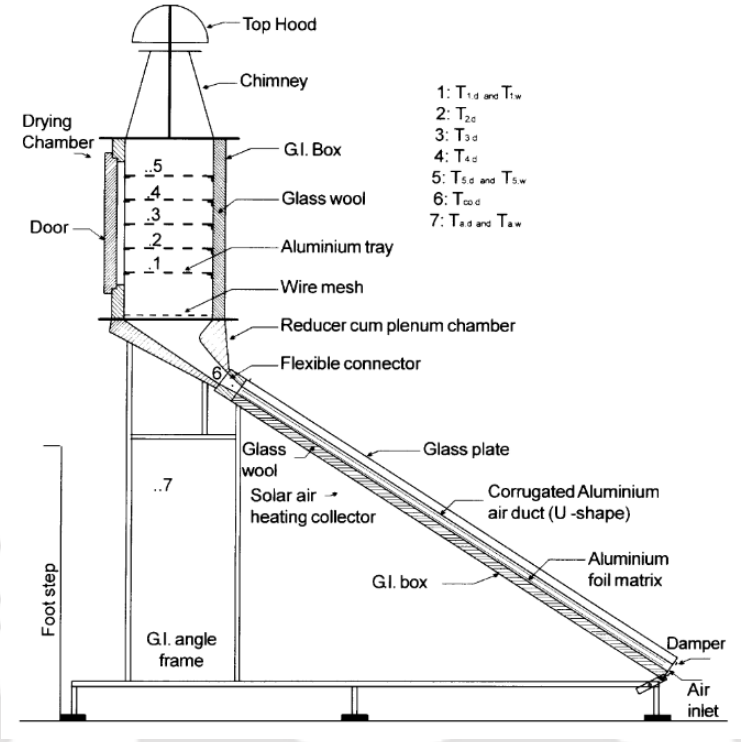

Fig. 1.5 Indirect type solar dryer (Pangavhane et al., 2002). Adapted with copyright permission 2022, Elsevier

1.5.2.3 Active or forced circulation types of dryers

Active solar dryers are designed by including external means, like fans or pumps, for extracting the heated air from the collector area to the drying bed. Thus, all active solar dryers are forced convection dryers by their application. A typical active solar dryer depends on solar energy only for the heat source, while air circulation uses motorized fans or a ventilator. These dryers find major applications in large-scale commercial drying operations in combination with conventional fossil fuel to have better control over-drying by minimizing the effect of fluctuations of the solar insolation on the drying air temperature. Active solar dryers are known to be suitable for drying higher moisture content foodstuffs such as papaya, kiwi fruits, brinjal, cabbage, and cauliflower slices.

1.5.3 Mechanical drying

Based on the capacity and methods of drying, mechanical dryers are classified as low-temperature drying and hot air drying.

1.5.3.1 Low-temperature drying

Low-temperature drying systems take advantage of the natural drying potential of the warm air. The process often needs less energy but more time than hot air drying. Compared to high-temperature grain drying, low-temperature drying may take weeks or months. This type of dryer is used for low moisture content product drying with ambient air or slightly pre-heated air.

1.5.3.2 Hot air drying

Hot air drying, heated air enters the drying chamber, moves over the grains, and absorbs moisture while passing through the grain. The grain at the inlet dries faster because at the inlet the drying air has the highest water absorbing capacity. Because of the shallow bed and relatively high airflow rates, drying occurs in all layers of the grain bulk, but fastest at the inlet and slowest at the outlet. As a result, a moisture gradient develops at the end of the drying process. The drying process is stopped when the average moisture content of the grain is equal to the desired moisture content. When the grain is unloaded and filled in bags the individual grains equilibrate. That means wetted grains release water which dried grain absorbs so that after some time all grains have the same moisture content. However, the re-wetting of the dried grains leads to fissuring in the milling process. This explains why the milling recovery and head rice recovery of grains dried in fixed bed batch dryers are not optimal. One way to minimize the moisture gradient during drying is to mix the grains in the drying bin after around 60-80% of the drying time has passed.

1.5.3.3 Fluidized bed drying

In this drying technique, either the hot air is supplied across the fluidized bed of granular materials. These apply to a wide range of non-heat sensitive and heat sensitive products. Under controlled fluids (~ 2.3 m/s), the air is passed through the product layer to form a fluidized bed. It is the state in which the wetted particle is exposed to the dry air. The capacity of the commercial fluidized bed drying unit is 1–10 tons/hour. The most commonly used fluidized bed dryer is the rotating fluidized bed dryer. These are different from the conventional type of fluidized bed because their body force in the centrifugal bed is adjustable by the radius and rotating speed of the air distributor. In the RFB, the strong centrifugal field is much higher than gravity. The advantages/disadvantages of the drying methods are presented in Table 1.1.

Table 1.1 The advantages/disadvantages of the drying methods.

Drying methods	**Advantages/disadvantages**
Open sun-drying	Limited drying capacity, labor-intensive, and unavailability of the sun at night and in the rain. Due to this delay in fungal growth in the seeds, Re-wetting or overheating of grains can result in low milling quality, cracks in the kernels.
Field drying	Damage to rodents and birds when it spreads in the area. When the paddy poured as the pile and it re-wetted with straw in a pile.
Panicle drying	The moisture removal rate inside the panicle is very slow.
Mat drying	The main disadvantage of this process is the Re-wetting of paddy in the bottom location by the moisture of the soil.
Pavement drying	However, it has high capacity, and it can partially mechanize, but it has few demerits of pollution with dirt transpire in cereal.
Fluidized bed drying	The fluidized bed drying method has some advantages as compared to other methods of drying. It is a continuous drying process and it achieves relatively higher thermal efficiency. Its main drawback is that it works on high-grade energy as an input source and it has many mechanical components which directly related to the cost. Hence, it is a costly drying process.
Direct solar dryers	This dryer is cheap, comparatively more hygienic, and drying faster than sun drying. The efficiency of this dryer declines during rainy or cloudy weather and it is not usable at night. The major hindrance of this dryer is the low drying capacity and no control over it.
Indirect solar dryer	The thermal efficiency of this dryer declines during rainy or cloudy weather and is difficult to use at night. It has relatively more control over the drying process as compared to the direct solar dryer.

Active solar dryer	This dryer is used to get proper control over the drying process but it is also not usable during the night/cloudy weather. The drying rate is relatively higher as compared to the other solar drying process. Its thermal efficiency is comparatively higher.

In the last few years, many different types of dryers have been developed to enhance the dried products' storage life and quality till now no ideal dryer is developed. Each dryer has its advantage and disadvantage. The solar dryer has got considerable attention due to its reliability and low cost but its major drawback is the dependency on solar radiation. People cannot use this dryer during the cloudy weather/night. This drawback makes this technique not suitable for commercial applications. This problem can be overcome by integrating a suitable backup heater with a thermal storage medium.

Therefore, the present work is an endeavor towards the design and development of a continuous dryer for the quality drying of agricultural products. In this study, a biomass-operated grain dryer coupled with solar air heaters has been designed and developed for the quality drying of agricultural products. The thermodynamic analysis of the developed dryer has been performed to optimize the performance of the dryer.

1.6 Outline of the thesis

This thesis comprises of six chapters which are outlined as follows:

Chapter-1 introduces the motivation, background, types of dryers, mechanism of the drying process, and outline of the thesis. In Chapter-2, the detailed literature survey in relation to the proposed research is discussed. The literature related to the energy-exergy analysis of the different types of dryers, drying kinetics of agricultural products, mathematical modelling of the drying process, and a summary of the literature survey are included in this chapter. Based on the literature survey, the research gaps are identified, and the objectives of the thesis are formulated. The description of the experimental setup and procedures along with design analysis of the components of the dryer are presented in Chapter-3. The mathematical equations used for the design and performance analysis of the dryer have also been presented in this Chapter. In Chapter-4, the performance analysis of the dryer for the paddy drying process in the biomass-operated natural convection dryer, natural convection solar dryer, forced convection solar dryer, and the solar-

biomass hybrid dryer is presented. The energy efficiency analysis of the biomass-operated natural convection dryer, solar air heaters and the solar dryer under natural and forced convection mode is reported in Chapter 5. The major conclusions of the present work and the scope for future work are presented in Chapter-6. Uncertainty analysis in investigating the dryer performance and the experimental data under different operating conditions during drying of paddy are presented in appendices I and II, respectively.

Chapter 2

Literature Review

2.1 Introduction

Drying is one of the important post-harvest processes for food/agricultural produce. It can extend the shelf life of harvested products, improve quality, reduce post-harvest losses, and lower the transportation cost since most of the water is taken out from the product during the drying process. Hence, designing an efficient dryer for the agricultural products drying process is a major challenge. The present study is focused on the design of an efficient dryer by combining biomass and solar energy. Hence, the literature survey related to the different techniques of drying such as convective drying, energy-exergy analysis of the dryers, and drying kinetics of the agricultural products is discussed in this chapter. A summary of the literature review, research gaps, and objectives of the present study is presented.

2.2 Convective dryers

Bala and Woods (1994) performed the study of an indirect type natural convection solar dryer for the rice drying process. In this analysis, solar energy was collected in the solar air heaters and the hot air passes through the grain bed for the drying process. The temperature along the collector was described by a numerical solution. The drying of grain was described by introducing a deep-bed solution procedure. Due to variation in temperature in the collector plate and across the air bed, a thermal buoyancy effect was observed. Due to natural convection, a low airflow rate was produced and the drying wave moves slowly. In this study, a temperature drop across the bed was observed, which causes a little contribution to buoyancy in the chimney height. The deep bed analysis of the drying process showed that the assumption of uniform layer drying of grain is not valid, although the layer is thin.

Pangavhane and Sawhney, (2002) developed a natural convection solar dryer and performance testing of the dryer was performed. In this study, the thermal performance of the solar air heater and the drying chamber was evaluated for the natural convection mode under no-load condition, and the solar drying unit was tested under grapes-loaded condition. The drying test was carried out in the solar dryer with manually harvested fresh Thompson seedless grapes. The dryer consists of

a solar air heater, flexible connector, reducer-cum plenum chamber with chimney, and a supporting stand. During the five days of the experiment, the diurnal variation of the ambient air temperature, solar irradiance, collector outlet air temperature, and the dryer outlet air temperature for the solar dryer were plotted. During the drying process, the daily mean values of air temperature at the dryer inlet and solar radiation intensity were varied from 51.9–64.6 °C, and 605–673 W/m^2, respectively. The daily mean thermal efficiency of the collector was varied from 48–56%. During the study, relatively higher values of the SAH thermal efficiency were obtained in the afternoon hours and its value varied with air flow rate. The developed dryer reduced the drying time by 43% as compared to open sun drying.

Bena and Fuller (2002) conducted a study of a natural convection solar dryer coupled with a biomass backup heater. This dryer was developed to demonstrate the drying technology suitable for small-scale farmers for the fruits and vegetables drying in non-electrified areas of developing countries. A simple biomass burner was demonstrated in combination with a solar dryer. In the experiment, a series of experimental trials were performed and the capacity of the dryer was found to be 20 to 22 kg of fresh pineapple arranged in the slice thickness of 10 mm. The drying efficiency of the unit was found to be 9%. Further modifications were suggested to improve the performance of the solar and biomass component of the dryer, which includes (i) using two layers of glazing to reduce the thermal losses from the cabinet, (ii) increasing the diameter of the flue gas pipe to increase the flow of air through the burner, (iii) increasing the thickness of the central area of the thermal mass to reduce the differences in drying temperatures in the cabinet, and (iv) diverting the flue gas through the drying chamber. The schematic of the dryer is shown in Figs. 2.1 and 2.2.

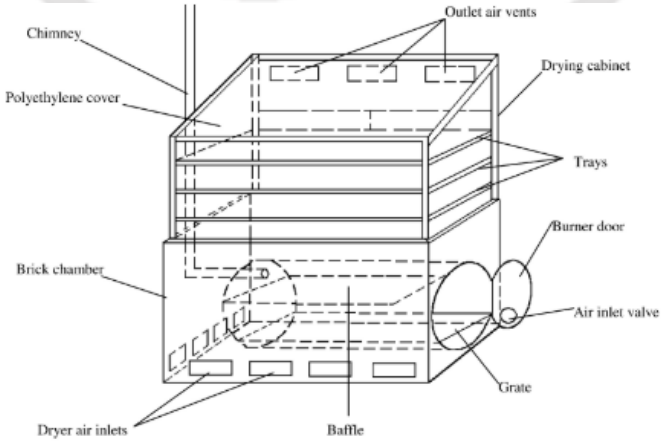

Fig. 2.1 Natural convection solar dryer (Bena and Fuller, 2002). Adapted with copyright permission 2022, Elsevier

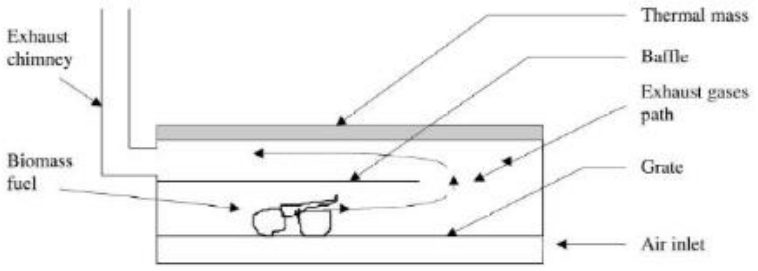

Fig. 2.2 Cross-section through biomass burner (Bena and Fuller, 2002). Adapted with copyright permission 2022, Elsevier

Prasad and Vijay (2005) presented the experimental study for ginger, turmeric, and Guduchi drying in a solar dryer. In this study, an integral type of natural convection solar dryer coupled with a biomass stove was developed. During the study, 18 kg fresh ginger with an initial moisture content of 319.74% (db) was dried to a final moisture content of 11.8% (db) in 33 hours. In the study, the moisture content of turmeric and Guduchi were reduced from 358.96% to 8.8% and 257.45 to 9.67%. These products were also dried under solar drying and open sun drying separately in the same climatic condition and faster product drying was observed in the hybrid dryer.

Jain and Tewari (2015) studied the performance of an indirect type natural convection solar crop dryer with latent thermal energy storage. In this study, the solar crop dryer was developed with thermal energy storage to maintain continuity of herbs drying for their color and flavor vulnerability. The dryer consists of a flat plate solar absorber, packed bed latent energy storage, drying plenum with crop trays, and natural air ventilation. The dryer was designed with a maximum collector area of 1.5 m^2 six crop trays with an effective area of 0.5×0.75 m^2 can hold 12 kg of fresh leafy herbs. The dryer was attached with a packed bed with thermal energy storage material of 50 kg PCM. The dryer system works in such a way that the PCM stores the thermal energy during sunshine hours and releases it in the evening. This stored energy help in maintaining the drying air temperature between 40 °C and 45 °C for 5 to 6 hours. The schematic of the dryer is shown in Fig. 2.3.

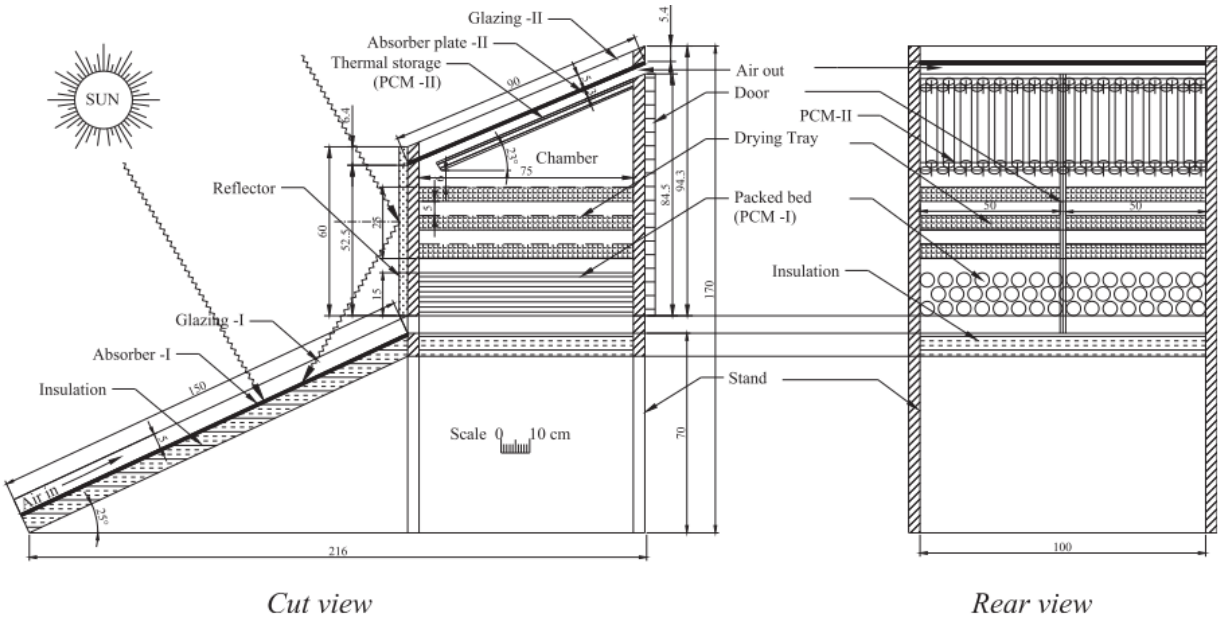

Fig. 2.3 Schematic of natural convection solar dryer with thermal storage (Jain and Tewari, 2015). Adapted with copyright permission 2022, Elsevier

Sallam et al., (2015) reported the solar drying of the whole mint plant under natural and forced convection mode. In this study, two identical prototype solar dryers (direct and indirect) having the same dimensions were used to dry the whole mint, both prototypes were operated under natural and forced convection mode. Ten empirical models were used to fit the drying curves; nine models were showing a good agreement with the drying curve of mint. The results indicate that the drying of mint under different operating conditions occurred in the falling rate period and the constant rate period of the drying curve was not observed. From the results, it was obtained that the drying rate of mint under forced convection is higher than that of under natural convection, especially during the first hour of drying.

Sekyere et al., (2016) performed the experimental investigation to analyze the drying characteristics of pineapples in a mixed-mode natural convection solar crop dryer coupled with a backup heater. During this study, the moisture content was monitored continuously until the desired moisture content is achieved. In the solar heating mode of operation, results showed that the thermal mass is capable of storing part of the absorbed solar energy but the quantities involved were insufficient to sustain night drying. In this study, it was observed that the developed dryer is capable to dry a batch of pineapples in each mode of operation. The drying analysis was performed for four different scenarios namely, (i) continuous drying with solar energy during the day and

back up heater during the night; (ii) drying with back up heater; (iii) combination of solar energy and energy from back up heater during the day; and (iv) solar energy. The four drying Scenarios presented correspond to specified drying periods for four typical conditions in Ghana. The and the moisture content of pineapple slices were reduced from 924–106% in 19 h, 1049–184% in 10 h, 912–155% in 7 h, and 1049–144% in 23 h for drying scenarios (i), (ii), (iii), and (iv), respectively. In this study, the average moisture pickup efficiency values were obtained as 27%, 24%, 11%, and 32% for drying scenarios (i), (ii), (iii), and (iv), respectively. The schematic of the dryer is shown in Fig. 2.4.

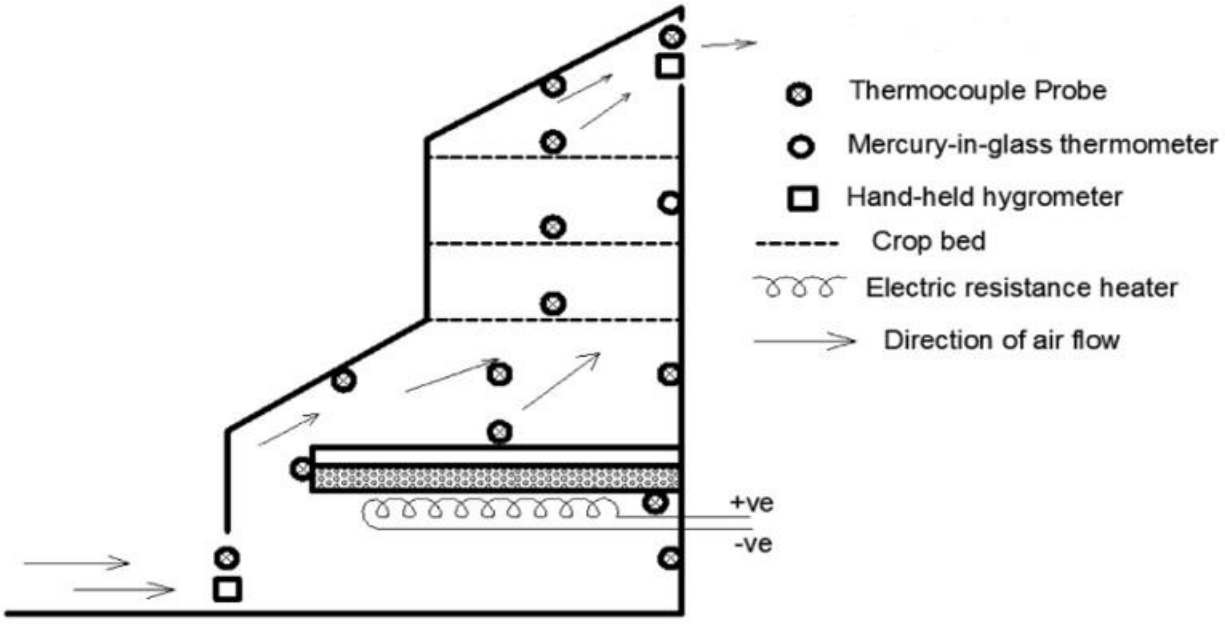

Fig. 2.4 Schematic of the laboratory dryer (Sekyere et al., 2016). Adapted with copyright permission 2022, Elsevier

(Bosomtwe et al., 2019) developed a solar-biomass hybrid dryer and performed the drying of maize. During the experiments, the temperature in the dryer was recorded as 52 °C and 41.4 °C in the hybrid drying and solar drying mode. In this study, relatively good drying characteristics of maize were obtained in the case of a solar-biomass hybrid dryer. Shreelavaniya et al. (Shreelavaniya et al., 2021) developed a solar-biomass hybrid dryer for drying small cardamom. This study was reported for the biomass-operated mode and solar-biomass hybrid mode of drying. The cardamom having a moisture content of 83.2 was dried to the final moisture content of 9.5 % (w.b) in the biomass operated mode while cardamom with a moisture content of 82.4 % was dried

to 9.1 % (w.b) in solar-biomass hybrid mode. In this study, the color retention ability of the products was found to be better in the hybrid mode of drying.

2.3 Energy and exergy analysis of the dryers

Midilli and Kucuk (2003) performed the energy and exergy analysis of a solar drying cabinet for the drying of shelled and unshelled pistachios. Energy analysis was performed to estimate the amount of energy gain in the solar air collectors and the energy utilization ratio. Exergy analysis was conducted to determine the location, type, and magnitude of exergy losses during the drying process. In this study, the shelled and unshelled pistachios were dried in the temperature range of 40–60 °C. The highest exergetic efficiency was obtained during the solar drying of shelled pistachios. Syahrul et al., (2003) performed the thermodynamic analysis of a fluidized bed dryer for the quality drying of wheat and corn. During this study, a relatively lower value of thermal efficiency was observed at the end of the process. In this study, it was observed that the inlet air temperature has a strong effect on the thermodynamic efficiency of the wheat drying process, while in the case of the corn drying process, an increase in inlet air temperature does not increase the thermal efficiency.

Dincer and Sahin (2004) performed the thermodynamic analysis of a new model. In this paper, exergetic efficiency was derived as a function of heat and mass transfer parameters. This model was developed to optimize the design of the drying systems and their components to identify the appropriate applications and optimal configurations for drying systems. The purpose of this study was to optimize the thermal efficiency of the dryer. Goswami et al., (2004) developed a thermodynamic cycle that reduces the capital cost by 50%. In this study, the solar energy was converted into electrical energy by emphasizing nanoscale antennas and achieved conversion efficiency in the range of 80–90%. Akpinar, (2004) reported the energy and exergy analysis of the convective type electric heating dryer for the red pepper slices drying process. In this study, the exergetic efficiency and energy utilization ratio were achieved in the range of 67.28–97.92% and 1.109–18.854%, respectively. During this study, it was observed that the exegetic efficiency has a direct relation with drying time while the energy utilization ratio has an indirect relation.

Akpinar (2005) reported that the exergy efficiency of the dryer increases with progressing drying time, increasing drying air temperature, and velocity. The exergy efficiency of the drying chamber was inversely proportional to the moisture content of the product and increased with

removing water from the samples. The exergy utilization for moisture evaporation from the product exponentially diminished towards the end of the drying process. In this study, it was found that the major part of supplied exergy to the drying chamber is wasted in exhaust air.

Zvolinschi et al., (2006) studied the second law analysis of a paper drying machine. In this study, entropy was controlled by increasing inlet air humidity and maintaining lower temperatures. During this study, the entropy generation was reduced by 35% by an increase in 5 times inlet air humidity. Gupta and Kaushik, (2008) established the optimal performance parameters for the maximum exergy delivery during the collection of solar energy in a solar air heater. The procedure to determine optimum aspect ratio (length to width ratio of the absorber plate) and optimum duct depth (distance between the absorber and bottom plate) for maximum exergy delivery was developed. The energy and exergy output rates of the solar air heater were evaluated for various values of collector aspect ratio, mass flow rate, and solar air heater duct depth. During the study, it was found that lower mass flux, higher aspect ratio, and lower duct depth give higher exergy output.

Tyagi et al., (2007) performed the exergy analysis of a concentrating type solar air heater and found that the thermal and exergetic efficiency of the SAH increases with an increase in air mass flow rate for a constant solar radiation intensity. Ghandoor et al., (2008) investigated a survey of two hundred households of Jordanian residents and performed the energy and exergy analysis. The energy and exergy efficiency were obtained as 66.6% and 15.4%, respectively. Tiwari et al., (2009) performed the energy analysis to predict fish surface temperature, greenhouse room air temperature, and moisture evaporated during the drying of Prawn under natural and forced convection mode. In this study, the predicted values showed a good agreement with experimental data. The obtained exergy efficiencies under natural and forced convection mode were lower than the corresponding energy efficiencies. The exergetic performance of forced convection drying was better than natural convection.

Coskun et al., (2009) performed the first & second law analysis for the wood chips drying process. This analysis was performed to enhance the performance of the industrial chips dryer and the energy and exergy efficiency were obtained as 34.07% and 4.39%, respectively. During this study, it was observed that the energy and exergy efficiency can be increased by the energy recovery process. Akbulut and Durmus, (2010) analyzed the energy and exergy of the thin layer drying process of mulberry in a forced convection solar dryer. The drying experiments were

conducted at varying air mass flow rates from 0.014–0.036 kg/s. The effects of inlet air velocity and drying time on both energy and exergy were studied. In this study, the maximum value of energy utilization ratio and exergy loss were found as 55.2% and 10.82 W, respectively. During this study, it was observed that the energy utilization ratio and exergy loss decreases with increasing airflow rate while the exergetic efficiency increases.

Celma and Cuadros (2009) performed the energy and exergy analysis of an indirect type natural convection solar dryer in the olive mill wastewater drying process. In this study, the temperature and exergetic efficiency of the drying chamber was achieved in the range of 34–52 °C and 34.4–100%, respectively. Akpinar and Koçyiĝit, (2010) performed the energy and exergy analysis of a solar air heater for the four different cases with and without obstacles on the collector and compared the results. In this study, it was observed that the obstacle on the collector enhances the performance of the solar air heater. The energy and exergy efficiency was achieved in the range of 20–82% and 8.32–44.00%, respectively. Chowdhury et al., (2011) presented the energy and exergy analysis for the Jackfruit leather drying process of a mixed-mode solar tunnel dryer consisting of solar air heaters connected in series with a transparent drying chamber. The investigators reported that the energy efficiency of the solar air heater and the drying chamber varied from 27.45–42.50% and 32.34–65.30%, respectively. The thermal efficiency of the solar air heater varied linearly with solar radiation. The exergy inflow and losses of the dryer increase with an increase in solar radiation.

Padilla et al., (2011) performed the energy analysis of a parabolic trough solar receiver and found that this model is suitable for heat losses and collector efficiency calculation. Results obtained in this study showed the best agreement compared to the other models. The development of this parabolic trough receiver reduces the convective heat losses by 41.8% which leads to enhancement in the performance of the heat transfer model. From the results, it was concluded that this model is suitable for the calculation of heat losses and collector efficiency under different flow and operating conditions.

Sami et al., (2011) performed the energy and exergy analysis of an indirect type forced convection solar cabinet dryer. During this study, the highest value of exergy loss was observed at noon. The total energy efficiency was high despite low total exergy efficiency, it showed the thermodynamic irreversibility in the dryer. The maximum value for the outlet air temperature, exergy, and energy were obtained as 69 °C, 2.5 kW, and 1.12 kW, respectively. Caliskan et al.,

(2012a) conducted the thermodynamic analysis of thermochemical and sensible energy storage at different ambient conditions for building heating applications and found that sensible thermal storage is exergetically more efficient than thermochemical thermal storage. Tyagi et al., (2012) studied the solar air heater performance with and without latent heat storage material (paraffin wax) and found that solar air heater with latent heat storage gives higher outlet air temperature and works as a backup heater for about four hours in the evening.

Fudholi et al., (2013) performed the exergy analysis of a solar air heater with fins for the airflow rate range of 0.03–0.1 kg/s under the solar radiation intensity variations 400–800 W/m^2. In this study, the maximum value of SAH thermal efficiency was obtained at 77% for the airflow rate of 0.09 kg/s. The exergy efficiency and improvement potential were varied in the range of 15–28% and 740–1070 W, respectively. Kazemi and Ahmadifard, (2013) studied the energy and exergy analysis of a solar air heater having a flat plate collector. The theoretical and comprehensive studies were performed for energy and exergy analysis. The highest value of energy and exergy efficiency were obtained as 80% and 8%, respectively.

Bhaskaran Anangapal, (2014) performed the thermodynamic analysis of a system to reduce fuel consumption. In this study, it was obtained that the 1.1–1.2 air factor is sufficient for the combustion of liquid fuel and 1.15–1.3 for the combustion of solid fuel. The maximum exergy efficiency of fuel was found as 73%. Vijayan et al., (2016) reported the performance analysis of a solar dryer with a sensible thermal storage medium for the bitter gourd drying process. The performance of the dryer was investigated for the various mass flow rate of air. The bitter gourd dried from initial moisture content of 92% (wb) to 9% (wb). The thermal efficiency of the collector and the dryer were obtained as 22% and 19%, respectively for the air mass flow rate of 0.0636 kg/s. Behnaz et al., (2016) designed sensible heat storage and performed the thermodynamic analysis. During this investigation, it was found that the increase in input energy flowrate and a decrease in outlet energy flowrate, increases the charging temperature of the energy storage system. The discharging temperature of the thermal energy storage was also increased with an increase in the input energy flow rate.

Singh and Dhiman (2016) performed the exergy analysis of a solar air heater for the building heating process. From the study, it was found that the energy and exergy efficiency of the solar air heater increases with mass flowrate reaches a maximum value after that its value decreases. Rabha and Muthukumar, (2017) studied the performance of a forced convection solar dryer integrated

with paraffin wax as a heat storage system. In this study, 20 kg of red chili having a moisture content of 73.5% (wb) was dried to 9.7% (wb) in four consecutive days. This dryer saved the drying time up to 128% as compared to open sun drying. The average energy efficiency of the SAH-1 and SAH-2 was found as 32.5% and 14.1% and the exergy efficiency as 0.9% and 0.8%, respectively. The exergy efficiency of the drying chamber was varied in the range of 24.2–98.9% with an average of 52.2%.

Rabha et al., (2017a) studied the energy and exergy analysis of a solar dryer for the Ghost Chilli pepper and ginger drying process. In this study, a forced convection tunnel dryer coupled with shell and tube-based latent heat storage modules was designed and fabricated. During this study, Ghost Chilli and ginger were dried in 42 h and 33 h at the drying air temperature range of 42–61 °C and 37–57 °C respectively. The results of this study showed that the thermal efficiency of the first and second solar air heater varied between 22.1–40.24% and 9.64–19.5%, respectively. The thermal efficiency of the solar air heaters array varied between 22.95% and 23.3%. The exergy efficiency of the drying chamber for chili and ginger drying were ranged from 21–98% and 4–96% with an average of 63% and 47%, respectively. The photograph of the solar dryer is shown in Fig. 2.5.

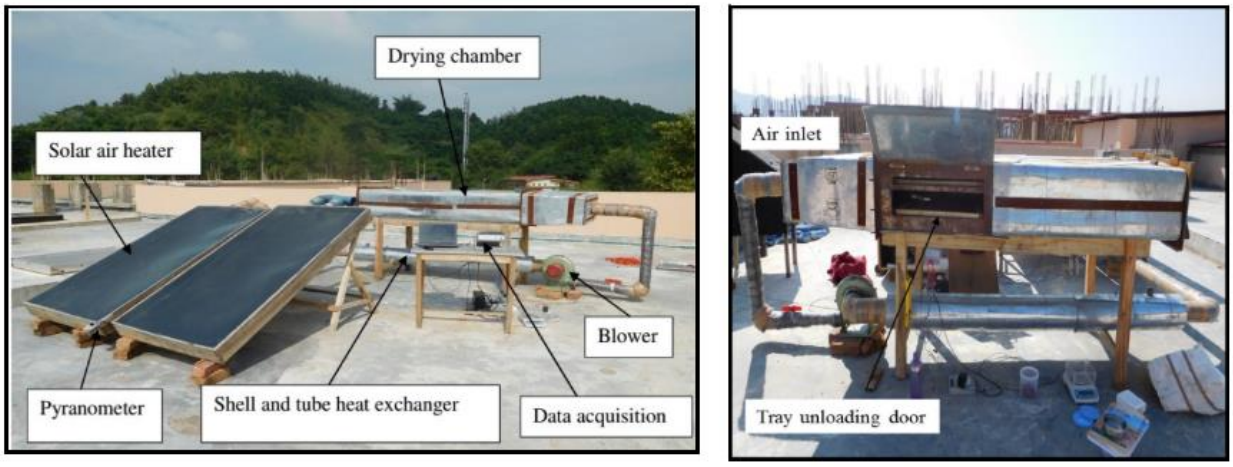

Fig. 2.5 Photograph of the solar dryer (Rabha et al., 2017a). Adapted with copyright permission 2022, Elsevier

Baniasadi et al., (2017) studied the performance of a mixed-mode solar dryer. The paraffin wax of melting point 70 °C was used as latent heat storage in the drying process of apricot. The maximum temperature achieved in the drying process was 65 °C. Minaei et al., (2017) studied the drying behavior of St John's wort leaves and evaluated the energy consumption, specific energy,

and thermal utilization efficiency for varying thickness of the St. John's wort leaves at different temperatures. In this study, it was observed that the drying rate is almost constant along with the drying chamber. The overall thermal efficiency and pick-up efficiency of the dryer were obtained as 10% and 11%, respectively. Swami et al., (2018) developed a dryer integrated with phase change material as a thermal storage medium, which was suitable for fish drying. In this study, two types of phase change material (C_{31-33} & C_{23-24}) were used and found that C_{23-24} is the most suitable for the drying temperature range of fish.

Kalapala and Devanuri (2018) reported a review study on the performance of energy storage by varying the design and operational parameters. This study was performed to analyze the performance of a PCM-based heat exchanger. In this study, it was concluded that the performance of multiple PCMs thermal storage can be enhanced by keeping their melting points in geometric progression. Folayan et al., (2018) reported the drying characteristics of onion on a batch dryer and performed the thermodynamic analysis of the dryer for different air temperatures and thickness of the products. The energy, exergy, and sustainability index of the dryer was evaluated for the varying temperature and thickness of the onion slices. From the results, it was observed that as the air temperature increases the exergy at the dryer inlet increases.

Abuşka et al., (2019) performed the energy and exergy analysis of a forced convection solar air heater with cherry stone/powder as thermal energy storage and found that the performance of the solar air heater with cherry stone is higher than that of the cherry powder. Yilmaz (2019) performed the energy, exergy, and economic analysis of an ocean thermal energy conversion system and a hybrid wind turbine. In this study, relatively higher values of energy and exergy efficiency were obtained in the wind turbine hybrid system.

Singh et al., (2019) reported the double pass forced convection solar air heater combined with porous media to enhance heat transfer. In this study, optimization analysis was conducted by varying the air flow rate and found that the airflow rate of 0.023 kg/s is the best condition for the developed dryer. Li et al., (2019) studied the energy and exergy analysis of a heat pump and a gas separation unit. The gas separation unit was used to recover waste heat. The coefficient of performance of the system was found as 4.45 and 8.05 in the absence and presence of the gas separation unit. Al Siyabi et al., (2019) analyzed the effect of thermal energy storage system inclination angle variation on the melting of latent heat storage material. In this study, the

investigations were conducted for 0°, 45°, and 90°. From the results, it was observed that 45° inclination angle from the horizontal is most suitable as compared to 0° and 90° inclination angle.

Fudholi et al., (2019) performed the exergy analysis of a photovoltaic thermal collector. In this study, a performance analysis of a v-corrugated collector was performed. This collector was used to convert solar energy into electrical and thermal energy. Experimental and theoretical exergy efficiency were obtained as 12.89% and 13.36%, respectively. The sustainability index was obtained as 1.1685 and 1.148, respectively. Sevik et al., (2019a) studied the performance analysis of a double pass solar dryer integrated with an infrared solar air dryer for the mint and apple drying process. In this study, the maximum thermal efficiency of the collector was achieved as 83.56%. This study was performed in summer and autumn; a relatively higher thermal efficiency was obtained during the summer.

Gautam and Saini (2020) reported a review study on the applications and economic analysis of solar thermal storage and found that the packed bed solar system is the most suitable thermal storage in the wide temperature range of application. Kalidasan et al., (2020) developed a thermal system integrated with PCM and reviewed the application of PCMs for low, medium, and high-temperature solar systems. In this study, PCM was integrated with the PVT system and found that the PV cells are capable to produce electricity with only 15% of absorbed solar energy, and the remaining is converted into heat. Guerraiche et al., (2020) performed the experimental and numerical study of a collector using latent heat storage material for water heating. The used thermal energy storage material consists of 40% potassium nitrate and 60% sodium nitrate. In this study, the relatively higher water temperature at the outlet of the collector was obtained in the case of thermal energy storage as compared to without thermal storage.

2.4 Drying kinetics of agricultural products

2.4.1 Drying kinetics of grains and kernels

Chen and Wu, (2001) studied the thin-layer drying model for rough rice having high moisture content. In this study, thin-layer drying tests were conducted for rough rice in the temperature range of 35–60 °C for five different relative humidity from 10–50%. The temperature and relative humidity of the drying air was controlled by mixing two air streams. The goodness-of-fit of the drying curve was examined by statistical regression technique. Correlation coefficients and residual plots were used as a criterion for evaluating the goodness of fit. The two-compartment

model with a two-term exponential function was found as the best fit to the experimental data and recommended as the thin-layer model for rough rice. Four important drying constants of the model were quantified as a function of temperature and relative humidity of drying air.

Panchariya et al., (2002) studied the thin layer drying modeling for the black tea drying process. The drying characteristics of tea were explained in the drying air temperature range of 80–120 °C and air velocity of 0.25–0.65 m/s. The data of sample weight, wet-bulb temperature, and the velocity of drying air were recorded continuously during the test. The drying data were fitted to the different semi-theoretical models such as Lewis, page, modified page, two-term, and Henderson and Pabis models. In this study, the lewis model gave a better prediction and described the thin-layer drying characteristics of black tea particles. The coefficients of determination were obtained above 0.996 for both relationships. The result illustrates that despite high initial moisture content, the drying of tea particles takes place in the falling rate period.

Jain and Tiwari (2004) studied the thermal aspects of open sun drying for various crops. The thermal behavior of open sun drying of green chili, green peas, white gram, onions, potatoes, and cauliflower was studied. During this study, it was observed that the heat transfer mainly depends on the rate of moisture transfer. In this study, a mathematical model was developed to predict the crop temperature and the rate of moisture removal for a steady-state condition. The rate of moisture transfer from the potato slices and cauliflower was significantly higher than that of other crops. In this study, the predicted values of crop temperature, temperature above the crop surface, and mass of the crop were in fair agreement with the experimental result. The goodness-of-fit was determined with the help of the coefficient of correlation and root mean square error.

Farias et al., (2004) performed a numerical solution for the grain drying in a conveyor dryer using the finite-volume method. Mathematical modeling was developed and considered the influence of bed porosity and transient terms in the drying process. The finite volume method and upwind formulation were used to solve the governing equations. The relative humidity, temperature, and moisture content of the corn in the drying process were analyzed. In this study, it was found that the air temperature has more effect on the drying rate of corn than the airflow rate. In the drying process, it was observed that the grains reached the inlet air temperature very quickly in all drying conditions.

Prachayawarakorn et al., (2005) studied the performance analysis of a dryer for the paddy drying process. This dryer consists of three main units, a fluidized bed dryer, a tempering unit, and

ambient-air ventilation. The tempering unit was responsible for grain relaxation after drying. In this study, three drying systems were proposed, first system was the simple system, in which paddy was first dried in a fluidized-bed dryer and then held temporarily in the tempering unit, after which it was ventilated with ambient air. The second system consists of two sub-drying systems; each of the system components was arranged as in the first system. The two sub-drying systems were connected in series with a tempering unit between the sub-systems to equalize the moisture content inside the kernels. In the third system, grains after relaxing in the first tempering unit were dried immediately in the second fluidized-bed dryer without ambient-air ventilation. Heat and mass transfer equations were applied to predict the change in moisture content for each drying system. From the results, it was found that the second system has a higher drying capacity and thermal efficiency than the others.

Siebenmorgen et al., (2005) studied the influence of drying rate on rice fissure formation rate and mechanical strength distribution. In this study, the test was conducted to determine the effect of drying conditions on the rate of fissure formation and the resultant mechanical strength distributions of individual rice kernels. In this study, the long-grain varieties cypress, dew, and wells at 21% harvest moisture content (MC) was dried to 12% at 40 °C, 45 °C, 50 °C, 55 °C, and 60 °C. Immediately after drying, the sample was placed in sealed plastic bags at 21 °C. In this study, fissure enumeration, milling test, and individual kernel breaking force measurements were done at 1 h, 24 h, 48 h, and 120 h after drying ceased. It was found that the head rice yields decrease as drying temperature increases and very few fissures were visible immediately after drying. Most fissures appeared within 24 hours of the drying process. During the study, it was found that there is no difference in the kernel's thickness distributions of fissured and non-fissured kernels in the dried sample. The drying treatments produced samples having greater variation in the kernel braking forces than the control sample and the breaking force distributions were affected by the drying treatment.

Ondier et al., (2010) reported the drying of rough rice at low temperatures. In this study, the drying operation was performed at the air temperature range of 26–34 °C and relative humidity 19–68%. The drying rates and their effect on quality parameters such as head rice yield, color, and pasting viscosity of long and medium-grain rice were investigated. The rice was harvested at the moisture content of 19.6% and 17.5%. In this study, results showed that the dehumidification of the drying air had a high potential for increasing drying rates at 26 °C, 30 °C, and 34 °C. Low

drying air temperature and relative humidity had no adverse effect on head rice yield and color. It was observed that the drying duration could be shortened by reducing the RH at a given temperature, particularly at a lower temperature.

Li et al., (2011) studied the equilibrium moisture content and sorption isosteric heats of five wheat varieties in China. In this study, the moisture sorption isotherm data of five Chinese wheat varieties were investigated by the gravimetric static method at five different temperatures 10 °C, 20 °C, 25 °C, 30 °C, and 35 °C and relative humidity ranged from 11.3–96%. It was observed that the sorption data of wheat decreases with an increase in temperature at constant relative humidity, and the hysteresis effect was observed between adsorption and desorption isotherms. In this work, six models namely the Chen Clayton, Modified-BET, Modified-Chung-Pfost, Modified-Henderson Modified-Oswin, and Strohman-Yoerger were employed to describe the experimental data. The BET, MCPE, and MOE were selected to describe the sorption isotherms of wheat for the relative humidity in the range of 11.3–49.9%, 11.3–96%, and 11.3–96%, respectively. During the study, a big difference was found between adsorption and desorption isosteric heats of wheat below 20% moisture content.

Torki Harchegani et al., (2012) studied the deep-bed drying kinetics of rough rice. In this experiment, a deep bed dryer was designed and constructed for rough rice drying. The study was performed on different operating conditions to evaluate the effect of influential parameters such as air temperature, velocity, and relative humidity. During the experiment, it was found that the air temperature has the highest contribution to the drying time for a specific reduction in the moisture content. In this study, relative error and mean relative error was calculated for the simulation results and found to be in the acceptable range of 10–15% and below 10%. In the study, a non-equilibrium model for numerical simulation of rough rice drying in a deep-bed dryer was evaluated for predicting the variation of average grain moisture content and finally, this model proved its ability with good accuracy.

Asiru et al., (2013) studied the mathematical modeling for the drying of cashew kernels. In this work, a mathematical model describing the thin-layer drying of cashew kernels in a batch dryer was presented. In this study, the drying air temperature ranged from 70–110 °C. During the study, cashew kernels were dried from the initial moisture content of 9.29% (db) to 3.5% (db). Seven thin layer mathematical drying models were compared based on the coefficient of determination (R^2), mean square error (MSE), and mean relative deviation modulus (p) to estimate the drying curves.

The effects of the drying air temperature and time on the drying model constants and coefficients were predicted by multiple regression analysis using linear and non-linear type models. The page model was best fitted to describe the drying behavior of cashew kernels with R^2, MSE, and P values of 0.9830, 0.00311, and 5.046, respectively.

Chukwunonye et al., (2016) performed the literature survey for the thin layer drying modeling for some selected Nigerian products. The drying data fitted to the different thin-layer drying models. The fitting of the models was investigated by comparing the coefficient of determination (R^2), the sum of square error (SSE) and root mean square error (RMSE) between observed and predicted moisture ratio. The model having the highest value of R^2, and the lowest value of SSE and RMSE was considered as the best model for the drying process. In this study, the raw agricultural products with 80% to 90% moisture content were brought down to equilibrium moisture content. From the study, it was observed that the relevant and adequate pretreatment is before the drying enhances the quality of the product. From the study, it was observed that the drying behavior, moisture migration, design of effective drying equipment, and optimization of the drying process are essential parameters to understand the drying kinetics of crops.

2.4.2 Drying kinetics of fruits and vegetables

Rafiee (2009) studied the mathematical modeling of thin-layer drying kinetics of apples and verified with experimental data. In this paper, fourteen different mathematical drying models were compared to three statistical parameters such as root mean square error (RMSE), chi-square, and modeling efficiency. The thin-layer drying kinetics of apple slices were investigated in a laboratory convective dryer and the mathematical modeling of the drying process was performed. The experimental study was performed at the air temperature between 40 °C and 80 °C for the air velocity 0.5, 1, and 2 m/s and the thickness of the layer 2 mm, 4 mm, and 6 mm, respectively. Besides the effect of drying air temperature and velocity, the effect of slice thickness on drying characteristics was also performed. Drying curves obtained from the experimental data were fitted with the thin-layer drying models. In the study, the modeling efficiency, RMSE, and chi-square were obtained as 0.99972, 0.00292, and 0.00001, respectively. Which is suitable to describe the drying curves of apples. The effect of air temperature, velocity, and layer thickness on the drying constant and coefficient was reported. From the study, it was found that the increase in drying air temperature results in a decrease in drying time.

Goyalde et al., (2009) studied the mathematical modeling for the drying kinetics of sugarcane slices. The drying characteristics of the sliced sugarcane were investigated and fitted to semi-theoretical models to describe the drying behavior. The drying test was performed in an experimental fixed-bed dryer with upward airflow. The drying was carried out at two air temperatures 50 °C and 60 °C with air relative humidity of 17.9–11.1%. The sugarcane slices were dried from the initial moisture content of 70% (wb) to 6% (wb). This operation took 7.5 h and 3.5 h for the drying temperature of 50 °C and 60 °C, respectively. In this study, experimental data were adjusted to four traditional mathematical models to represent the drying process of agricultural products.

Darvishi (2012) reported the effect of the shape of potato chips on drying characteristics. In this study, the effect of microwave power and shape of samples on the moisture ratio, drying rate, effective moisture diffusivity, energy efficiency, and energy consumption for potato drying was investigated. The drying experiments were carried out at 200 W, 300 W, and 400 W for the rectangular (S_2) and cylindrical (S_1) shapes with dimensions of 1 mm ×1 mm × 0.5 mm, 5 mm × 0.5 mm, respectively. The results showed that the power and shape of samples significantly influenced the total drying time, effective diffusivity, energy efficiency, and energy requirement for the drying process. As the drying progress, the loss of moisture in the product causes a decrease in the absorption of microwave power and results in a fall in the drying rate. It was observed that the average effective diffusivity varied from 2.33×10^{-8}–7.60×10^{-8} m^2/s for S_2 and 1.39×10^{-8}–3.17×10^{-8} m^2/s for S_1 in the microwave power range of 200–400 W. Energy efficiency increases with an increase in microwave power and moisture content. The minimum specific energy requirement for the drying of potatoes was determined as 4.24 MJ/kg and 5.70 MJ/kg for S_1 and S_2, respectively at the power of 400 W.

Zarein et al., (2013) studied the mathematical modeling, energy consumption, and thin layer drying kinetics of carrot slices under a microwave oven. This study was performed to investigate the thin-layer drying characteristics of carrot slices under 4 different microwave power; 100 W, 300 W, 500 W, and 700 W. In this study, five mathematical models for describing the thin slices of carrot were investigated, out of the five models, the Midilli model was considered as the most appropriate model for carrot slices. During the study, the effective diffusivity varied from 4.23×10^{-7}–7.34×10^{-6} and the activation energy was obtained as 92.33 kW/kg. The specific energy consumption values were ranged from 10.27–23.29 kWh/kg and the optimized specific energy

consumption obtained as 300 W. During the experiment, it was found that the increase in microwave power increases the drying rate and reduces the energy consumption.

Borah and Nayak (2013) studied the quality characteristics of dried jahaji banana chips after deep fat frying. A study on drying behavior and the quality of dried banana chips was performed. Experiments were conducted at three drying temperatures 40 °C, 60 °C, and 80 °C for the initial moisture content of 200%, 100%, and 50%. The effect of moisture loss and oil absorption during frying indicates that the drying temperature does not have any significant effect on the oil content or moisture content of chips. The color and hardness of chips change significantly during the frying. A significant effect of temperature, moisture content, and drying time on the hardness of chips was observed. Based on overall acceptability and other sensory ratings the banana chips dried at 60 °C up to 200% (db) moisture content and fried for 180 sec at 170 °C results in the best quality of banana chips.

Tavakolipour and Zirjani (2014) studied banana chips drying by hot air and microwave dehydration methods. In this study, banana slices of Cavendish variety having slice thicknesses 3 mm, 5 mm, and 10 mm first pretreated with blanching and chemical treatments followed by the hot air drying at 60 °C, 70 °C, and 80 °C and microwave drying at 300 W, 500 W, and 700 W microwave power intensity. Dried samples were evaluated for color, sugar content (sucrose), ascorbic acid, rehydration ratio, drying time, and drying rate. Pretreatments enhance the drying rate and decrease the drying time. From the study, it was observed that the drying rate in microwave drying is ten times that of hot air drying.

Dagde and Nmegbu (2014) studied the mathematical modeling of a tray dryer for the drying of potato chips using a hot air medium. In this study, a mathematical model for the batch tray dryer for the drying of potato chips was developed. During the study, the conservation principle was applied to the fundamental quantities of moisture, humidity, energy in potatoes, and energy in the air. The model equations were solved using the fourth-order Runge-Kutta algorithm and implemented in a visual basic program. The results showed that the moisture content in the potato chips reduces as time increases, and the potato chip's temperature increases with time, while the air humidity increases. Functional parameters in the dryer such as the quantity of heat supplied and airflow rate were also simulated for process control and optimization.

Singh et al., (2014) developed a mathematical model to study the drying characteristics of apples and potatoes. During the study, a mathematical model was proposed to study the drying

characteristics of apples and potatoes. The model was validated with the help of several experimental data and the proposed model was compared with the mathematical drying models based on RMSE, reduced chi-square, and coefficient of determination for different food products. During the study, it was observed that moisture removal is the main factor for the reduction of mass and volume of food products. Time and temperature have a significant effect on moisture removal in the drying process. The results of this study showed that the proposed model is better as compared to existing models. This model may be helpful for food industries to analyze the drying kinetics of apple and potato maintaining the product quality.

Ayala and Topete (2014) studied the pineapple drying process in a solar hybrid dryer. In this study, the experimental analysis of pineapple drying in a solar hybrid dryer was presented. A direct and integrated type of solar dryer was designed and the copper helical tube was used to conduct heat from hot water at 80°C. The tube was located at the bottom of the dryer pan, the wall and the base of the dryer were isolated by fiberglass. During this study, the honey variety of pineapple was used and each slice of pineapple was 5 mm thick having a density of 2.83 kg/m^2. The drying tests were performed during winter and spring, using both the hybrid and traditional solar dryers. The evaporation efficiency of the traditional solar dryer was obtained approximately twice that of the hybrid dryer, ranging from 22.7–24% for traditional and 9.3–14% for hybrid dryer.

Huirem and Shakya, (2015) studied the thin layer drying kinetics of kiwifruits. In this study, the thin layer drying kinetics of kiwifruit slices were experimentally investigated in a laboratory-scale vacuum oven. An experimental study was performed to dry the kiwi-fruits slices from initial moisture content of 86% (wb) to 2% (wb) at three different temperatures 50 °C, 60 °C, and 70 °C, under 630 mm Hg vacuum (17.33 kPa) pressure. The time required for drying kiwifruits slices at 50 °C, 60 °C, and 70 °C plate temperatures were 12 h, 9 h, and 6.5 h, respectively. In this study, the drying takes place in the falling rate period. The four mathematical drying models Lewis, Page, Modified Page, and Henderson and Pabis model were used to fitting the experimental result. The moisture reduction data obtained as a function of drying time. The page model was considered the best model to describe the vacuum drying characteristics of kiwifruits.

Jabeen et al., (2015) studied the drying kinetics of potatoes in a cabinet dryer. In the study, a laboratory-scale cabinet dryer was constructed with an attached weighing balance to calculate changes in the weight of the product without removing it from the dryer. Experiments were conducted to study the effect of process parameters (temperature and thickness) on the drying

kinetics of potatoes. The drying process was characterized by a decrease in the moisture ratio with time and showed a non-linear behavior. No constant drying rate was observed in the entire drying process and the drying occurred in the falling rate period, showing that the drying process was mainly controlled by the diffusion mechanism. From the study, it was observed that the drying rate increases with an increase in air temperature.

Ashaolu and Akinbiyi (2015) studied the effect of chip size on thin-layer drying characteristics of plantain. This study investigates the effect of varying chip sizes of plantain varieties in the drying process. In the study, the drying was carried out at 50 °C, 60 °C, 70 °C, and 80 °C at the air velocity of 2.2 m/s. The plantain samples were cut into equal sizes of thicknesses 2 cm, 3 cm, 4 cm, and 5 cm for two varieties. It was observed that the drying period for each variety was not the same and a higher drying rate was obtained at 80 °C than 50 °C. The drying time varied from one variety to another, depending on the initial moisture content, pretreatment, and drying air temperature. The study indicates that the drying of 2 cm thick chips takes lesser time than 5 cm thick chips, especially in the Musa Sapientum variety of bananas. The Musa Sapientum variety had the highest drying rate than the Dwarf Cavendish variety in almost all temperatures and treatment variations. In this study, the moisture diffusivity was obtained in the range of 0.0118–0.0373 m^2/s, while the activation energy was found as 0.2 kJ/mole for the temperature range of 50–80 °C.

2.5 Overall observations

The previous research work on the various types of the dryer for the different types of agricultural product drying process has been reviewed. The energy and exergy analysis of the dryer becomes an important tool to analyze the performance of the dryer. The energy and exergy efficiency of the various types of dryers have been reported by different researchers as shown in Table 2.1.

Table 2.1 Performance analysis of the dryers reported by different researchers

Type of dryer	**Product**	**Collector efficiency (%)**	**Drying chamber exergy efficiency (%)**	**Dryer efficiency (%)**	**Reference**
NCHD	Pineapple	NA	NA	9	Bena and Fuller (2002)
Convective Dryer	Red pepper	NA	67.28–97.92	NA	Akpinar et al., (2004)
NCSD	olive mill wastewater	NA	34.4–100	NA	Celma and Cuadros, (2009)
FCSAH	NA	20–82	NA	NA	Akpinar and Koçyiğit, (2010)
STD	Jackfruit leather	27.45–42.5	NA	NA	Chowdhury et al., (2011)
FCSAH	NA	70–80	NA	NA	Fudholi et al., (2013)
FCSAH	NA	Max. 80	NA	NA	Jafarkazemi and Ahmadifard, (2013)
FCSD	Bitter gourd	22	NA	19	Vijayan et al., (2016)
FCSD	Ghost Chilli pepper	22.95– 23.3	21–98	NA	Rabha et al., (2017a)

2.6 Summary of the literature review

Solar dryer makes the drying process hygienic, pollution-free, reduces the wastage of agricultural products, and enhances the product quality. From the literature survey, it was found

that the hybrid dryer reduces the drying period over open Sun drying and makes the drying process continues throughout the day. The use of a solar hybrid dryer is one of the best drying techniques in terms of product quality in the non-electrified areas of developing countries. It reduces the drying time up to 50% as compared to open sun drying. Energy and exergy analysis of the dryers plays a key role in performance optimization. From the literature, it was found that the thermal performance of the solar dryers increases with an increase in the airflow rate. Energy analysis is not a sufficient condition to design a thermodynamic system, it does not consider irreversibility. Hence, to analyze the performance of the thermodynamic system, exergy analysis must be carried out. Exergy analysis is a practical approach to design a thermodynamic system.

The energy and exergy efficiency of the solar dryer mainly depend on the solar intensity and airflow rate. Several studies reported different energy and exergy efficiency of the dryer with the types, sizes, and shapes of the products. Hence, from the literature, it can be concluded that the performance of the dryer varies with the types, shape, and size of the product. Thin layer drying kinetics of the agricultural product is an important tool to evaluate the quality of the dried products and it helps to optimize the drying process. It reduces the drying time and enhances the quality of the dried product. Numerous literatures related to the thin layer drying kinetics of agricultural products such as grains, vegetables, fruits, etc. is reported. The thin layer drying kinetics of the products depend on the types of agricultural products, temperature, and layer thickness. In the literature, researchers conducted the statistical analysis for the best fitting of the drying model based on the highest value of R^2 and the minimum value of chi-square, and RMSE.

2.7 Climatic information in Northeastern India

The climatic conditions and the soil of the NER are suitable for the cultivation of varieties of agricultural products such as rice, ragi, jowar, maize, cotton, sugarcane, tobacco, tea, rubber, ginger, turmeric, chili, cardamom, cashew nut, and black pepper. Rice is the most important cereal crop of the North Eastern Hill Region covering an area of about 998000 hectares producing about 2154000 tonnes of rice with average productivity of 2.00 t/ha. It is the major crop, and claims over 85 % of the cropped area. These agricultural products have high demand in the global market. Assam is the largest rice producer state in the NE region. The demand for these agricultural goods is very high on the international market. All of these agricultural goods have a significant economic impact on India's NER. Most of these products are typically dried in the open sun or by burning

wood logs in open furnaces. The quality of the dried goods deteriorates due to unregulated heating, as well as direct exposure to smoke and sunlight. The frequent rainfall, high humidity, low yearly average solar radiation, and lengthy rainy days characterize the NER's climate. Due to the presence of clouds in the sky, particularly in the summer, solar radiation varies during the day. On a day with plenty of sunshine, however, the average daily solar radiation is relatively high, the upper limit of the solar intensity at Guwahati is ~1000 W/m^2. Therefore, the agricultural products drying must be completed during sun hours, hence the drying duration is restricted by daily solar radiation. The relative humidity of NER region recorded in the range of 60–85% A solar dryer coupled with a thermal energy storage device or an additional heat source may be the most appropriate for the NER region because sun radiation fluctuates regularly as a result of cloud cover.

2.8 Research gaps

In this chapter, an extensive literature survey is reported for the various drying aspects such as energy-exergy analysis, drying characteristics, and mathematical modeling for the drying process of agricultural products. Amongst the dryers, solar dryers are more preferable due to their reliability, clean energy input, quality of the product, and environment friendly. However, the solar dryer can only be operated when sufficient solar insolation is available. Hence, the integration of biomass-operated dryer to the solar dryer makes it continuous throughout the day and enhances the product quality. In the literature, study related to the performance analysis of the hybrid dryer for the cereal grains drying is found to be very limited. A very few studies related to the energy-exergy analysis, mathematical modeling, and drying kinetics of the paddy drying process in the biomass-solar hybrid dryer have been found. Throughout the literature survey, none has conducted the performance analysis of the biomass-solar hybrid dryer coupled with the sensible and latent thermal storage medium. Hence, the study on performance analysis of the biomass-operated dryer having sensible and latent thermal storage medium coupled with solar air heaters for crop drying is an emerging area of research. To analyze the performance of the biomass-solar hybrid dryer coupled with a thermal storage medium for the grains drying in the climatic condition of North-East India, a throughout experimental study is required. Hence, in the present study, the performance analysis of a natural convection biomass-operated grain dryer with sensible and latent storage medium coupled with solar air heaters has been investigated experimentally. Coupling the biomass-fired dryer to the solar dryer continues the drying operation throughout the day. The

sensible thermal storage stores the flue gas energy and extend the drying operation for the same energy input. Paraffin wax in the tray controls the energy and provides uniform heat to the product. Hence, the thermal energy storage saves the product from overheating and enhances the dried product quality. The energy-exergy analysis will help to optimize the drying operation.

2.9 Objectives of the present work

This research work aims to develop an experimental setup for the quality drying of the agricultural product in the climatic condition of North-East India. Experimental investigations have been performed to enhance the performance of the developed dryer. The solar air heaters have been coupled to the biomass-operated dryer so that the biomass consumption could be reduced.

In view of the above closure of literature review, the following objectives are considered in the present work:

- Development of the biomass-operated dryer coupled with solar air heaters
- Performance evaluation of biomass operated and solar operated dryers
- Performance evaluation of biomass operated dryer coupled with solar dryer
- Energy efficiency analysis of the developed dryers

2.10 Summary of the chapter

This chapter thoroughly reviewed the literature related to the different types of dryers such as convective dryers, solar dryers under natural and forced convection mode, and hybrid dryers for the various types of agricultural products drying process. The energy-exergy analysis of the dryers and drying kinetics of the agricultural products have also been reviewed. Based on the review a critical summary has been formulated and research gaps have been identified. To address the objectives, a methodology has been formulated and the methodology (experimental setup and procedure) of the present study is presented in chapter 3.

Chapter 3

Experimental setup and procedure

3.1 Introduction

In the present study, a solar-biomass hybrid dryer has been developed. The experimental investigations for the drying kinetics of paddy under biomass-operated dryer, natural convection solar dryer, forced convection solar dryer, and the solar-biomass hybrid dryer has been performed. The thermodynamic analysis of the natural convection biomass-operated dryer with and without sensible thermal storage, solar air heater, and solar dryer under natural and forced convection mode has been conducted. The experimental set up and procedures of the study has been presented in this Chapter. Mathematical formulations for the performance investigation of the dryer are also discussed in the subsequent sections.

3.2 Solar-biomass hybrid dryer

The solar-biomass hybrid dryer has been developed for the drying of agricultural products. The dryer is developed especially for the farmers in the underdeveloped and developing countries. This dryer mainly consists of two solar air heaters, conical furnace, rectangular chamber with pebbles, phase change material (paraffin wax) and drying chamber. During the sunshine hours, solar dryer is used for the drying of products and the biomass operated dryer is used after the sunset (whenever sunshine is not present). Sensible (pebbles) and latent thermal storage (paraffin wax) in the biomass operated dryer is used to store the energy during the biomass burning period so that the temperature in the drying chamber can be controlled for the quality drying of the products. The performance analysis of the biomass operated dryer and solar dryer has been analyzed. The performance analysis of the solar-biomass hybrid dryer has also been performed for the paddy drying process. The study of the biomass operated dryer is performed for the natural convection mode while the solar dryer is studied under natural and forced convection mode. The schematic and the photograph of the experimental setup are shown in Figs. 3.1 and 3.2. Figure 3.3 shows the energy flow diagram of the dryer.

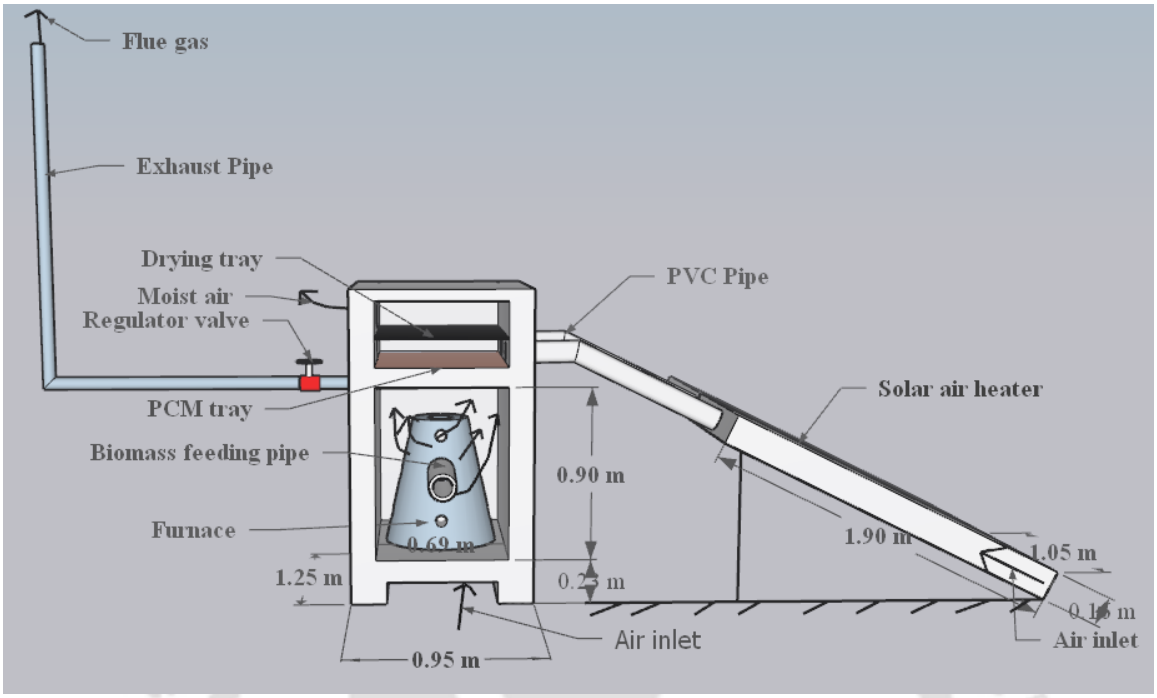

Fig. 3.1 Schematic diagram of the experimental setup

Fig. 3.2 Photograph of the experimental setup

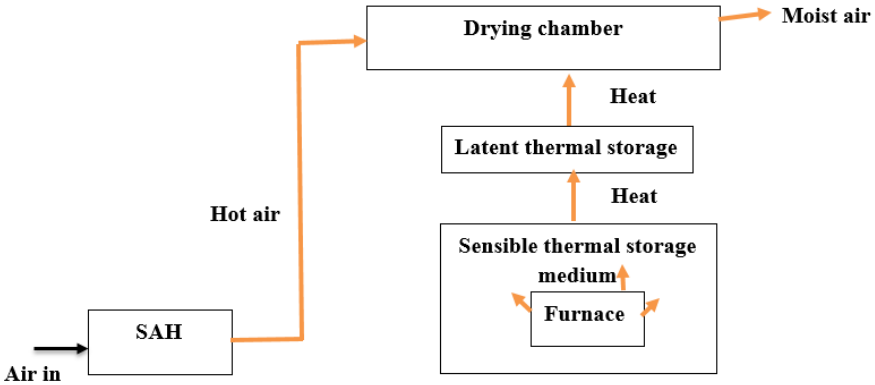

Fig. 3.3 Energy flow diagram in the dryer

3.3 Biomass-operated natural convection grain dryer

3.3.1 Description of the dryer

The natural convection biomass-operated dryer mainly consists of a conical furnace, a brick-wall rectangular chamber, sensible heat storage material (pebbles), latent heat storage material (paraffin wax), and an exhaust pipe. The conical furnace (mild steel) having a bottom diameter, top diameter, height, and exhaust pipe diameter are 0.60 m, 0.30 m, 0.68 m, and 0.0635 m respectively are kept in the rectangular chamber of 0.13 m thick brick wall having inside dimension of 1.25 m × 0.95 m × 0.90 m. At the top of the rectangular chamber, a mild steel tray is kept at a height of 0.9 m from the base of the furnace, in which paraffin wax is kept which acts as latent heat storage for the quality drying of agricultural products. Above the paraffin wax tray, a mild steel wire mesh tray is kept for the drying of agricultural products. For supplying fresh air in the rectangular chamber, eight holes of dimension 0.15 m × 0.10 m are made at the bottom of the rectangular chamber. For the proper combustion in the conical furnace, a rectangular hole of dimension 0.63 m × 0.23 m is made through which fresh air enters the conical furnace. At the bottom of the furnace, a perforated mild steel tray of thickness 5 mm is attached at which wood is being burnt and also provides sufficient air for the burning of biomass. The provision for the collection of ash is also maintained. The concept of this dryer is studied by Mohapatra and Mahanta, 2013. This natural convection dryer is an example of an indirect type of application of heat to food/agricultural products. The schematic of the natural convection biomass-operated dryer is shown in Fig. 3.4. The specifications of the furnace are shown in Table 3.1.

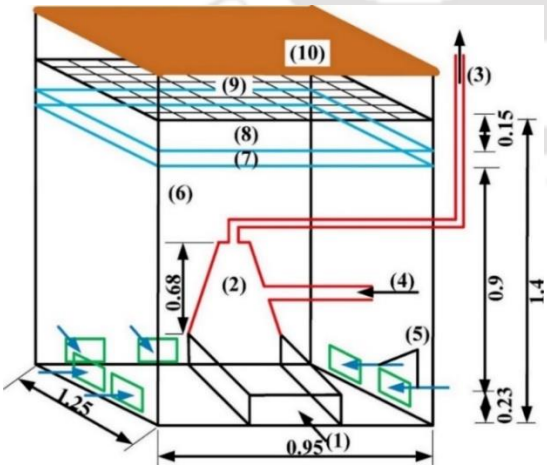

(1) Ambient air enters the furnace (2) Conical furnace (3) Exhaust pipe (4) Biomass feeding pipe (5) Ambient air enters the rectangular chamber (6) Rectangular chamber (7) Paraffin wax tray (8) Drying chamber (9) Drying tray (10) Cover plate.

Fig. 3.4 Schematic diagram of natural convection biomass-operated dryer (dimensions are in meter)

Table 3.1 Components and Specifications of the furnace

Components	Specifications	Components	Specifications
1.Furnace		5. Exhaust pipe (Horizontal)	
a. Shape	Conical	a. Shape	Circular
b. Dimension	$Ø_1$=0.6 m $Ø_2$=0.3 m	b. Dimension	L = 2 m, Ø= 0.063 m
c. Thickness	0.003 m	c. Thickness	0.001 m
d. Height	0.6 m	d. Material	GI sheet
e. Material	Mild steel		
2. Biomass burning plate		6. Exhaust pipe (Vertical)	
a. Shape	Rectangular	a. Shape	Circular
b. Dimension	0.59 m×0.59 m	b. Dimension	L = 1.8 m,
c. Thickness	0.005 m		Ø = 0.063 m
d. Material	GI sheet	c. Thickness	0.005 m
		d. Material	GI sheet
3. Biomass feeding pipe		7. Cover plate	
a. Shape	Circular	a. Shape	Rectangular
b. Dimension	Ø = 0.13 m	b. Dimension	0.43 m×0.62 m
c. Thickness	0.005 m		×0.22 m
d. Material	Mild steel	c. Thickness	0.005 m
		Material	Mild steel
4. Ash tray		8. Stand (Base)	
a. Shape	Rectangular	a. Shape	Rectangular
b. Dimension	0.6 m×0.6 m×0.05 m	b. Dimension	0.61m×0.61m×0.22 m
c. Thickness	0.005 m	c. Thickness	0.005 m
d. Material	Mild steel	d. Material	Mild steel

3.3.1.1 Basic consideration for the furnace

The basic criteria of the furnace are considered as follows:

- The heating is indirect, i.e., flue gases from the chimney and the drying air flow in two different circuits. This arrangement protects the product from contamination by smoke, soot, and ash of the flue gases.
- Sufficient air should flow to the furnace for the complete burning of biomass.
- Passage of flue gases through the exhaust pipe by creating sufficient draft.
- Care should be taken for making holes in the biomass burning plate (BBP) so that easy removal of ash to the ash tray and no burning pieces of wood chips drop to the ash tray through the hole.
- Removal of ash outside the chamber should be easy.
- The biomass feeding process should be easy so that labor charges can be minimized.
- All the parts of the furnace are assembled simply so that the maintenance and redesign cost of the dryer can be reduced.
- The material cost should be less and easily available throughout the year.

The following basic equations are used for design calculations:

The energy loss to the ambient in the flue gas passes through the exhaust pipe can be evaluated with the help of Eq. (3.1):

$$Q_f = \dot{m}_f C_f (T_f - T_{amb}) \tag{3.1}$$

Pressure drop through the biomass burner can be evaluated by using Eq. (3.2):

$$\Delta p = gH(\rho_a - \bar{\rho}_f) \tag{3.2}$$

where

$$\rho_a - \bar{\rho}_f = \frac{p}{R}(T_a - \bar{T}_f) \tag{3.3}$$

where Q_f is the heat carried by the flue gas, m_f is the mass flow rate of flue gas, Δp is the pressure difference, H is the chimney height, ρ_a is the density of ambient air, $\bar{\rho}_f$ is the mean density of flue gas, p is the atmospheric pressure, T_a is the ambient air temperature, and $\bar{T}_f$ is the mean temperature of flue gas. The conical furnace efficiency can be defined as the ratio of heat transfer

to the rectangular chamber of the dryer to the energy input in the conical furnace. It can be calculated by using Eq. (3.4):

$$\eta_{furnace} = \frac{Q_{chamber}}{E_{in}} \tag{3.4}$$

The air circulation is generated in the dryer due to the density difference of the air in the chamber and ambient air. Thermal buoyancy produced due to density difference can be obtained by using Eq. (3.5):

$$\Delta p = g\beta H\rho_a(\Delta T) \tag{3.5}$$

3.3.1.2 Basic consideration for the drying chamber

It is very difficult to control the drying air temperature in the drying chamber during drying without a thermal storage medium. Hence, it is necessary to store the energy and used it for the further drying process. To store the thermal energy in the rectangular chamber below the drying chamber a sensible thermal storage medium (pebbles) is used. For quality drying of agricultural products, a uniform temperature is required. By using only sensible thermal storage in the rectangular chamber will not solve the problem of quality drying. Hence, to achieve uniform temperature in the drying chamber a latent heat storage medium is required. Properties of the thermal storage medium is shown in Table 3.2. The basic criteria for the thermal storage medium are considered as follows:

- The specific heat capacity of sensible heat storage materials should be high.
- There should be sufficient void space between the storage materials so that air flow between the materials is possible.
- The amount of heat storage materials used depends on the amount of heat produced.
- The latent storage materials should be nontoxic, non-reactive, and non-hazardous.
- The evaporation temperature and flash point of the latent storage material should be high so that there is no contamination of material with the drying product and no chance of getting fire on the material.
- It should store a sufficient amount of heat during phase change from solid to liquid and release heat for a longer period at a constant range during the solidification.
- The cost of storage material should be less.

- The storage materials should be locally available.

Table 3.2 Properties of the thermal storage medium

Particulars	Parameters	Value
Phase change material (Paraffin wax)	Density	900 kg/m^3
	Specific heat	2.384 kJ/kg K
	Latent heat of fusion	189 kJ/kg
	Thermal conductivity	0.22 W/m K
	Melting point temperature	58–60 °C
	Flash point	200–240 °C
	Boiling point	370 °C
sensible thermal energy storage material (Pebbles)	Density	2260 kJ/kg
	Specific heat	1 kJ/kg K

3.3.1.3 Experimental procedure for the biomass operated dryer

In this dryer, biomass is burnt in a conical furnace. From the heat generated by burnt biomass, the surface of the conical furnace becomes hot, which makes surrounding air/pebbles (which are kept in the rectangular chamber) heated up. Due to density difference, the heated air moves upward and passes through the paraffin wax tray, which causes to increase in the paraffin wax temperature. Once the temperature of the paraffin wax becomes equal to its melting point, the paraffin wax melts and supplies uniform heat for the quality drying of the food/agricultural products. In the study, the energy and exergy analysis in the rectangular chamber below the paraffin wax tray for two cases viz. (i) without sensible thermal storage medium in the rectangular chamber, and (ii) with sensible thermal storage medium has been studied. In the above two cases, hot air from the rectangular chamber is allowed to flow into the drying chamber through the cylindrical tube in the paraffin wax tray.

In the first case, the investigation is done without sensible heat storage material and performed the energy-exergy analysis in the rectangular chamber. In case-II, pebbles are used as sensible heat storage material surrounding the conical furnace in the rectangular chamber. Pebbles (which are kept in the chamber) stores energy from the hot air and retain heat for a longer time in the chamber. For proper analysis, the study in the rectangular chamber is done for four sections. The temperature at each section in the rectangular chamber is measured by using J-type thermocouples at 20 points

and an average value of temperature at the corresponding sections is taken for the performance analysis. The temperature is recorded in 80 different locations across the rectangular chamber and an average of all point temperatures (T_{ch}) is considered. For the measurement of the conical surface temperature, six thermocouples at six points are attached at the outer surface of the conical furnace and an average of all six-point temperature (Ts) is taken. Brick wall temperatures are measured by using Laser Beam Temperature Gun GM-300. Subsequently thermodynamic analysis of the dryer has been performed. For all cases of studies, locally available wood (lebbeck) is burnt continuously in the conical furnace for three hours. The schematic of the position of the thermocouples with coordinate at one section in the rectangular chamber is shown in Fig. 3.5.

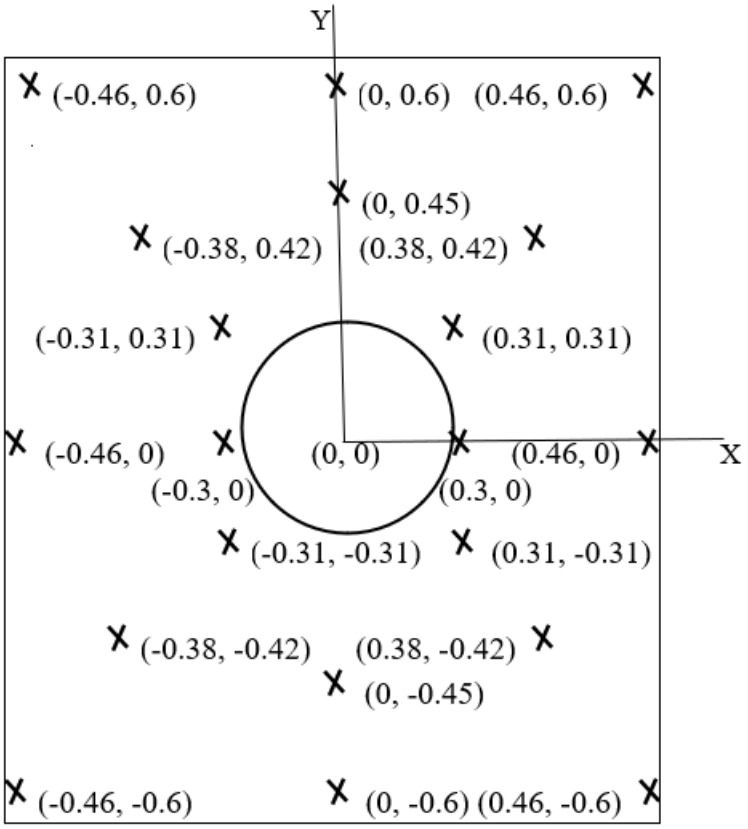

Fig. 3.5 Schematic representation of the position of the thermocouples at one section in the rectangular chamber (co-ordinates are in meter)

In this figure, the circle at the center of the rectangular chamber represents the position of the furnace and points represent the thermocouple position. For the coordinates at the position of the thermocouple in the rectangular chamber, the center of the section is taken as the origin. After performing the above two cases of studies, another case study (case-III) is performed. In case–III,

the sensible heat storage medium is filled up to the paraffin wax tray but hot air is not allowed to flow from the rectangular chamber to the drying chamber. In this case, the temperature in the paraffin wax tray and just below the paraffin wax tray are measured. After studying the above three cases, it was observed that a significant amount of energy is lost in the flue gas through the exhaust pipe. Hence, the biomass-operated dryer has been modified in such a way that the flue gas energy could be utilized in the rectangular chamber. In the modified biomass-operated dryer, several holes are made in the conical furnace and the flue gases are directly allowed to enter the rectangular chamber so that sensible storage materials (pebbles) can store most of the flue gas energy and that stored energy could be utilized for the drying process. The schematics of the modified natural convection biomass-operated dryer is shown in Figs. 3.6 (a) and (b). For the drying kinetics analysis, paddy was brought from the local farmer near to IIT Guwahati campus (26.1445° N and 91.7362° E). All the experimental data have been recorded at an interval of 30 minutes.

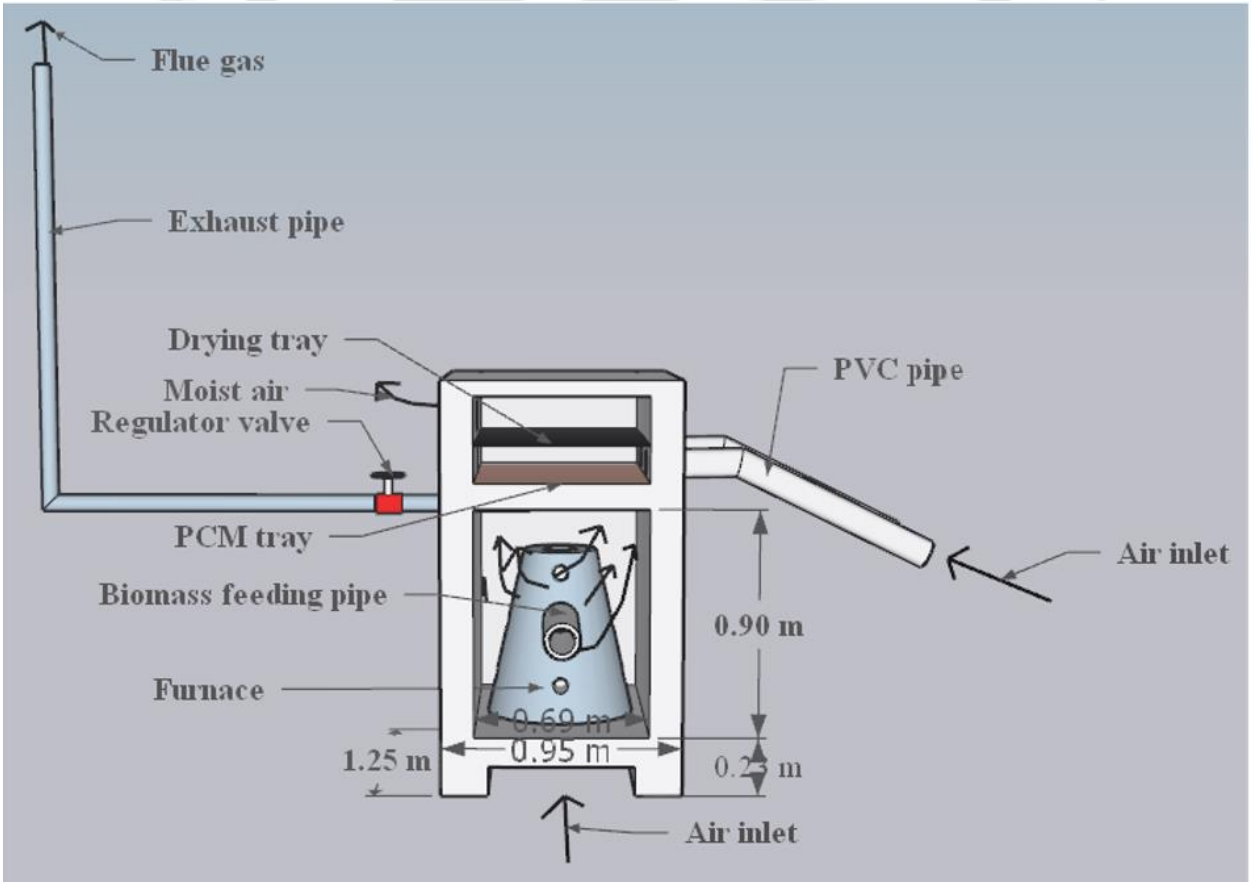

Fig. 3.6 (a) 3-D schematic of the modified natural convection biomass-operated dryer

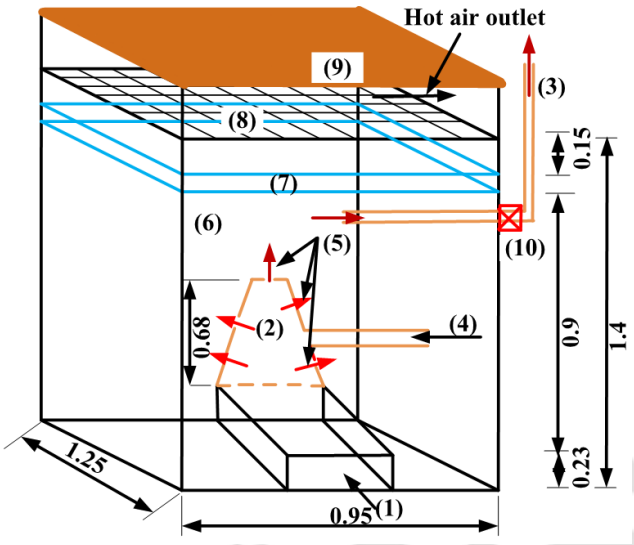

(1) Fresh air enters the furnace (2) Conical furnace (3) Exhaust pipe (4) Biomass feeding pipe (5) Flue gas enters the rectangular chamber (pebbles) (6) Rectangular chamber (pebbles) (7) Paraffin wax tray (8) Drying tray (9) Cover plate (10) Flow regulator valve.

Fig. 3.6 (b) Schematic of the modified natural convection biomass-operated dryer (dimensions are in meter)

3.4 Design of the solar dryer

3.4.1 Description of the dryer

In the study, solar dryer having flat plate collector has been designed. The designed solar dryer consists of a copper flat plate collector, glass cover, plywood, glass wool, and a wooden frame. In the present study, two solar air heaters (SAHs) of dimension 1.9 m × 1.05 m × 0.16 m have been designed and hot air from the SAH flows into the drying chamber through the PVC pipes. To maximize the utility of solar energy, a fan is attached to each PVC pipe at the inlet of the drying chamber.

3.4.1.1 Solar air heater (SAH)

The SAH consists of a 0.004 m thick glass cover, copper plate collector of thickness 0.0005 m, 10 copper tubes of diameter 0.0125 m, glass wool insulation of thickness 0.04 m, and a plywood sheet of thickness 0.006 m. The components are fitted in a wooden frame of dimension 1.90 m × 1.05 m × 0.16 m. The clear glass is placed at the top of the wooden frame followed by the collector, insulation, and plywood sheet. The wooden frame inner face is also insulated with 40 mm thick glass wool. To enhance the absorption of solar energy, the collector plate is black painted. The distance between the insulation and the flat plate is 50 mm, and that is between the flat plate and glass cover is 70 mm. The space in the SAH allows the hot air to flow into the drying chamber. In

the present study, two solar air heaters have been designed and attached to the drying chamber having dimension 1.25 m × 0.95 m × 0.30 m through the PVC pipes. The air present in the SAH gains energy from the absorber employing natural convection and moves upward due to the natural draft created by density difference. The hot air flows into the drying chamber through PVC pipe and drying of the paddy takes place. The photograph of the absorber plate is shown in Fig. 3.7. The schematic of the SAH is shown in Figs. 3.8 (a) and (b). Table 3.3 presents the materials and properties considered for designing the collector plate.

Table 3.3 Materials and properties used for the design of flat plate collectors

Particulars	**Materials/properties**
Absorber plate	Copper
Casing	Wood
Insulation	Glass wool
Thermal conductivity of the plate	385 W/m K
Density of the plate material	8960 kg/m^3
Absorptivity of the collector plate	0.95
Glass cover transmittance	0.897
Thermal conductivity of the insulation	0.044 W/m K
Location of the collector	26.1445° N, 91.7362° E

The solar air heaters have been developed with the help of the following correlations:

The solar air heaters have been designed to dry 24 kg of paddy per day under natural convection mode. To dry the required amount of paddy under the natural convection mode, sizing of the SAHs has been performed. The total area of the SAH has been estimated so that the designed SAH can produce the required amount of heat to remove the moisture of the paddy. Hence, the required area of the SAH for the moisture removal from the paddy can be estimated by using Eq. (3.6):

$$Q_{req.} = \eta_{SAH}(G\alpha_c\tau_g t)A_{SAH} \tag{3.6}$$

where $Q_{req.}$ is the energy required to dry paddy in kJ. The G, α, τ and t are the solar irradiance, absorptivity of collector, transmittance of the glass cover and drying time. The amount of heat required for the moisture removal is estimated with the help of Eq. (3.7):

$$Q_{req.} = m_p c_p (T_{pd} - T_{pi}) + m_w H_{wvap.} \tag{3.7}$$

where, m_p, c_p, T_{pi}, T_{pd}, m_w, H_{wvap} are the mass of paddy (kg), specific heat of paddy (kJ/kg k), initial paddy temperature, dried paddy temperature, mass of water removed (kg), and the latent heat of vaporization of water. From the literature survey, the average thermal efficiency of the SAH under natural convection mode is found as 15.31% (Sevik and Abuşka, 2020; Fakoor Pakdaman et al., 2011). Hence, the thermal efficiency is assumed as 15.31% for the design of a flat plate solar air heater in the present study. The collector area of the solar dryer has been evaluated with the help of Eqs. 3.6 and 3.7. The design summary of the solar air heater is shown in Table 3.4.

Table 3.4 Summary of the design of the solar air heater

Particulars	**Value**
Expected sunshine hour per day (h)	10
Average drying air temperature (ºC)	50
The amount of heat required to raise the temperature of paddy to 50 °C (MJ)	0.662
Amount of heat required to dry the 24 kg of paddy (MJ) (12 kg/batch)	11.352
The total amount of heat required per day (MJ)	12.014
Average solar radiation intensity (W/m^2)	646
The average thermal efficiency of the natural convection solar air heater (%)	15.31
The total area of the solar air heater (m^2)	3.99

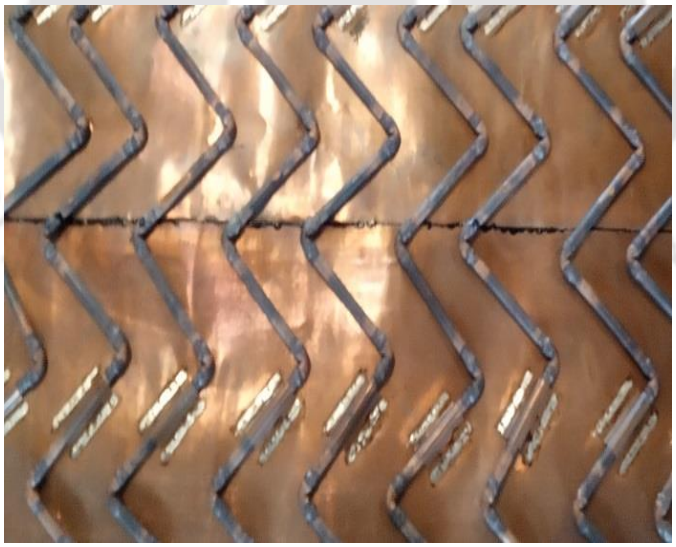

Fig. 3.7 Photograph of the collector with copper tubes

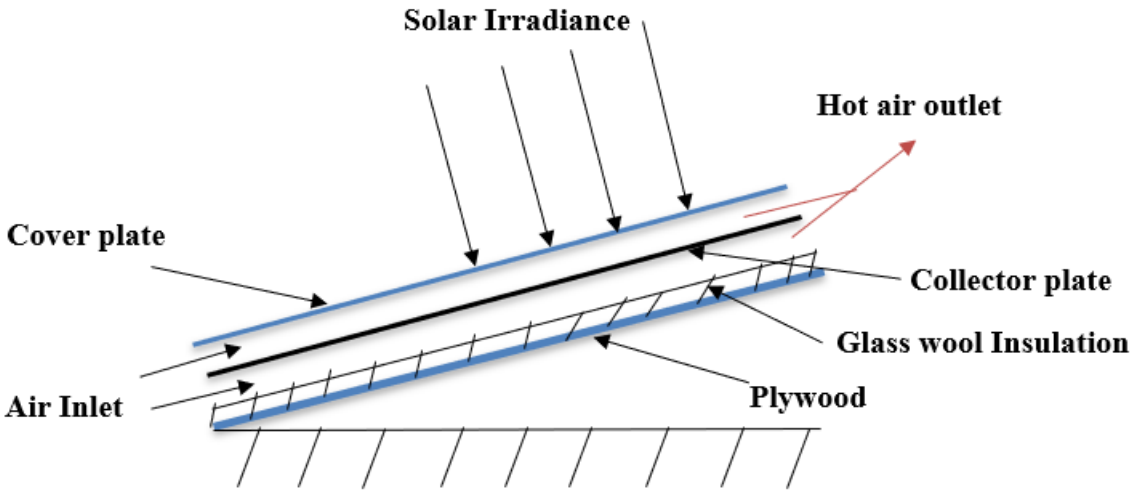

Fig. 3.8 (a) Schematic of the SAH.

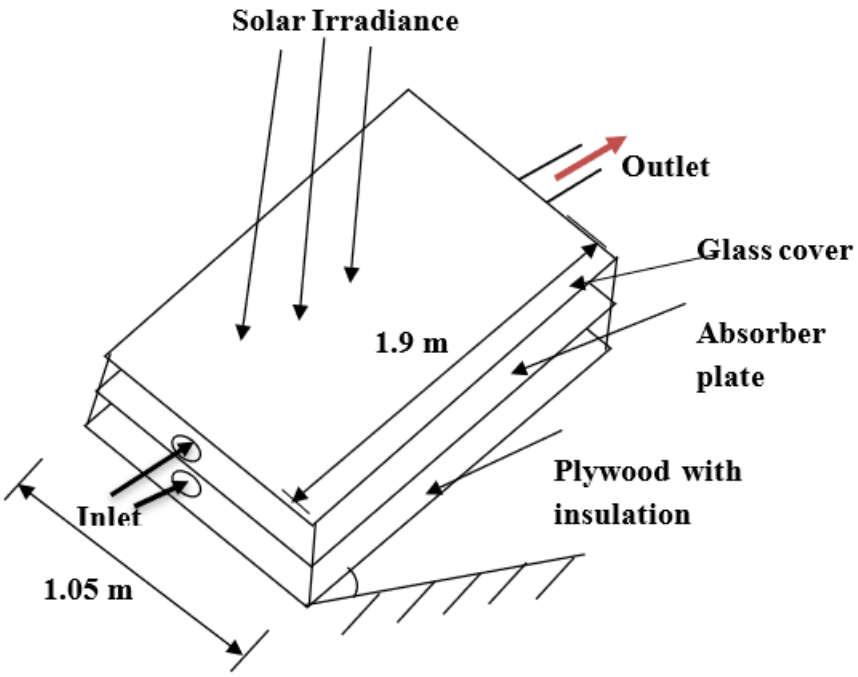

Fig. 3.8 (b) Schematic of the SAH

3.4.1.2 Drying chamber

The drying chamber is constructed just above the paraffin wax tray having dimension 1.25 m × 0.95 m × 0.30 m with a mild steel wire mesh drying tray of dimension 1.25 m × 0.95 m is placed in the drying chamber. Paddy is kept at the wire mesh tray and drying starts during the sunshine hours.

3.4.1.3 Natural draft

A natural draft is inbuilt in both the solar air heater with the collector adjusted to the south at the inclination of 26.14°. A glass cover is kept at the top to prevent the losses from the top and at the bottom, plywood is placed with insulation. Space above and below the flat plate absorber provides the natural draft.

3.4.1.4 Experimental procedure for the solar dryer

This experimental study has been performed to evaluate the performance of the developed dryer. The solar air heater is adjusted in such a way that it can utilize maximum solar energy received by the sun to heat the air. To maximize the absorption capacity of the collector, it is black painted. The temperature at various points in the solar dryer is measured by using J-type thermocouples, the solar radiation intensity is measured by using a pyranometer (Model MP-200) and for the measurement of paddy moisture, a moisture meter (Grain moisture tester PM-410) is used. The developed natural convection solar dryer works on the buoyancy principle. The black painted absorber absorbs the solar energy that falls on the solar collector plate. Due to absorbed solar energy, the absorber plate becomes hot and the air present in the space surrounding the absorber plate in the SAH gets heated up. Due to increase in air temperature, air density decreases and starts moving upward in the inclined SAH and higher density, ambient air enters into the SAH, this way a continuous airflow in the dryer system is developed. The SAHs and drying chamber are connected via PVC pipe hence the hot air moves to the drying chamber and dries the products. In the forced convection solar dryer, a fan of 33W rating is attached to each PVC pipe at the drying chamber inlet so that the hot air energy from the SAH could be utilized properly.

3.5 Mathematical equations used for the thin layer drying kinetics of paddy

The thermal performance of the dryer can be defined in terms of moisture removal rate, drying rate, and drying efficiency. The product moisture content (M_{db}) can be evaluated by using Eq. (3.8) (Karthikeyan and Murugavelh, 2018):

$$M_{db} = \frac{m_{pi} - m_{pd}}{m_{pd}} \tag{3.8}$$

where m_{pi} and m_{pd} are the initial and dried mass of paddy. The moisture ratio (MR) of the product can be determined by Eq. (3.9) (Chauhan et al., 2018b; Ekka et al., 2020):

$$MR = \frac{M_t - M_e}{M_i - M_e} \tag{3.9}$$

where M_t, M_i, and Me are the instantaneous, initial, and equilibrium moisture content respectively. The moisture ratio obtained from the experimental study is plotted with time and fitted to the eight mathematical models of the drying curve as shown in Table 3.5. These mathematical models are solved with the help of the Microsoft excel solver. The reduced chi-square (χ^2), root mean square error (RMSE), and the determination coefficient (R^2), and the constants were evaluated for all the models. The regression analysis was also performed for the selected model. From the literature, it was found that the lower values of (χ^2) and (RMSE) and the higher value of (R^2) gives the best fit of the drying curve (Rabha et al., 2017b). Hence the best drying model is selected on the above criteria. The values of R^2, RMSE, and χ^2 were calculated in the Eqs. (3.10–3.12) (Rabha et al., 2017b):

$$R^2 = 1 - \frac{\sum_{i=1}^{n}\left(MR_{pred.} - MR_{\exp.}\right)^2}{\sum_{i=1}^{n}\left(\overline{MR}_{pred.} - MR_{\exp.}\right)^2} \tag{3.10}$$

$$RMSE = \left(\frac{\sum_{i=1}^{n}\left(MR_{\exp.} - MR_{pred.}\right)^2}{N}\right)^{\frac{1}{2}} \tag{3.11}$$

$$\chi^2 = \frac{\sum_{i=1}^{n}\left(MR_{\exp.} - MR_{pred.}\right)^2}{N - n} \tag{3.12}$$

The drying rate (DR) can be defined as in Eq. (3.13):

$$DR = \frac{dM}{dt} = \frac{M_{t+\Delta t} - M_t}{\Delta t} \tag{3.13}$$

Mass of water removed and water evaporation rate from the product can be calculated by using Eqs. (3.14) and (3.15):

$$m_{water} = \frac{m_p(M_i - M_f)}{100 - M_f} \tag{3.14}$$

$$\dot{m} = \frac{m}{t} \tag{3.15}$$

where m_{water}, $M_{i,}$ and M_f are mass of water removed, moisture content at the initial time, and moisture at the end, respectively. Specific moisture evaporation rate (SMER) is the amount of moisture removed per kilowatt of energy supplied to the dryer system. It is a useful parameter to characterize the performance of the dryer. It is expressed as in Eq. (3.16) (Khanlari et al., 2020):

$$SMER = \frac{m_w}{IA} \tag{3.16}$$

Several mathematical models are developed by the researchers to determine the best fitting of the drying curve. In the present study, eight mathematical models are used for the best fitting of the drying curve. The mathematical models used for the drying kinetics analysis of paddy in the present study are shown in Table 3.5.

Table 3.5 Mathematical models used to describe the drying kinetics of paddy

Model No.	Model Name	Model	References
1	Newton	$MR = \exp(-kt)$	(Ayensu, 1997)
2	Page	$MR = \exp(-kt^n)$	(Diamante and Munro, 1993)
3	Modified page	$MR = \exp(-(kt)^n)$	(Panchariya et al., 2002)
4	Logarithmic	$MR = a\exp(-kt) + c$	(Toĝrul and Pehlivan, 2004)
5	Two-term	$MR = a\exp(-k_1 t) + b\exp(-k_2 t)$	(Yaldiz et al., 2001)
6	Wang and Singh	$MR = 1 + at + bt^2$	(Rabha et al., 2017b)
7	Diffusion approach	$MR = a\exp(-kt) + (1-a)\exp(-kbt)$	(Akpinar et al., 2003)
8	Verma	$MR = a\exp(-kt) + (1-a)\exp(-g t)$	(Akpinar, 2010b)

3.6 Summary

This chapter discusses the different parts of the experimental setup and procedure of the present study. This dryer is developed based on the principle of thin-layer drying. It is designed on the assumption that the volume of drying air is much higher than the grain volume (Belessiotis and Delyannis, 2011). The mathematical equations used for the performance evaluation of the dryer have also been discussed. Based on the experimental procedure described in this chapter experiments were performed. The results of the experiments are presented and discussed in the following chapters.

Chapter 4

Performance analysis of the developed dryer

4.1 Introduction

In this chapter, the drying characteristics of paddy on the biomass-operated dryer, solar dryer, and solar-biomass hybrid dryer have been analyzed. The drying parameters such as moisture content variations, drying rate, moisture evaporation rate, and specific moisture extraction rate have been reported. The drying curves obtained in the present study are fitted with eight mathematical models to obtain the best fitting curve. The values of model constants, root mean square error, chi-square, and the determination coefficients are also reported in this chapter.

4.2 Drying characteristics of paddy in the biomass operated dryer

4.2.1 Drying kinetics of paddy

In this study, the drying characteristics of paddy has been analyzed in the biomass-operated grain dryer. This study has been performed for three different cases viz. (i) without sensible thermal storage medium in the rectangular chamber, (ii) with sensible thermal storage medium (pebbles) in the chamber, and (iii) with sensible thermal storage medium and exhaust valve is closed at the end of biomass burning. The latent heat thermal storage medium (paraffin wax) was present in all three cases of study. Three sets of experiments were performed for each case of studies and average values of the results are presented. In all the three cases, biomass was burnt at the rate of 2.5 kg/h for three hours for drying process. In each set of experiment inventory considered for drying is 12 kg. The paddy has been loaded on the drying tray after 1.5 hours of initiation of biomass burning. The input parameters of the study are presented in Table 4.1. The moisture content and the drying rate variations of paddy with time for the case-I, case-II, and case-III are shown in Figs. 4.1 (a), (b) and (c), respectively. In this study, the average initial moisture content of the paddy is found to be 33 %. The paddy was loaded on the drying tray after 1.5 hours of initiation of biomass burning. The drying has been performed for 7.5 hours in all three different cases. From Fig. 4.1 (a), it was observed that the moisture content of paddy decreases sharply between 1 and 2 hours and a sharp increase in the drying rate was observed during this period.

Table 4.1 Input parameters for the biomass-based dryer

Different cases	Initial moisture content (%)	Biomass (kg)	Drying time (h)	Inventory (kg)
Case-I (without sensible thermal storage)	33.1	7.5	7.5	12
Case-II (with sensible thermal storage)	33.2	7.5	7.5	12
Case-III (with sensible thermal storage and exhaust valve closed at the end of biomass burning)	33	7.5	7.5	12

It indicates that the paddy achieved required amount of energy for the moisture removal in 1 hour and thereafter the moisture removes sharply. During the study, a relatively lesser reduction in moisture content and lower values of drying rate was observed after 2 hours, that is because once the surface moisture removed, the internal moisture evaporates by the diffusion process. In this study, the moisture content of paddy was reduced from 33.1% to 16.9% in 7.5 hours and the drying rate varied from 0.004–0.062 kg/kg h with an average of 0.0216 kg/kg h. From the results, it can be seen that the final moisture content of the paddy achieved in the study is higher than the equilibrium moisture content (EMC). Figure 4.1 (b) shows the moisture content and drying rate variations of paddy for case-II. During the study, similar variations of the moisture content and the drying rate were observed as shown in Fig. 4.1 (a). In this study, the moisture content of paddy was reduced from 33.2% to 16.1% and the drying rate varied from 0.008–0.064 kg/kg h with an average of 0.0228 kg/kg h. A relatively lower value of final moisture content and the higher average value of the drying rate of paddy was observed in this case as compared to case-I. However, the paddy did not reach the EMC. Figure 4.1 (c) shows the moisture content and drying rate variations of paddy for case-III. During this study, the moisture content of paddy reduced from 33% to 13.2% in 7.5 hours, while the EMC of paddy was achieved in about 5.5 hours. A similar trend of moisture content variations for paddy drying was reported by (Utari et al., 2022; Wincy et al., 2022). The values of drying rate of paddy increases initially, reaches its maximum value and then decreases. The values of the drying rate were ranged from 0.002–0.056 kg/kg h with an average of 0.032 kg/kg h. A similar trend of drying rate variations for paddy drying was reported by (Sitorus et al., 2021). In this study, a relatively higher average value of the drying rate was

obtained as compared to case-I and case-II. From the results, it can be seen that the EMC of paddy was only achieved in case-III. Hence, case-III can be considered as best for paddy drying process.

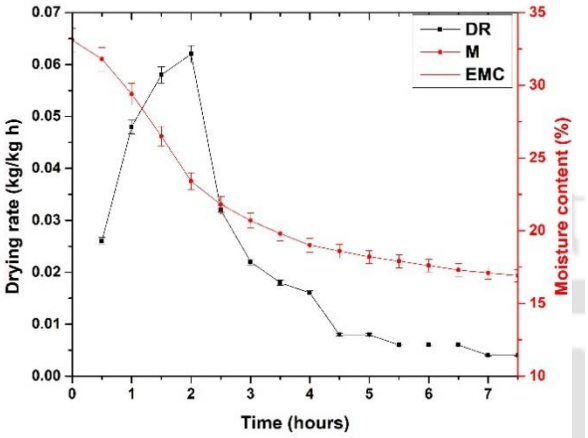

Fig. 4.1 (a) Variations of moisture content and drying rate of paddy for case-I

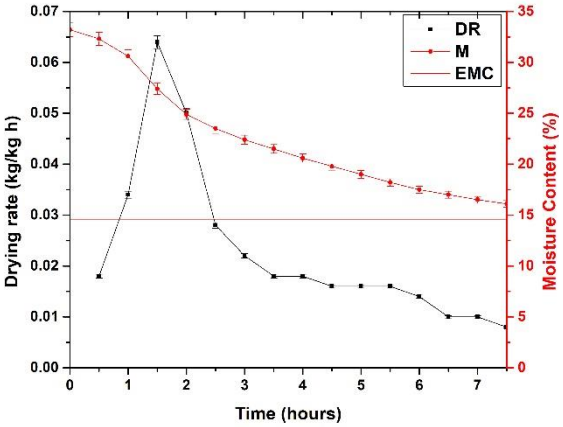

Fig. 4.1 (b) Variations of moisture content and drying rate of paddy for case-II

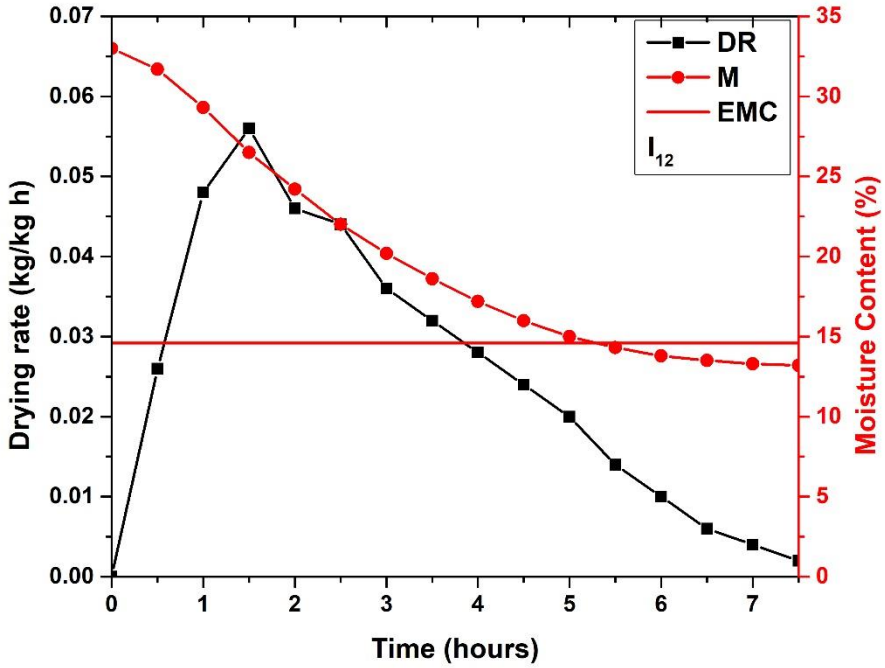

Fig. 4.1 (c) Variations of moisture content and drying rate of paddy for case-III

Figure 4.2 shows the moisture evaporation rate of paddy during the drying process for all three different cases of study. From the results, it can be seen that the moisture evaporation rate of the paddy reaches the maximum value between 1–2 hours from the loading in all three cases of study. The average values of the moisture evaporation rate were obtained as 5.7 g/min, 6 g/min and 6.81 g/min for the case-I, case-II, and case-III, respectively. From the results, it was found that the moisture evaporation rate increases initially as the surface moisture removal takes place, once the surface moisture removed its value decreases with time. Because the internal moisture removal takes place by the diffusion process and required relatively high energy. During the study, a relatively higher values of the moisture evaporation rate were obtained in the case-III.

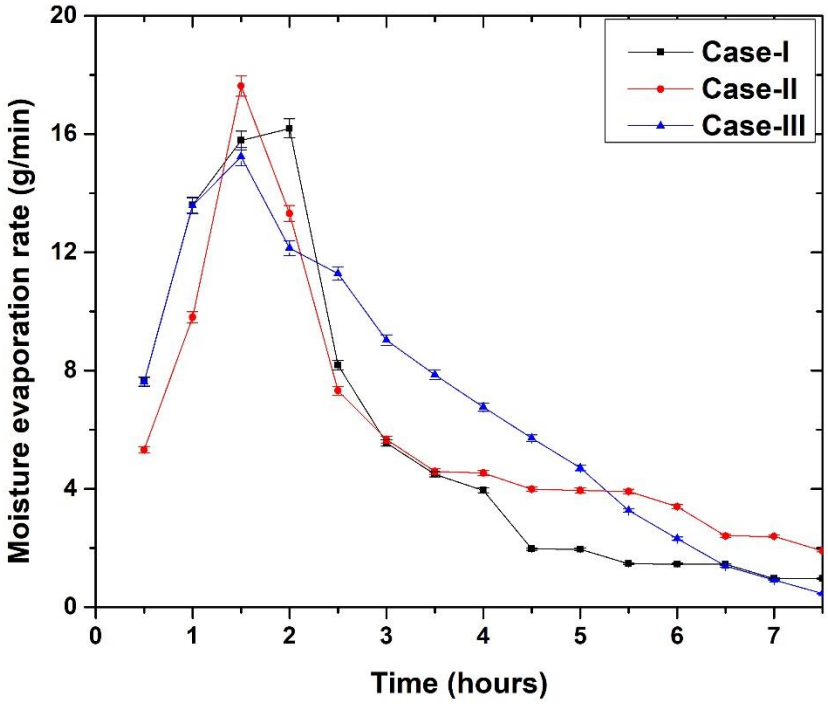

Fig. 4.2 Variations of moisture evaporation rate with time for the inventory of 12 kg

4.2.2 Mathematical modeling

The experimental and predicted moisture ratio of paddy for case-III (sensible energy storage medium in the rectangular chamber and exhaust valve is closed at the end of biomass burning) is shown in Fig. 4.3. From the figure, it was observed that the experimental and predicted moisture ratio varies with similar trends. From Fig. 4.1 (c), it can be seen that the paddy achieved the

equilibrium moisture content in about 5.5 hours. Hence, the experimental and predicted moisture ratio in Fig. 4.3 is presented for 5.5 hours of the drying process. The linear regression analysis using the microsoft excel solver has been performed to find the best fitting of the curve. The fitness of the model's was considered on the basis of lowest values of χ^2 and RMSE, and the highest value of R^2 (Rabha et al., 2017b). In this study, the Wang and Singh model was best fitted to the paddy drying curve. The values of χ^2, RMSE, and R^2 in the Wang and Singh model was obtained as 0.001079, 0.032856, and 0.99964, respectively. Hence, the Wang and Singh model can be assumed to represent the drying kinetics of paddy in the biomass-operated dryer in the range of obtained experimental moisture ratio. Table 4.2 presents the constants and coefficients for the drying models. The values of a and b for the Wang and Singh model was obtained as -0.28506 and 0.018613. The comparison of the experimental and the predicted moisture ratios is shown in Fig. 4.4. From the curve, it was observed that the curve fitting is relatively better for the lower moisture ratio. The drying model for paddy drying can be expressed as in Eq. (4.1):

$$MR = 1 + at + bt^2 \tag{4.1}$$

Table 4.2 Modeling of moisture ratio for thin-layer drying of paddy in the biomass-operated dryer

Model Name	Model constants	R^2	RMSE	χ^2
Newton	k= 0.51493	0.9522	0.11446	0.0131
Diffusion approach	a= 1 k= 0.51493 b= 1	0.9522	0.11446	0.0131
Verma	a= 40.2419 k= 1.24143 g= 1.3803	0.97665	0.46253	0.21393
Two-term	a= 4.3097 k_1= 1.068 b= 4.3097 k_2= 1.068	0.97853	2.6	6.6726
Page	k= 0.0909 n=2.2327	0.9828	0.08255	0.006815
Modified Page	k= 0.34179 n= 2.2327	0.9828	0.08255	0.006815
Logarithmic	a= 1.962 k= 0.462 c= -0.15896	0.99938	0.028678	0.08224
Wang and Singh	**a=-0.28506** **b= 0.0186**	**0.99964**	**0.032856**	**0.001079**

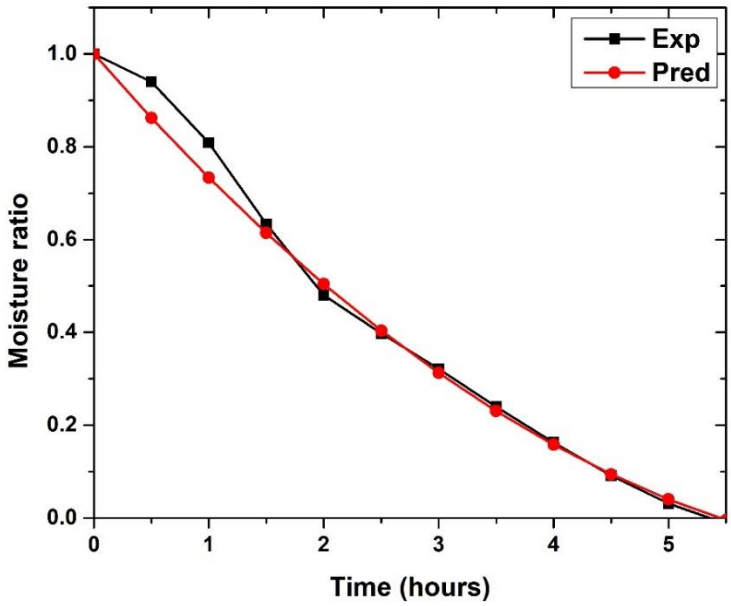

Fig. 4.3 Variations of experimental and predicted moisture ratios (Wang and Singh model) with time

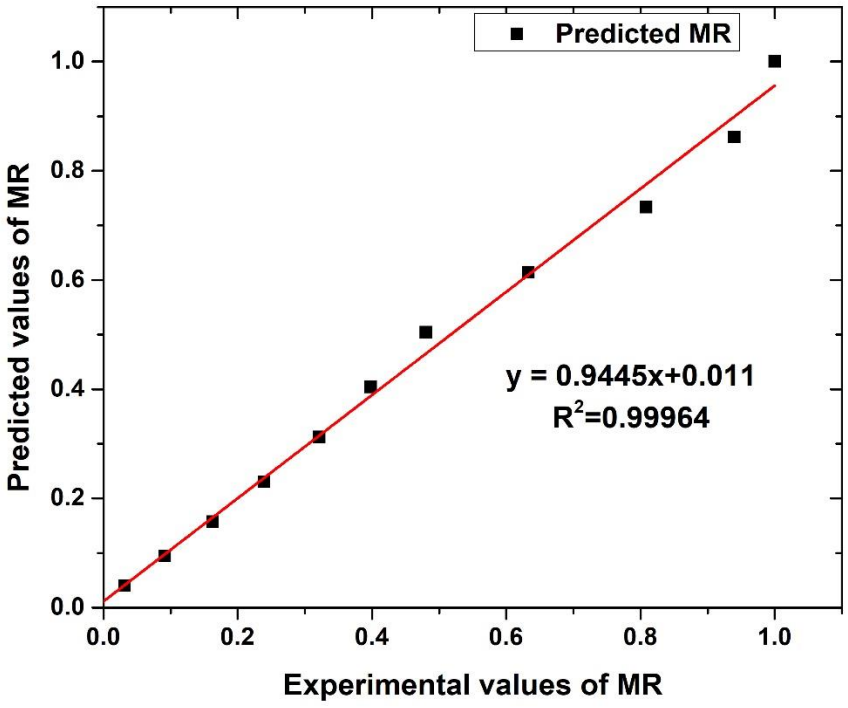

Fig. 4.4 Comparison of the predicted and experimental moisture ratios

4.2.3 Performance analysis of the dryer for different inventory

From the study in the above section, it was observed that the case-III (sensible energy storage medium in the chamber and exhaust valve is closed at the end of biomass burning) is the best drying condition for the modified biomass-operated dryer. Hence, the performance of the dryer was optimized with varying quantities of the product (paddy) for the case-III. Figure 4.5 shows the moisture content variations of paddy in the drying process. In this study, four different inventories 8 kg, 10 kg, 12 kg, and 14 kg having moisture content of 33.5%, 33.1%, 33%, and 34% were successfully dried. From the drying curve, it has been found that about 4.5 hours, 5 hours, 5.5 hours and 7.25 hours is required to achieve EMC for the inventories 8 kg, 10 kg, 12 kg, and 14 kg, respectively. From the results, it was found that the 10 kg and 12 kg inventories took 0.5 hours and 1 hour more than that of 8 kg while 14 kg inventory took around 2.75 hours more than that of 8 kg inventory. However, the capacity of the dryer is higher for the drying of 14 kg inventory per batch but it required relatively more time. Hence, for the continuous drying of the products, 12 kg inventory is considered optimum for the designed biomass operated dryer.

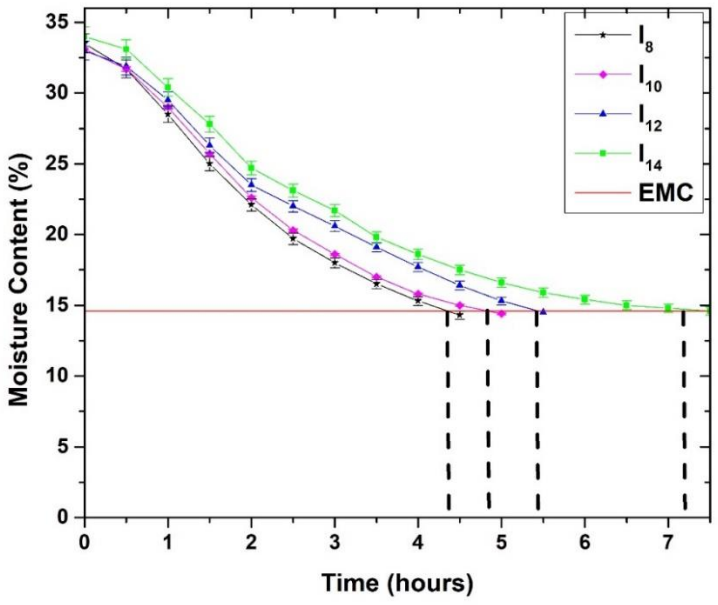

Fig. 4.5 Variations in the moisture content of paddy for different inventories

4.3 Drying characteristics of paddy in the natural convection solar dryer

4.3.1 Performance analysis of the dryer for different inventory

In this study, the experiments were performed for three different inventories viz. 10 kg, 12 kg, and 14 kg, and the drying characteristics were analyzed. The experiments were started at 9 AM for all three inventories. Figure 4.6 (a) shows the variations in the solar irradiance and the temperature at the inlet of the drying chamber with time for 10 kg inventory. During the study, the solar irradiance was varying from 762–967 W/m^2 and the temperature at the inlet of the drying chamber was ranged from 67.4–75.3 °C. From the results, it was observed that the temperature at the inlet of the drying chamber follows the similar trends with solar irradiance. This is because, the energy received by the hot air in the solar air heater varies with the solar irradiance. As the values of solar irradiance changes, the temperature achieved by the hot air in the solar air heater also change hence the temperature at the drying chamber varies accordingly. Figure 4.6 (b) shows the moisture content variations of paddy for 10 kg inventory. During the study, paddy having moisture of 33.4% was dried to the desired level of moisture content in about 4.5 hours.

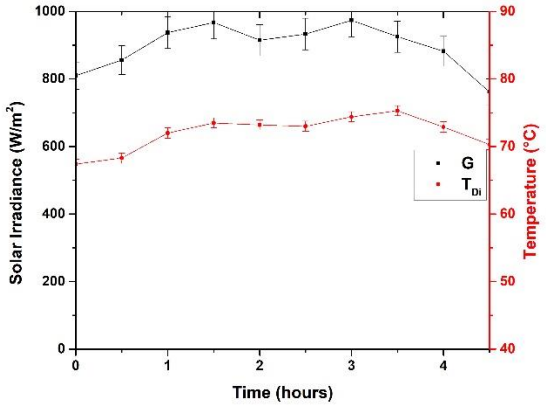

Fig. 4.6 (a) Variations in the solar irradiance and drying chamber inlet temperature

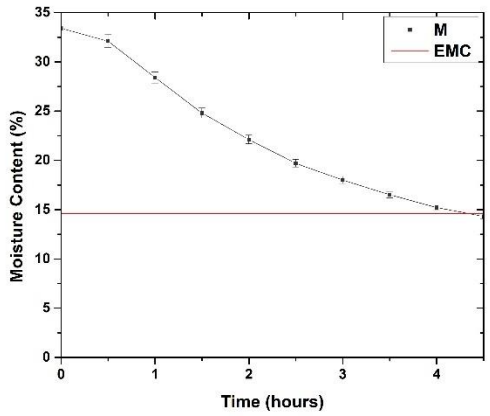

Fig. 4.6 (b) Variations in the moisture content for 10 kg inventory

The solar irradiance and the hot air temperature at the inlet of the drying chamber for the 12 kg inventory is shown in Fig. 4.7 (a). In this study, the solar irradiance was varied in the range of 745–970 W/m^2 and the air temperature were ranged from 64.3–72.8 °C. During the study, the strong dependency of hot air temperature with solar irradiance was observed. The temperature of hot air was varied with solar irradiance. Figure 4.7 (b) shows the moisture content variations of paddy for 12 kg inventory. In this study, paddy having an initial moisture content of 34.1% was dried to desired level of moisture content in 5 hours.

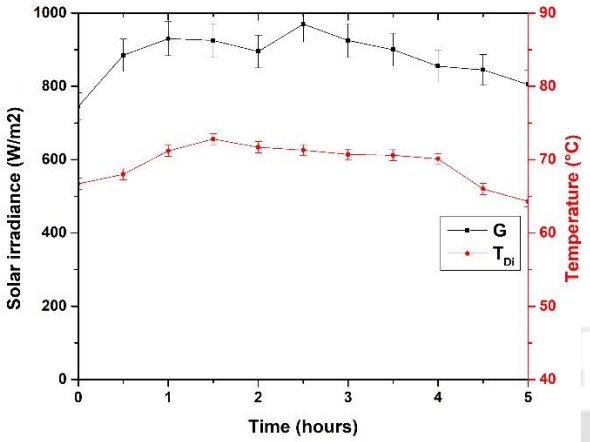

Fig. 4.7 (a) Variations in the solar irradiance and drying chamber inlet temperature

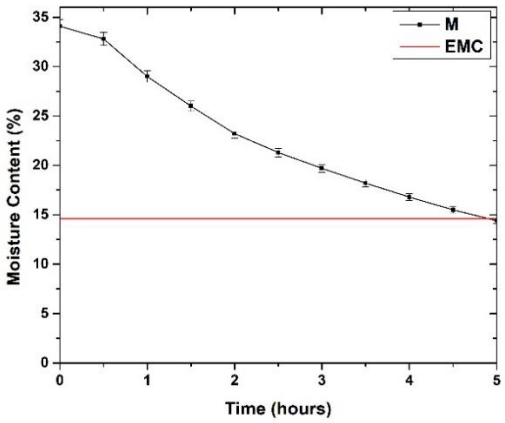

Fig. 4.7 (b) Variations in the moisture content of 12 kg inventory

The solar irradiance and hot air temperature at the inlet of the drying chamber for the 14 kg inventory is shown in Fig. 4.8 (a). During the study, the solar irradiance was varied in the range of 690–962 W/m^2 and the hot air temperature ranged from 56.8–73.8 °C, respectively. From the results, similarity in variations of the hot air temperature and the solar irradiance with time was observed. The value of the temperature was higher for the higher value solar irradiance and lower for the low value of solar irradiance. Figure 4.8 (b) shows the moisture content variations of paddy for 14 kg inventory.

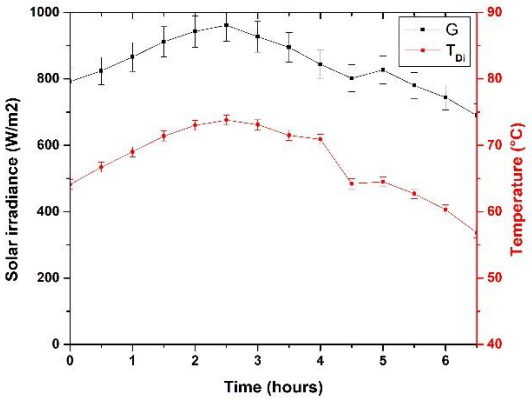

Fig. 4.8 (a) Variations in the solar irradiance and drying chamber inlet temperature

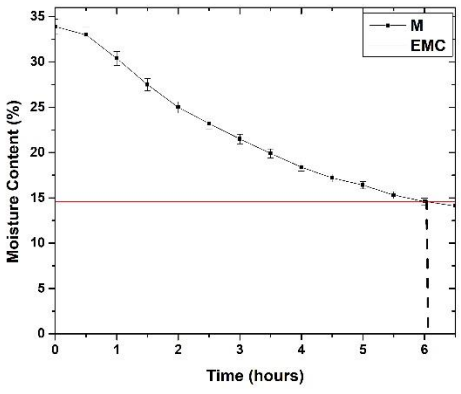

Fig. 4.8 (b) Variations in the moisture content of 14 kg inventory

During the study, paddy having initial moisture content of 33.9% was dried to the equilibrium moisture content (EMC) in about 6 hours. From the results, it was found that the 12 kg inventory took only 0.5 hour more than that of 10 kg while 14 kg inventory took around 1.5 hours more than that of 10 kg inventory. From the study, it can be seen that the 10 kg and 12 kg inventory required 4.5 hours and 5 hours to achieve EMC and as per the Indian weather conditions the solar dryer can be operated for 10 hours per day hence these inventories can be dried two batches per day. However, the capacity of the dryer is higher for the drying of 12 kg inventory per batch hence this inventory can be considered as optimum for the natural convection solar dryer.

4.3.2 Drying kinetics of paddy

From the results, it was evident that the natural convection solar dryer is suitable for drying of 12 kg inventory. Hence, in this study, the drying kinetics of 12 kg inventory is analyzed. For the drying process, the inventory was loaded on the drying tray at 9 AM. Figure 4.9 shows the variations in solar radiation intensity and the temperature of air at the inlet and outlet of the drying chamber for 12 kg inventory. The drying chamber inlet and outlet air temperature were ranged from 64–72.9 °C and 36.5–44.9 °C, respectively. During the drying operation, solar irradiance was varied from 745–970 W/m^2 with a mean of 880 W/m^2. From the results, it has been found that the drying chamber inlet temperature varies with solar irradiance and the drying chamber outlet temperature increases with drying time. The increase in outlet temperature may be due to the energy utilized in the drying chamber decreases with time.

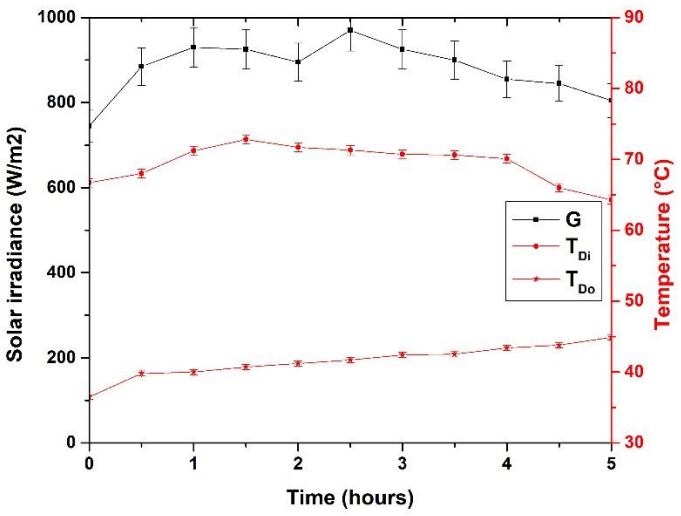

Fig. 4.9 Variations in solar irradiance and the drying chamber inlet and outlet temperature

Figure 4.10 shows the variations in the moisture content and drying rate of paddy for 12 kg inventory with time. In the present study, 12 kg of paddy having a moisture content of 34.1% was successfully dried to the desired level of moisture content. From the Figure, it was observed that the drying process takes 5 hours to reach the desired level of moisture content. From the results, it can be seen that the slope of the drying curve decreases with time. This indicates that the water evaporation rate from the inventory decreases with time. A similar trend of the curve for paddy drying was reported (Zare and Chen, 2009) and a similar decreasing slope of the drying curve was also reported (Bhardwaj et al., 2017) for the Valeriana jatamansi herb, (El-Sebaii and Shalaby, 2012) for mint drying process. From the drying rate curve, it was observed that at the start of the drying process, the drying rate of paddy increases sharply with time and after that, it decreases. During the study, a higher value of drying rate was observed for the high moisture content of paddy. The values of the drying rate were ranged from 0.022–0.076 (kg/kg h) with a mean of 0.0394 (kg/kg h). A similar trend of drying rate was reported by (Sitorus et al., 2021) for paddy drying and (Karthikeyan and Murugavelh, 2018) for turmeric drying process. Figure 4.11 shows the variations in the moisture evaporation rate and the specific moisture extraction rate of paddy with time. From the result, it was found that the moisture evaporation rate increases until 1 hour from the initiation of the drying process, and after that, it decreases. Its value was varied in the range of 4–20.99 g/min with an average of 9.345 g/min.

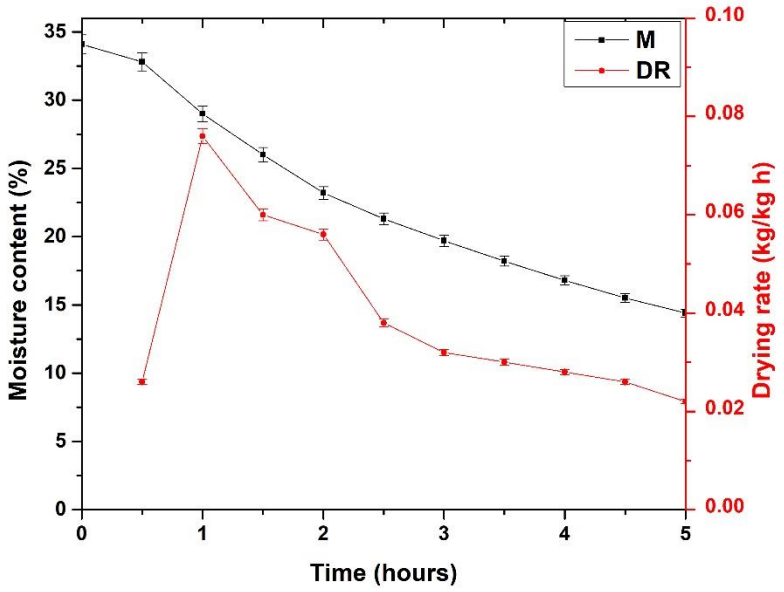

Fig. 4.10 Variations in the moisture content and drying rate of paddy with time

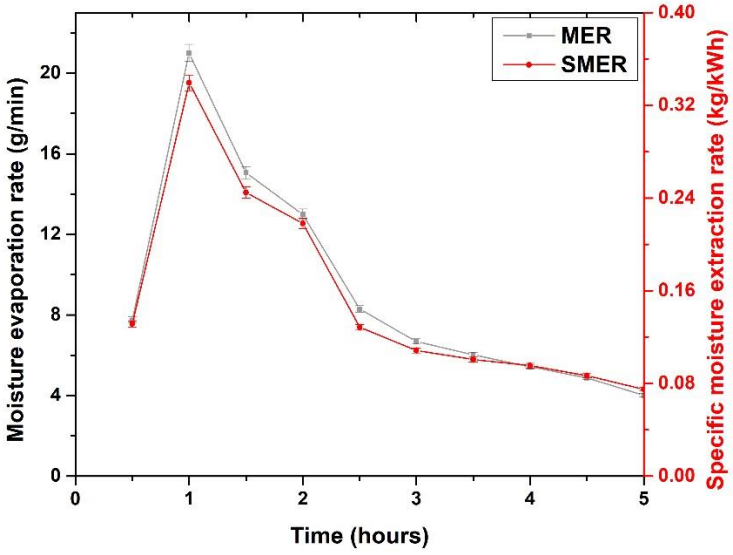

Fig. 4.11 Variations in the moisture evaporation rate and specific moisture extraction rate

From the figure, it can be seen that the specific moisture extraction rate increases at the initial period of the drying reaches maximum and after that decreases with time. It reaches its peak value at about 1 hour after the loading of paddy. Its value was ranged from 0.074–0.339 kg/kWh with a mean of 0.152 kg/kWh. During the study, a similar trend of variations was observed for the drying rate, moisture evaporation rate, and specific moisture extraction rate.

4.3.3 Mathematical modeling

The variations in the predicted and the experimental moisture ratios for the paddy drying process are shown in Fig. 4.12. The figure indicates that both the predicted and experimental moisture ratio decreases with time and the decreasing trend is almost similar. The value of the experimental moisture ratio was decreased from 1 to 0.047847 and the predicted moisture ratio values decreased from 1 to 0.07388. In this study, the Verma model was found to be best fit for the paddy drying process. The values of χ^2, RMSE, and R^2 were obtained in the selected model as 0.00065, 0.021752, and 0.995329, respectively. Hence, the Verma model can be assumed to represent the drying characteristics of paddy in the natural convection solar dryer. Figure 5.13 shows the comparison of the predicted and experimental MR by the most fitted drying model for

the natural convection solar dryer. Table 4.3 presents the constants and coefficients for the drying condition. The drying model for the paddy drying process can be written as in Eq. (4.2):

$$MR = 1.339\exp(-0.5295t) + (1-1.339)\exp(-2.815363\,t) \quad (4.2)$$

Table 4.3 Modeling of moisture ratio for thin-layer drying of paddy for the natural convection solar dryer

Model Name	Model constants	R^2	RMSE	χ^2
Newton	k= 0.39923	0.96269	0.06148	0.003780
Page	k= 0.27386 n=1.399641	0.99452	0.02356	0.00067
Modified Page	k= 0.3964 n= 1.39963	0.99452	0.02356	0.00067
Logarithmic	a= 1.38693 k= 0.25833 c= -0.3373	0.99124	0.02978	0.00122
Two-term	a= 0.54576 k_1= 0.43768 b= 0.54576 k_2= 0.43768	0.97567	0.04966	0.00387
Wang and Singh	a= -0.29564 b= 0.02106	0.98930	0.03292	0.00132
Diffusion approach	a= 1 k= 0.39923 b= 1	0.96269	0.06148	0.00519
Verma	**a= 1.33903** **k= 0.52951** **g= 2.81536**	**0.99533**	**0.02175**	**0.00065**

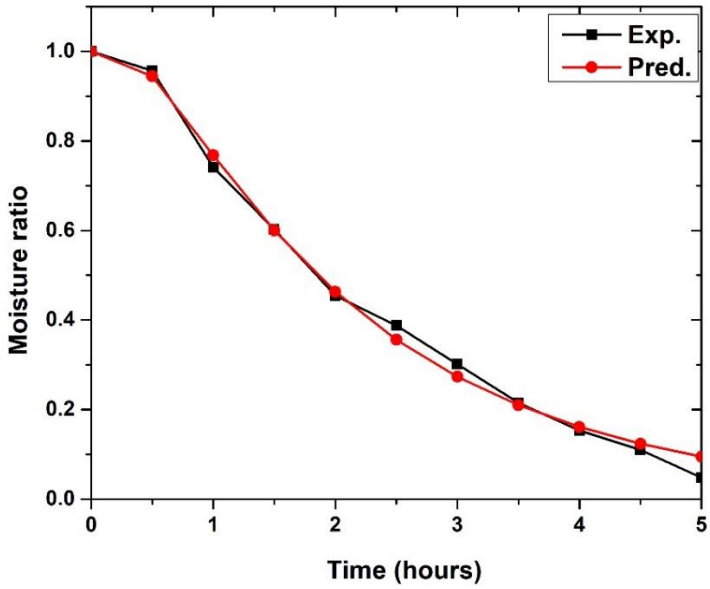

Fig. 4.12 Variations of experimental moisture ratio and predicted moisture ratio obtained in the Verma model

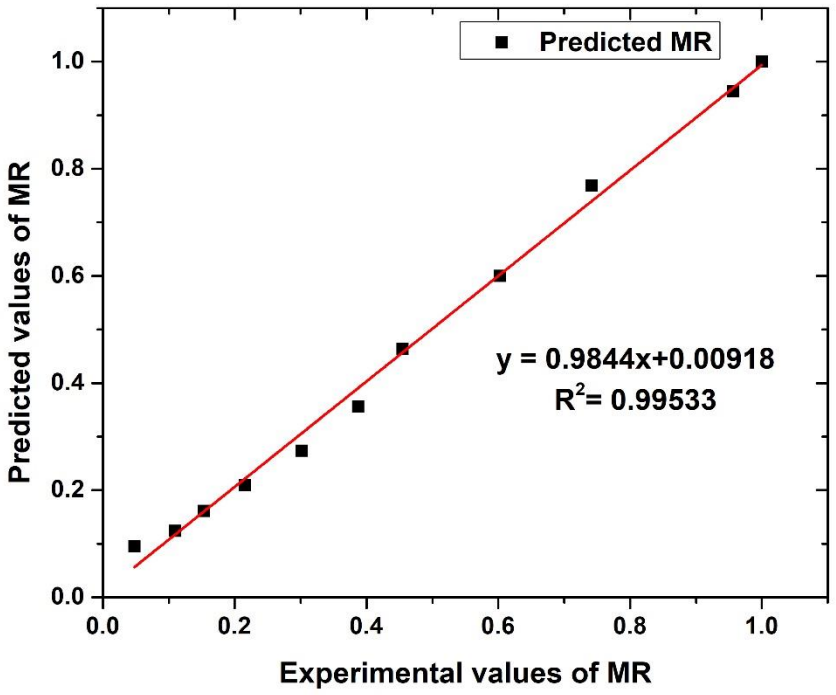

Fig. 4.13 Comparison of the predicted and experimental MR

4.4 Drying characteristics of paddy in the forced convection dryer

4.4.1 Performance analysis of the dryer for different inventory

In this study, the experiments were performed for 12 kg, 16 kg, and 20 kg inventory, and the drying behaviors of paddy were analyzed. The experiments were started at 9 AM. Figure 4.14 (a) shows the variations in the solar irradiance and the temperature at inlet of the drying chamber for 12 kg inventory. In the study, the solar irradiance was varied in the range of 693–970 W/m^2 and the drying chamber inlet temperature ranged from 56.7–78.2 °C. From the study, it was found that as the solar irradiance increases, the air temperature also increases. This is because the energy absorbed by the collector depends on the solar irradiance. The moisture content variations of paddy for 12 kg inventory is shown in Fig. 4.14 (b). In this study, paddy having initial moisture content of 34.2% was dried to the EMC in about 3 hours 45 minutes.

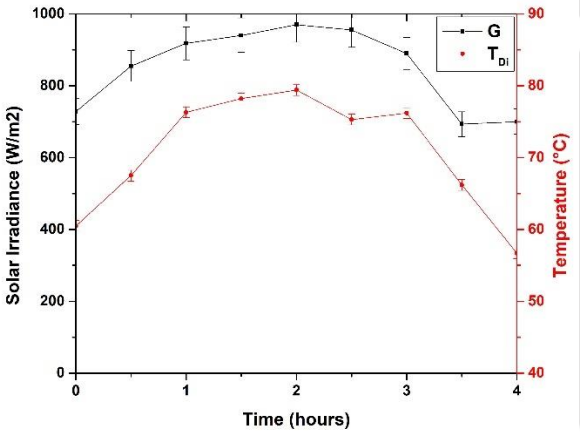

Fig. 4.14 (a) Variations in the solar irradiance and drying chamber inlet temperature

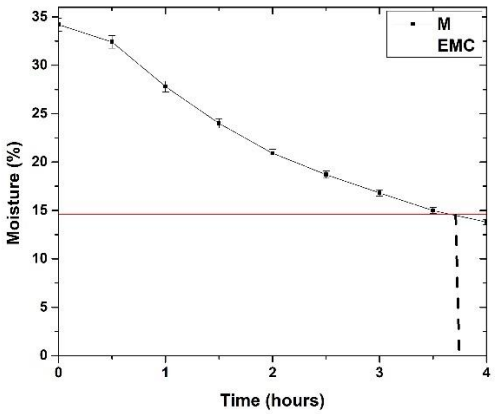

Fig. 4.14 (b) Variations in the moisture content of paddy with time

Figure 4.15 (a) shows the variations of solar irradiance and drying chamber inlet temperature during the drying of 16 kg inventory. During the study, the solar irradiance was found in the range of 676–924 W/m^2 and the drying chamber inlet temperature ranged from 64–75.2 °C. In this study, the air temperature shows a strong dependency on solar irradiance. Relatively higher values of temperature were observed for the high solar irradiance. The moisture content variations of paddy for 16 kg inventory is shown in Fig. 4.15 (b). The paddy having initial moisture content of 34.1% was dried to the EMC in about 4 hours 50 minutes. Figure 4.16 (a) shows the solar irradiance and

the drying chamber inlet temperature for 20 kg inventory. The solar irradiance was obtained in the range of 568–965 W/m^2 and the drying chamber inlet temperature ranged from 56–75.7 °C. From the results, a strong dependency of air temperature on solar irradiance were observed. The moisture content variations of paddy for 20 kg inventory is shown in Fig. 4.16 (b). In the study, paddy having moisture content of 34.6% was successfully dried to the equilibrium moisture content (EMC) in 6 hours 50 minutes.

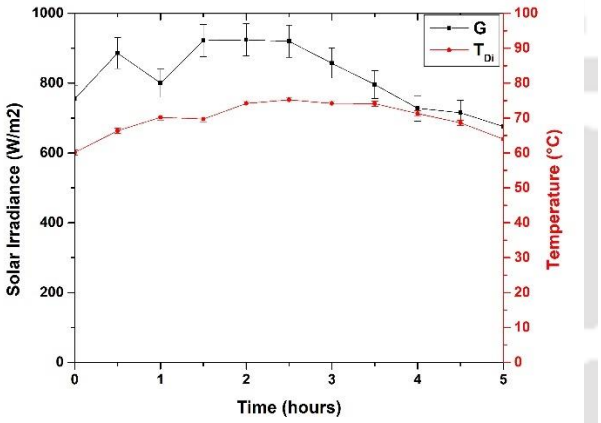

Fig. 4.15 (a) Variations in solar irradiance and drying chamber inlet temperature

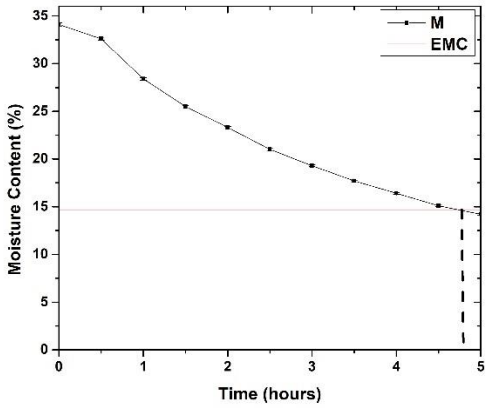

Fig. 4.15 (b) Variations in the moisture content of paddy with drying time

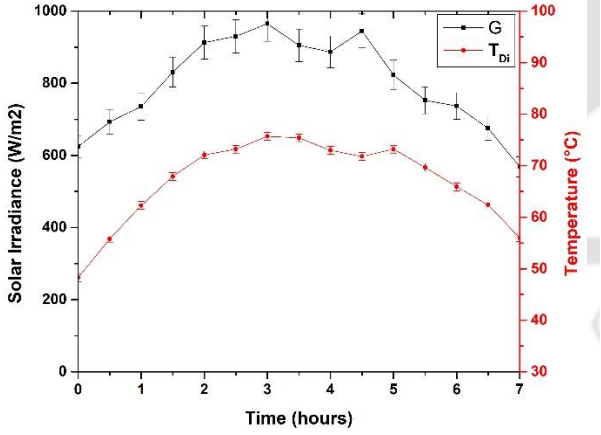

Fig. 4.16 (a) Variations in solar irradiance and drying chamber inlet temperature

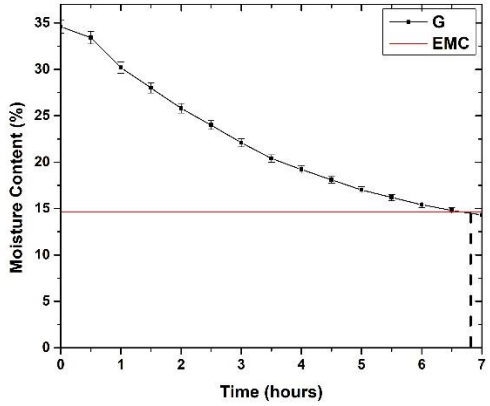

Fig. 4.16 (b) Variations in the moisture content of paddy with drying time

From the results, it was found that 16 kg paddy took 4 hours 50 minutes which is about 1 hour more than that of time required in 12 kg inventory drying while 20 kg inventory took about 3 hours more than that of 12 kg inventory. From the study, it can be seen that the 12 kg and 16 kg inventory required 3 hours 45 minutes and 4 hours 50 minutes to achieve EMC and as per the Indian weather conditions the solar dryer can be operated for 10 hours per day hence these inventories can be dried in two batches per day. However, the capacity of the dryer will be higher for the drying of 16 kg inventory per batch hence this inventory can be considered as optimum for the developed solar dryer under forced convection mode.

4.4.2 Drying kinetics of paddy

From the above study, it was found that the 16 kg inventory is suitable for the forced convection solar dryer. Hence, in the present study, the drying characteristics of 16 kg paddy is analyzed. This study has been performed from 9 AM to 2 PM. Figure 4.17 shows the air temperature at the inlet of SAH, inside the SAH, the outlet of SAH, collector temperature, and the temperature at the inlet and outlet of the drying chamber. The SAH inlet air temperature was varied from 32.6–37.1 °C with a mean of 35.47 °C and the temperature of hot air in the SAH ranged from 71.5–97.2 °C. The temperature of hot air at the SAH outlet was ranged from 63.5–81.2 °C with a mean of 74.5 °C. The temperature of the collector was varied in the range of 72–106.2 °C. The drying chamber inlet and outlet air temperature ranged from 60.1–75.2 °C and 37–45.3 °C, respectively. The moisture content and drying rate of the paddy is shown in Fig. 4.18. In the present study, paddy having the moisture content of 34.1% was successfully dried. From the results, it can be seen that the desired level of moisture content was achieved in 4 hours 50 minutes. From the moisture content curve, it was observed that the slope of the curve is lesser at the start of the drying process, that is because hot air energy is utilized to heat the grains. Once the grain achieved its desired temperature, moisture evaporation increases. When all the surface moisture evaporates, the slope of the curve decreases because the internal moisture removal takes place by the diffusion process. A similar trend of moisture content curve for paddy drying was reported (Zare and Chen, 2009). A similar decreasing slope of the drying curve was also reported (Bhardwaj et al., 2017) for the Valeriana jatamansi herb. From the drying rate curve, it was observed that the drying rate of paddy increases initially after that, its value decreases with time. In this study, higher values of the drying rate were obtained for the high moisture content of paddy. Its value was ranged from 0.018–0.084 (kg/kg h)

with a mean of 0.0398 (kg/kg h). A similar trend of drying rate was reported (Karthikeyan and Murugavelh, 2018) for turmeric drying.

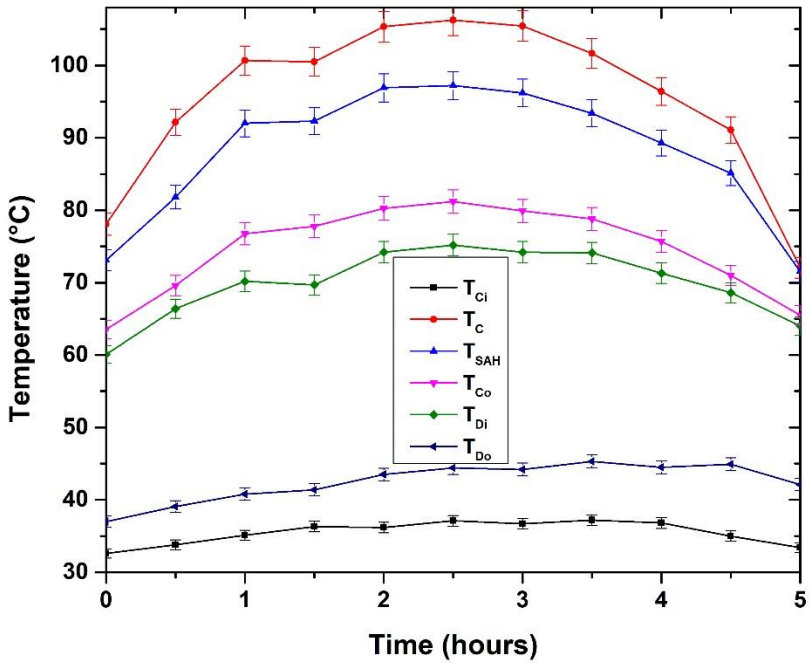

Fig. 4.17 Variations in temperature at various points in the dryer

Figure 4.19 shows the variations in moisture evaporation rate and specific moisture extraction rate with time. In this study, the maximum value of the moisture evaporation rate was obtained after 1 hour of the loading. Its value varied in the range of 4.34–30.58 g/min with an average of 12.37 g/min. From the figure, it can be seen that the SMER increases at the start of the drying process, reaches maximum and after that decreases as the drying process progress. It achieves maximum value after 1 hour of the loading of inventory. Its values were ranged from 0.096–0.579 kg/kWh with a mean of 0.22 kg/kWh.

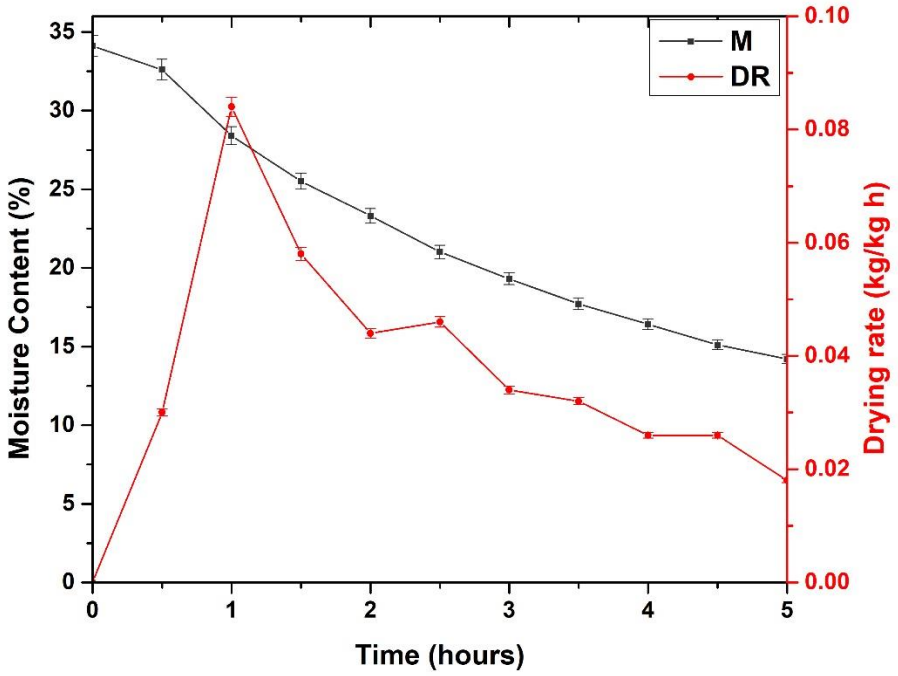

Fig. 4.18 Variations in the moisture content and drying rate of paddy with time

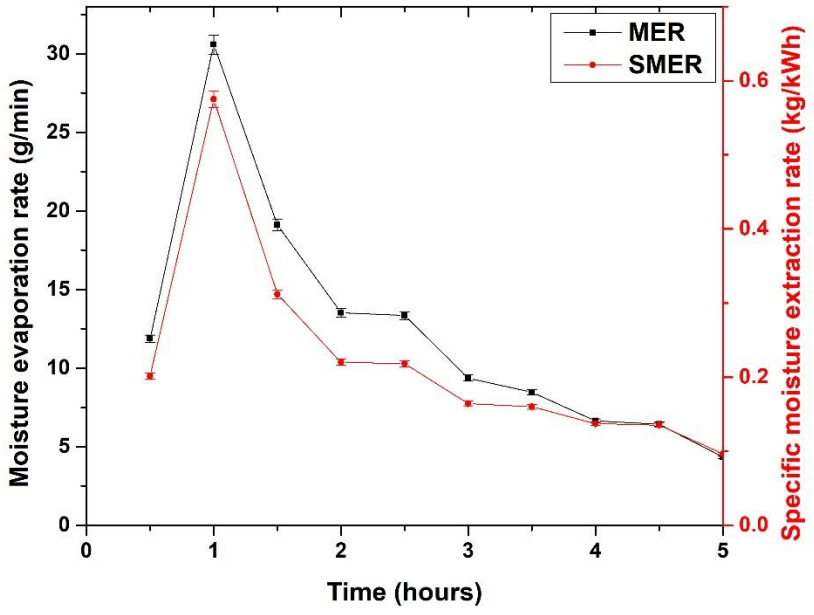

Fig. 4.19 Variations of moisture evaporation rate and specific moisture extraction rate

4.4.3 Mathematical modeling

The variations in predicted and experimental moisture ratios for the paddy drying process are shown in Fig. 4.20. The figure indicates that both predicted and experimental moisture ratio decreases with time and the decreasing trend is almost similar. The value of the experimental moisture ratio decreases from 1 to 0.033 and the predicted moisture ratio values decreased from 1 to 0.065. In this study, the Page model and the modified page model were found to be the best fit for the paddy drying curve. The values of χ^2, RMSE, and R^2 were achieved in this model as 0.000363739, 0.019071946, and 0.996443501, respectively. Hence, these models can be assumed to represent the drying kinetics of paddy in the designed forced convection solar dryer. So, the drying model for the paddy drying process can be written as in Eqs. (4.3) and (4.4):

$$MR = \exp(-0.287917t^{1.4}) \tag{4.3}$$

$$MR = \exp(-(0.4102t)^{1.4}) \tag{4.4}$$

Figure 4.21 shows the comparison of the predicted and experimental *MR* by the most fitted drying model for the forced convection solar drying of paddy. Table 4.4 presents the constants and coefficients for the drying models. Table 4.5 shows the values of χ^2, RMSE, and R^2 for the different modes of drying.

Table 4.4 Modeling of moisture ratio for thin-layer drying of paddy for the forced convection solar dryer

Model No.	Model constants	R^2	RMSE	χ^2
Newton	k= 0.41678	0.96575	0.05918	0.00350
Diffusion Approach	a= 1 k= 0.41678 b= 1	0.96575	0.05918	0.00350
Two-term	a= 0.54162 k_1= 0.45205 b= 0.54162 k_2= 0.45205	0.97622	0.04932	0.00243
Verma	a= 1 k= 1 g= 1	0.99186	0.02888	0.00083
Wang and Singh	a=-0.30399 b= 0.02200	0.99481	0.02303	0.00053
Logarithmic	a= 1.41360 k= 0.25195 c= -0.37678	0.99549	0.02146	0.00046
Page	**k= 0.28791 n=1.4**	**0.99644**	**0.01907**	**0.00036**
Modified Page	**k= 0.41020 n= 1.4**	**0.99644**	**0.01907**	**0.00036**

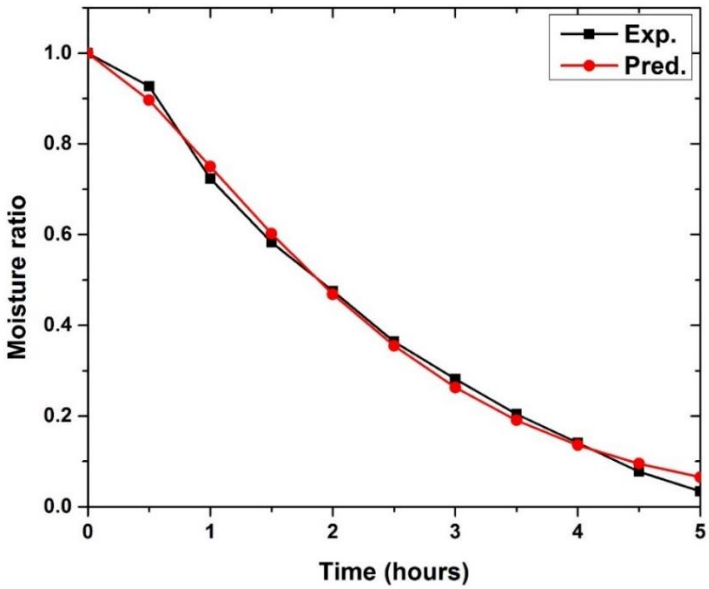

Fig. 4.20 Variations of experimental moisture ratio and predicted moisture ratio obtained in the Page model

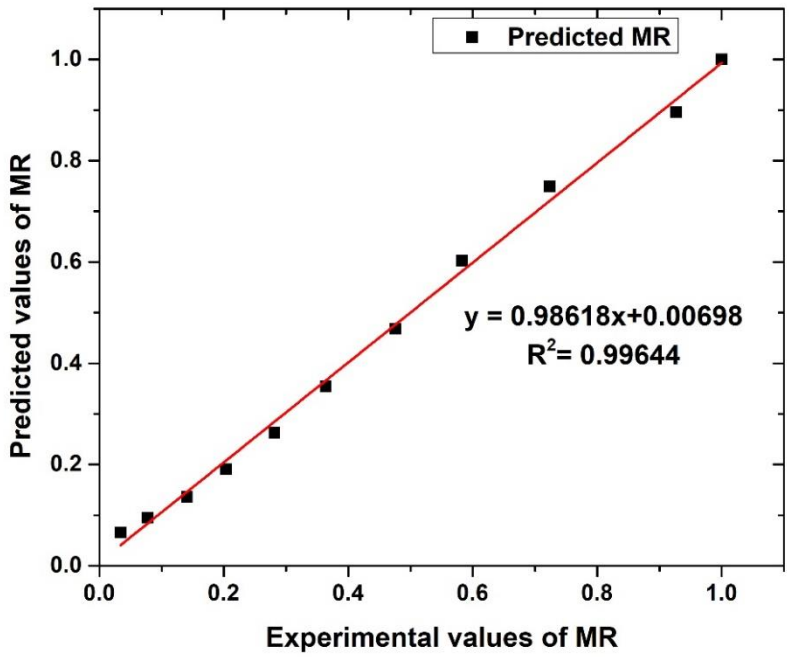

Fig. 4.21 Comparison of experimental moisture ratio and predicted moisture ratio

Table 4.5 Comparison of statistical analysis of mathematical models results for drying kinetics of the agricultural products.

S. No.	Drying mode	Product	R^2	RMSE	χ^2	Reference
1	Greenhouse	Bitter guard flakes	0.9855-0.9986	0.01038-05102	0.00301-0.07029	(Chauhan et al., 2018a)
2	Open Sun	Ghost chili pepper	0.94103-0.99719	0.01665-0.7628	0.00029-0.00589	(Rabha et al., 2017b)
3	Forced convection	Ghost chili pepper	0.96795-0.99696	0.01687-0.06653	0.00031-0.00453	(Rabha et al., 2017b)
4	Microwave	Paddy	0.91912-0.9798	0.01472-0.0319	0.00021-0.00102	(Jafari et al., 2017)
5	Oven drying	Paddy	0.9679-0.9903			(Xing-jun et al., 2016)
6	Biomass-operated dryer	Paddy	0.9522-0.99964	0.032856-2.6007	0.001079-6.7639	**Present study**
7	Natural convection solar dryer	Paddy	0.96269-0.99452	0.02356-0.06148	0.00076-0.00542	**Present study**
8	Forced convection solar dryer	Paddy	0.96575-0.99644	0.05918-0.01907	0.00350-0.00036	**Present study**

4.5 Performance comparision of solar dryer under natural and forced convection mode

This study was carried out to compare the performance of the solar dryer under natural and forced convection mode. From the study, 12 kg inventory was loaded on the drying tray under the natural and forced convection mode of drying. The solar irradiance and the moisture content variations is shown in Fig. 22. During the study, paddy having initial moisture content of 34.1%

was sucessfully dried to 14.4% in 5 hours under natural convection while the moisture content of 34.2% reduced to 13.8% in 3 hours 45 minutes under forced convection mode. The solar irradiance under natural and forced convection were varied in the range of 745–970 W/m^2 and 700–970 W/m^2 with an average of 880 W/m^2 and 849.8 W/m^2, respectively. In the study, it was found that the forced convection solar dryer dries the product faster even the average solar irradiance is lower as compared to natural convection solar dryer. However, the electrical energy required to run the fan under the forced convection drying was 66 J/s.

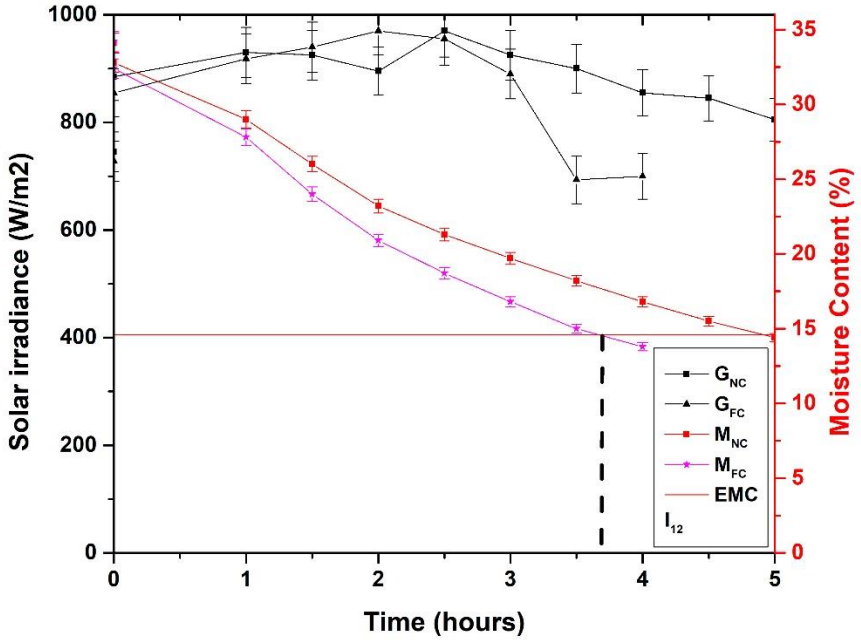

Fig. 22. Variations of solar irradiance and moisture content of paddy under natural and forced convection dryer for 12 kg inventory

4.6 Performance analysis of the biomass-solar hybrid dryer

This study was performed to analyze the performance of the hybrid dryer under natural and forced convection mode. In this study, the paddy was loaded on the drying tray at 7 AM. The drying of paddy progresses using solar energy on the day when sunshine was present. Once the solar irradiance decreased in the evening, the air temperature in the drying chamber starts falling, hence the biomass burning started in the furnace so that temperature could be maintained in the drying chamber. To continue the drying process, burning of the biomass started at 4 PM. During the study,

four batches of paddy were successfully dried under solar and biomass operated mode of dryer. The input parameter of the study is reported in Table 4.6.

Table 4.6 Input parameters for the biomass-solar hybrid dryer

Dryers	Solar intensity (W/m^2)	Biomass (kg)	Initial moisture content (%)	Inventory (kg)
Natural convection hybrid dryer	136–952	12.5	32.7–33.2	48 (4×12)
Forced convection hybrid dryer	127–966	12.5	32.2–33	56 (2×12, 2×16)

This study was started at 7AM and continued to 6 AM next day. To maintain the temperature in the drying chamber 12.5 kg of biomass (lebbeck wood) was burnt. Initially, 7.5 kg of biomass was burnt at the rate of 2.5 kg/h and after that, the biomass burning started at 11:30 PM, 5 kg of biomass was burnt at this time. The variations of solar intensity, drying chamber temperature, and moisture content of paddy for the natural convection hybrid dryer and forced convection hybrid dryer is shown in Figs. 4.23 and 4.24. In the natural convection hybrid dryer, four batches (12 kg/batch) of inventory were dried, 2 batches under solar energy and the other two batches under biomass-operated dryer. During the solar drying, the solar radiation intensity and temperature in the drying chamber were ranged from 136–952 W/m^2 and 36.4–48 °C, respectively. In the study, it was observed that the first batch of inventory dried in 5 hours while the second batch took 5.5 hour for the same amount of inventory. It may be due to the relatively lower value of solar irradiance during second batch drying. In the biomass-operated dryer, temperature in the drying chamber was ranged from 40.2–48.5 °C. From the results, it was found that the second batch of inventory took 6.5 hours to achieve final moisture content while the first batch achieved in 6 hours. This may be due to the relatively lower temperature in the drying chamber during the second batch drying.

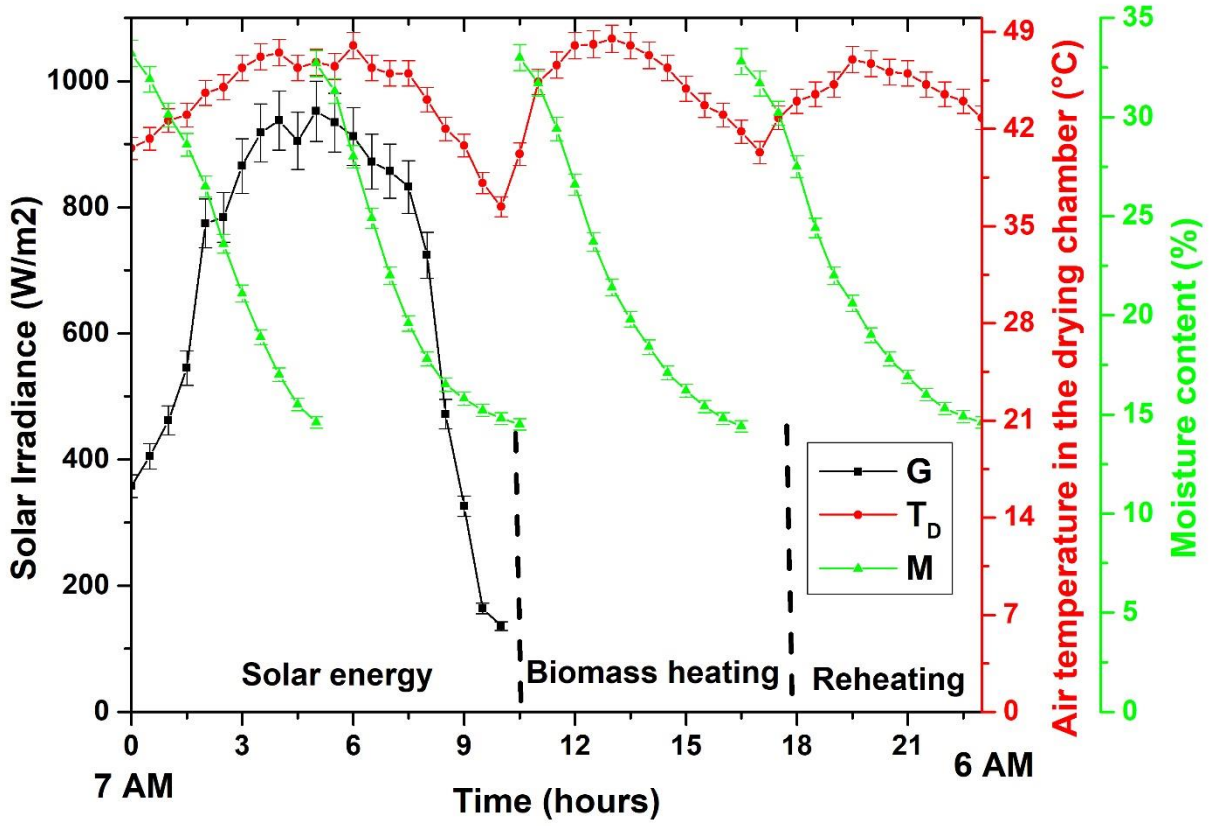

Fig. 4.23 Variations in solar intensity, drying chamber temperature, and moisture content of paddy for the natural convection hybrid dryer

Four batches of inventory were also dried in the forced convection hybrid dryer. In this study, 16 kg/batches of inventory were dried under solar energy and 12 kg/batch under biomass-operated mode. During the solar drying, the solar irradiance and the drying chamber temperature were ranged from 127–946 W/m^2 and 36.1–57.8 °C, respectively. In the study, it was found that the second batch of the inventory consumes 0.5 hour more as compared to the first batch in both mode of operation. That may be because of relatively lower temperature in the drying chamber during the second batch drying. From the study, it was found that the natural convection hybrid dryer could dry 48 kg (4×12 kg) inventory per day while the forced convection hybrid dryer could dry 56 kg (2×16 kg and 2×12 kg) per day. The amount of biomass burnt in the natural and forced convection solar-biomass hybrid dryer was 12.5 kg.

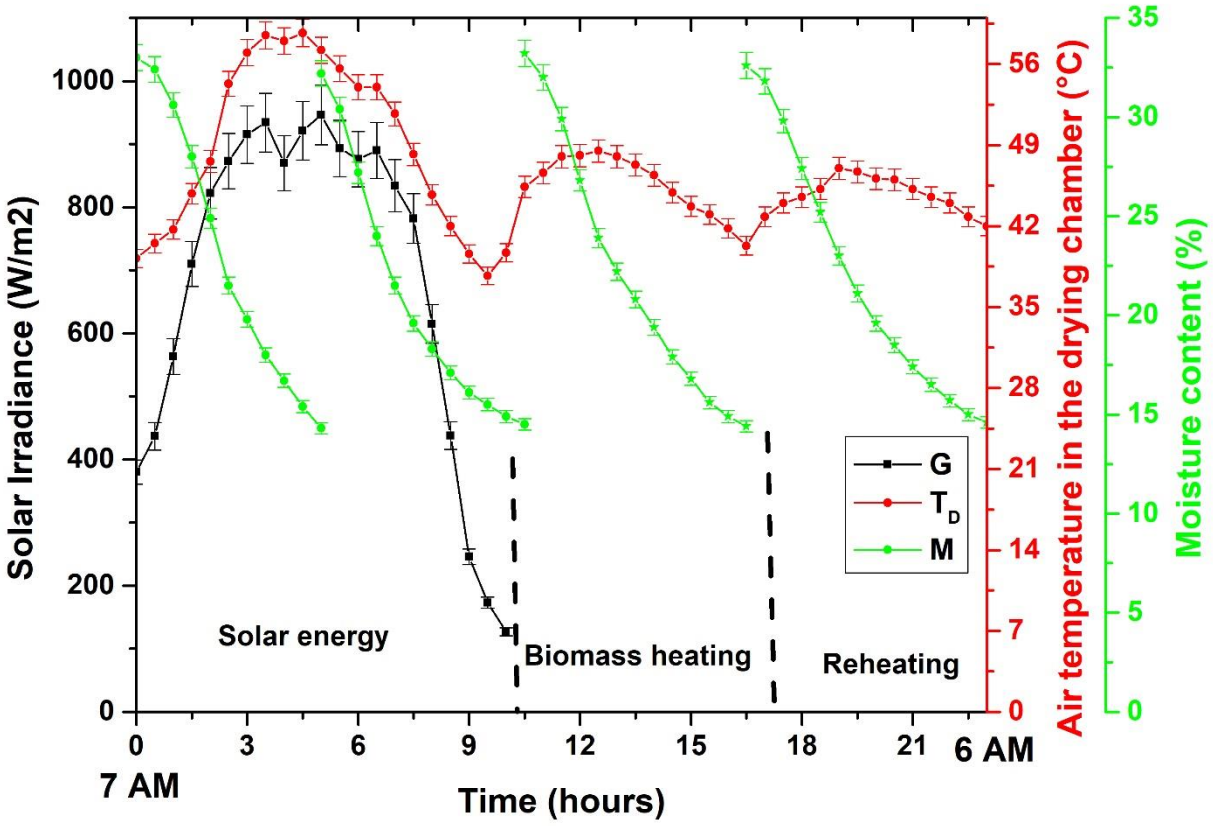

Fig. 4.24 Variations in solar intensity, drying chamber temperature at entry to paddy tray, and moisture content of paddy for the forced convection hybrid dryer

4.7 Summary

In the present study, the drying kinetics of paddy has been investigated in the biomass-operated dryer, natural convection solar dryer, forced convection solar dryer, and the solar-biomass hybrid dryer. The experimental moisture ratio obtained in the drying process was fitted with eight mathematical drying models for the best fitting of the curve. The performance of the biomass operated dryer, natural convection solar dryer, and the forced convection solar dryer was found to be optimum for 12 kg/batch, 12 kg/batch, and 16 kg/batch, respectively. The drying capacity of the forced convection solar-biomass hybrid dryer was found to be 56 kg paddy/day while it was 48 kg/day for the natural convection solar-biomass hybrid dryer. The energy and exergy analysis of the biomass operated dryer and the solar dryer are discussed in the next chapter.

Chapter 5

Energy efficiency analysis of the developed dryers

5.1 Introduction

In this chapter experimental findings of thermodynamic analysis (energy and exergy) of the natural convection biomass-operated dryer, natural convection solar dryer, and the forced convection solar dryer have been discussed. Finally, the optimized conditions for operation of dryers were investigated based on the energy consumption and reported.

5.2 Mathematical equations used for the energy and exergy analysis of the dryer

5.2.2 Energy analysis

Energy consumption is at the present scenario becomes a critical issue as the energy sources are depleting day by day. Hence, energy analysis of a thermodynamic system is important to optimize energy consumption.

5.2.2.1 Energy analysis of the biomass operated dryer

Convective heat transfer coefficient for the furnace outer surface and the vertical wall is calculated as in Eq. (5.1) (P K Nag, 2014):

$$h = \frac{Nu \times k}{L} \tag{5.1}$$

Radiative heat transfer coefficient for the outer surface of conical furnace can be calculated by using Eq. (5.2) (Evangelisti et al., 2017):

$$h_r = \sigma \times \varepsilon \times \left(T_{FS} + T_{RC}\right) \times \left(T_{FS}^2 + T_{RC}^2\right) \tag{5.2}$$

The heat transfer rate from the conical furnace to the rectangular chamber is evaluated by using Eq. (5.3) (P K Nag, 2014):

$$Q = h \times A_{FS} \times \left(T_{FS} - T_{RC}\right) \tag{5.3}$$

The heat loss rate through the rectangular chamber (brick wall) is defined as Eq. (5.4):

$$Q_l = h_w \times A_w \times (T_w - T_0) \tag{5.4}$$

5.2.2.2 Energy analysis of the solar dryer

Energy analysis of the dryer has been performed by using mass and energy conservation equations. During the analysis, it was assumed that the kinetic energy of the drying air remains constant throughout the drying process. Mass and energy balance of the air flowing through the SAH can be done by using Eqs. (5.5) (Arun et al., 2020; Jafari et al., 2017) and (5.6):

$$\sum \dot{m}_{Ci} = \sum m_{Co} = \dot{m}_a \tag{5.5}$$

$$Q_{rSAH} - Q_{lSAH} = Q_{Co} \tag{5.6}$$

where Q_{rSAH} and Q_{Co} are calculated by using Eqs. (5.12) and (5.13).

Energy absorbed by the collector from the sun is obtained from the Eq. (5.7) (Rabha et al., 2017a):

$$Q_{CS} = I\alpha\tau A_{SAH} \tag{5.7}$$

The heat gained by the air at the inlet of SAH is calculated with the help of Eq. (5.18)

$$Q_{Ci} = \dot{m}_a c_p (T_{Ci} - T_{amb.}) \tag{5.8}$$

The airflow rate in the drying system is calculated from Eq. (5.9) (Zuhur and Ceylan, 2019):

$$\dot{m}_a = \rho X V \tag{5.9}$$

The density of hot air can be written as in Eq. (5.10) (Abuşka et al., 2019):

$$\rho = \frac{353.44}{T_{air}(K)} \tag{5.10}$$

The hot air specific heat in the drying system is evaluated from Eq. (5.11) (Afzali et al., 2019):

$$C_p = 1002.9 + 0.0052T \tag{5.11}$$

Energy received by the solar collector is evaluated by Eq. (5.12):

$$Q_{rSAH} = \dot{m}_a c_p (T_{Ci} - T_{amb.}) + I\alpha\tau A \tag{5.12}$$

The energy gained by the air at the SAH outlet is calculated by Eq. (5.13) (A. Midilli and Kucuk, 2003; Singh, 2020):

$$Q_{Co} = \dot{m}_a c_p (T_{Co} - T_{amb.}) \tag{5.13}$$

The energy at the inlet of the drying chamber is evaluated by using Eq. (5.14):

$$Q_{Di} = \dot{m}_a c_p (T_{Di} - T_{amb.}) \tag{5.14}$$

Eq. (5.15) expressed the energy utilized in the drying chamber

$$Q_{uD} = \dot{m}_a c_p (T_{Di} - T_{Do}) \tag{5.15}$$

The thermal efficiency of the SAH, drying chamber, and the overall efficiency of the dryer are expressed with the help of Eqs. (5.16) (Kumar et al., 2021), (5.17) (Rabha et al., 2017a), and (5.18), respectively.

$$\eta_{SAH} = \frac{\dot{m}_a c_p (T_{Co} - T_{amb.})}{\left[I\alpha\tau A + \dot{m}_a c_p (T_{Ci} - T_{amb.}) \right]} \tag{5.16}$$

$$\eta_D = \frac{(T_{Di} - T_{Do})}{(T_{Di} - T_{amb.})} \tag{5.17}$$

$$\eta_{DSYS} = \frac{\dot{m}_a c_p (T_{Di} - T_{Do})}{\left[I\alpha\tau A + \dot{m}_a c_p (T_{Ci} - T_{amb.}) \right]} \tag{5.18}$$

5.2.3 Exergy analysis

The second law analysis of the dryer has been performed by using a steady flow equation for the dryer system. During the analysis, it was assumed that the drying air maintained a steady flow throughout the experiment. For the exergy calculation, reference (dead state) temperature is assumed as 300 K. The second law analysis of the dryer has been performed by using a steady flow equation for the dryer system. During the analysis, it was assumed that the drying air maintained a steady flow throughout the experiment.

5.2.3.1 Exergy analysis of the biomass operated dryer

For negligible changes in kinetic energy (K.E), potential energy (P.E), and available energy (exergy) at the corresponding sections in the rectangular chamber is calculated by using Eq. (5.19) (P K Nag, 2013):

$$Ex. = \left(e_i - e_0\right) - T_0 \times \left(s_i - s_0\right) \tag{5.19}$$

Exergy balance

$$Ex._{in} = Ex._{out} + Ex._{loss} + Ex._{destruction} \tag{5.20}$$

For the steady-state Eq. (5.21) can be used for the exergy destruction for the control volume in the rectangular chamber (P K Nag, 2013):

$$Ex._{Des} = \sum_j \left(1 - \frac{T_0}{T_j}\right)\dot{Q}_j + \left(Ex._i - Ex._{i+1}\right) \tag{5.21}$$

$$Ex._i - Ex._{i+1} = \left(e_i - e_{i+1}\right) - T_0 \times \left(s_i - s_{i+1}\right) + \left(\frac{V_i^2 - V_{i+1}^2}{2}\right) + g \times \left(z_i - z_{i+1}\right) \tag{5.22}$$

Exergy efficiency of the dryer can be expressed as in Eq. (5.23):

$$\eta_{Ex.} = \frac{Ex._{uD}}{Ex._{in}} \tag{5.23}$$

where, i represents the corresponding sections.

5.2.3.2 Exergy analysis of the solar dryer

Exergy received by the solar collector from the sun is calculated by the Eq. (5.24):

$$Ex._{CS} = I\alpha\tau A\left(1-\frac{T_0}{T_{Sun}}\right) \tag{5.24}$$

Exergy at the inlet of the SAHs and exergy received by the collectors is defined by Eqs. (5.25) and (5.26):

$$Ex._{Ci} = \dot{m}_a c_p\left[(T_{Ci}-T_0)-T_0\times ln\left(\frac{T_{Ci}}{T_0}\right)\right] \tag{5.25}$$

$$Ex._{rSAH} = \dot{m}_a c_p\left[(T_{Ci}-T_0)-T_0\times ln\left(\frac{T_{Ci}}{T_0}\right)\right]+I\alpha\tau A\left(1-\frac{T_0}{T_{Sun}}\right) \tag{5.26}$$

Exergy at the corresponding points in the dryer system can be calculated by the Eqs. (5.27), (5.28), and (5.29) (Ndukwu et al., 2017):

$$Ex._{Co} = \dot{m}_a c_p\left[(T_{Co}-T_0)-T_0\times ln\left(\frac{T_{Co}}{T_0}\right)\right] \tag{5.27}$$

$$Ex._{Di} = \dot{m}_a c_p\left[(T_{Di}-T_0)-T_0\times ln\left(\frac{T_{Di}}{T_0}\right)\right] \tag{5.28}$$

$$Ex._{Do} = \dot{m}_a c_p\left[(T_{Do}-T_0)-T_0\times ln\left(\frac{T_{Do}}{T_0}\right)\right] \tag{5.29}$$

Exergy at the various components of the dryer system is written as in Eqs. (5.30), (5.31), and (5.32): Exergy loss in the SAH is expressed with the help of Eq. (5.30):

$$Ex._{lSAH} = Ex._{rSAH} - Ex_{Co} \tag{5.30}$$

The exergy loss in the PVC pipe is evaluated in Eq. (5.31):

$$Ex._{lpipe} = Ex._{Co} - Ex_{Di} \tag{5.31}$$

Exergy used in the paddy drying process in the dryer system can be calculated as in Eq. (5.32):

$$Ex._{uD} = Ex._{Di} - Ex_{Do} \tag{5.32}$$

The components and the overall second law efficiency of the dryer are written as in Eqs. (5.33), (5.34), and (5.35):

The exergy efficiency of the SAH can be expressed as the ratio of outflow exergy to inflow exergy of the SAH. It can be written as the ratio of the exergy of air at the collector outlet to the exergy received by the collector plate (Akpinar and Koçyiĝit, 2010):

$$\eta_{Ex.\mathrm{SAH}} = \frac{Ex._{Co}}{Ex._{rSAH}} \tag{5.33}$$

The second law efficiency of the drying chamber is defined as the ratio of exergy used in the drying process to the exergy inflow into the drying chamber. In general, it can be written as in Eq. (5.34) (Ndukwu et al., 2017; Karthikeyan and Murugavelh, 2018):

$$\eta_{Ex.\mathrm{D}} = \frac{Ex._{Di} - Ex._{l}}{Ex._{Di}} = 1 - \frac{Ex._{l}}{Ex._{Di}} \tag{5.34}$$

The overall second law efficiency of the dryer is the ratio of exergy used or exergy destruction in the paddy drying process to the exergy received by the solar air heaters. It is expressed as in Eq. (5.35):

$$\eta_{Ex.\mathrm{DSYS}} = \frac{Ex._{uD}}{Ex._{rSAH}} \tag{5.35}$$

The improvement potential, sustainability index, and waste energy ratio are the major parameters of the exergy sustainability indicator, which identify how the exergy losses and exergy efficiency affect the sustainability of the drying process. The improvement potential in the second law efficiency for the drying process can be found by using Eq. (5.36) (Akpinar, 2010a):

$$IP = \left(1 - \eta_{Ex.D}\right)\left(Ex._{Di} - Ex._{Do}\right) \tag{5.36}$$

The sustainability index and waste energy ratio are evaluated by using Eqs. (5.37) and (5.38) (Vijayan et al., 2020):

$$SI = \frac{1}{1 - \eta_{Ex.}} \tag{5.37}$$

$$WER = \frac{Ex_{loss}}{Ex._{Di}} \tag{5.38}$$

5.3 Energy and exergy analysis of the biomass-operated dryer

In this study, biomass is burnt in the conical furnace for three hours, and the results obtained from the present investigation are discussed. Figure 5.1 shows the temperature of the outer surface of the conical furnace and the temperature of hot air in the rectangular chamber. The figure shows that the temperature of the conical furnace and the rectangular chamber is higher during the biomass burning period. When biomass burning stops, the temperature of the furnace and the chamber starts decreasing. Based on the measured temperature of the conical surface and hot air in the rectangular chamber. The heat transfer rate from the furnace to the rectangular chamber is calculated for the natural convection between the outer surface of the conical furnace and air in the rectangular chamber.

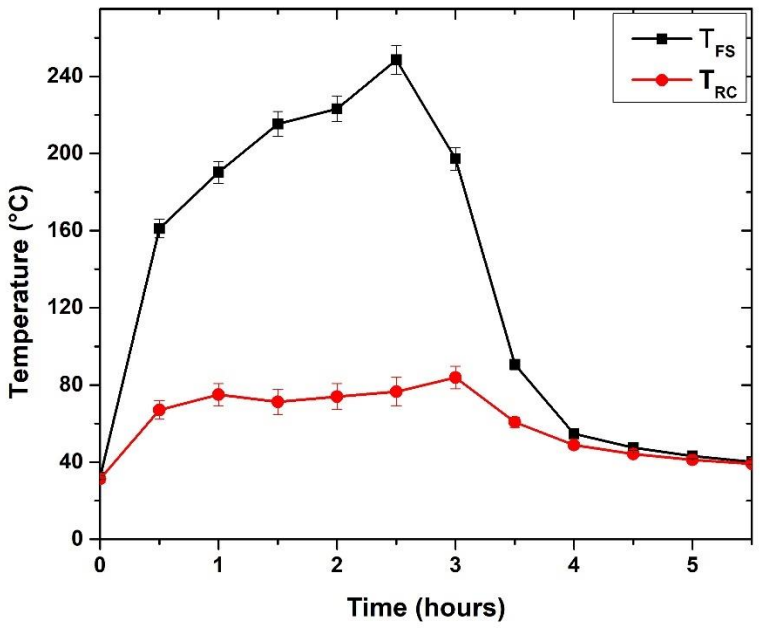

Fig. 5.1 Variations in temperature of the conical furnace outer surface and the hot air in the rectangular chamber

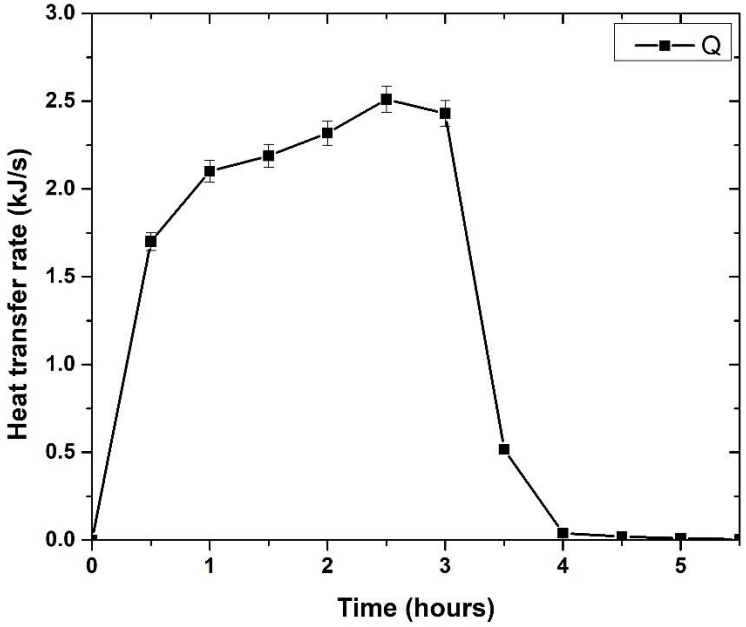

Fig. 5.2 Variations of heat transfer rate for the conical furnace to the rectangular chamber

The variations of heat transfer rate from the furnace to the rectangular chamber is shown in Fig. 5.2. In the study, the heat transfer rate from the conical furnace to the rectangular chamber was found to be higher during the time of biomass-burning in the furnace. That is because, during the biomass-burning, heat generation in the furnace was higher but once biomass-feeding stops; no longer has heat generation taken place in the furnace. Even though heat generation stops in the furnace, heat transfer takes place for a short period that is because, at the time of biomass-burning, some amount of heat was stored by the conical furnace. The maximum value of heat transfer rate was found as 2.51 kJ/s with an average of 2.2 kJ/s during biomass burning. Now, the study has been performed for two cases viz. (i) without sensible thermal storage in the rectangular chamber, (ii) with sensible thermal storage (pebbles) in the chamber. In both the cases of study, hot air from the rectangular chamber to the drying tray are allowed through the cylindrical holes in the PCM tray. The heat transfer coefficients and the heat loss rate for the outer surface of the rectangular chamber for case-(I) and case-(II) are shown in Figs. 5.3 (a) and (b). The maximum value of the heat transfer coefficients for the outer surface of the rectangular chamber was recorded as 5.26 W/m^2K and 4.48 W/m^2K with an average of 4.14 W/m^2K and 3.92 W/m^2K for the case-I and case-II, respectively.

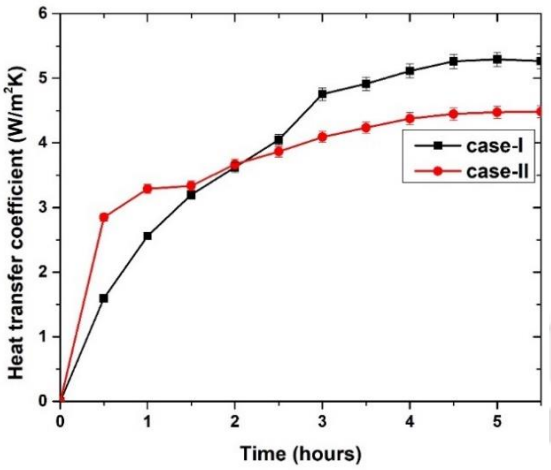

Fig. 5.3 (a) Heat transfer coefficient for the rectangular chamber outer surface for case-I and case-II

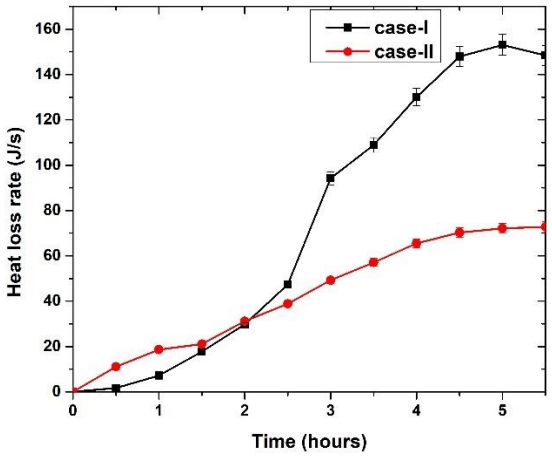

Fig. 5.3 (b) Heat loss rate from the rectangular chamber through the brick wall for case-I and case-II

From the results, it was observed that the heat transfer coefficient for the outer surface of the chamber for case-II is lower than that of case-I. In Fig. 5.3 (b), the heat loss rate through the rectangular brick wall was varied in the range of 1.67–153 J/s and 11–72.75 J/s with an average of 80.53 J/s and 46.14 J/s for case-I and case-II, respectively. In the study, a relatively lower heat loss rate through the rectangular chamber was observed for case-II. During the study, a relatively lower heat loss rate through the wall was found at the initial stage of biomass burning. That is because, most of the heat is absorbed by the pebbles due to which less amount of heat reaches the outer surface of the rectangular wall, which leads to lower temperature of the rectangular wall that's why heat loss from the wall is lower. However, after some time when pebbles stored their sensible energy, more amount of heat reaches the wall, due to which heat loss increases with time. Figure 5.4 shows the exergy destruction in the rectangular chamber for case-I and case-II. The exergy destruction in the rectangular chamber was obtained in the range of 0.528–7.35 kJ/kg and 0.125–3.251 kJ/kg with an average of 4.585 kJ/kg and 2.087 kJ/kg for case-I and case-II, respectively. From the result, it was observed that the exergy destruction in case-II is lower as compared to case-I. The lower exergy destruction means the most efficient energy utilization. Hence, the case-II (sensible heat storage material filled up to the paraffin wax tray) is the better condition as compared to case-I.

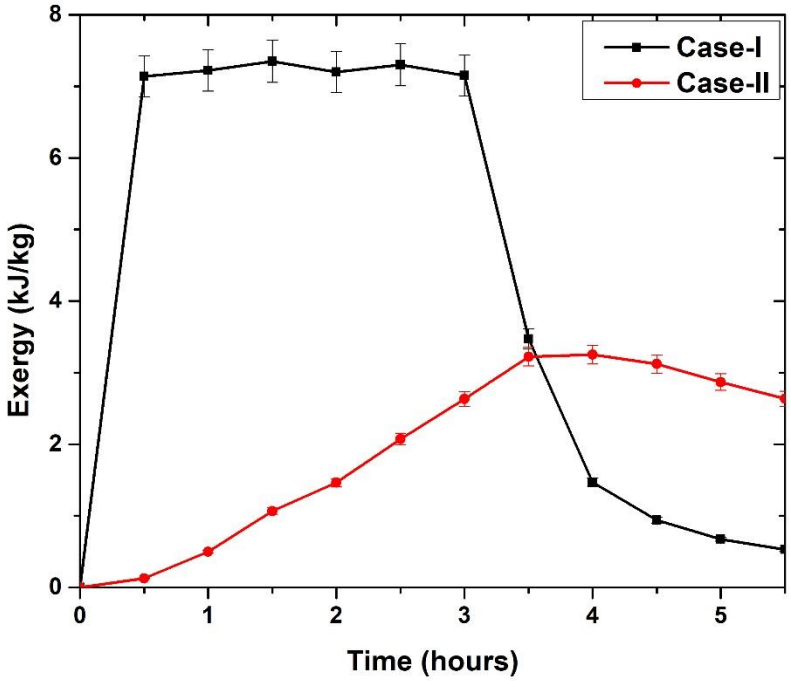

Fig. 5.4 Exergy destruction in the rectangular chamber for case-I and case-II

The variations in temperature and exergy of hot air just below the paraffin wax tray are shown in Figs. 5.5 (a) and (b). In this figure 5.5 (a), the temperature of hot air just below the Paraffin wax (PCM) tray for the case-I, case-II, and case-III (when sensible storage is present in the rectangular chamber and hot air from the rectangular chamber is not allowed to the drying tray), respectively. The temperature of hot air was varied in the range of 31.60–104.55 °C, 28.77–72.83 °C, and 29.64–81.22 °C for case-I, case-II, and case-III, respectively. In the study, temperature of hot air during the biomass-burning period was found higher in case-I. But once biomass burning stops, the temperature of the hot air in the rectangular chamber decreased sharply while in the case-II and case-III, even though the biomass feeding was stopped, the temperature of the hot air remains high for a longer period as compared to the case-I. In case-III, the temperature retains by the hot air is high for a longer period as compared to the other cases of studies. In figure 5.5 (b), the exergy of hot air just below the Paraffin wax (PCM) tray for the case-I, case-II, and case-III, respectively. From the result, it was observed that the exergy of the hot air just below the paraffin wax tray follows the same trend as the temperature profile. It retains for a longer period in the case-III.

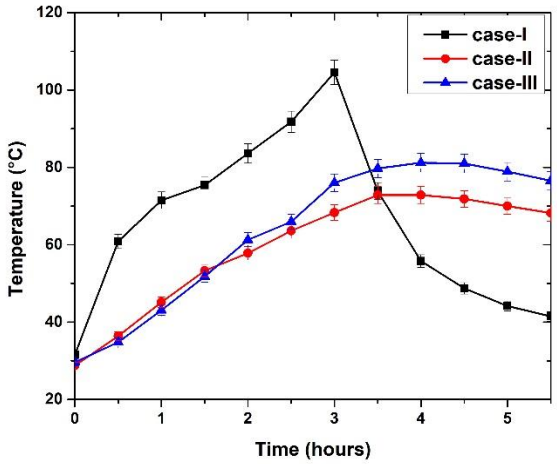

Fig. 5.5 (a) Temperature of hot air just below the PCM tray for three different cases

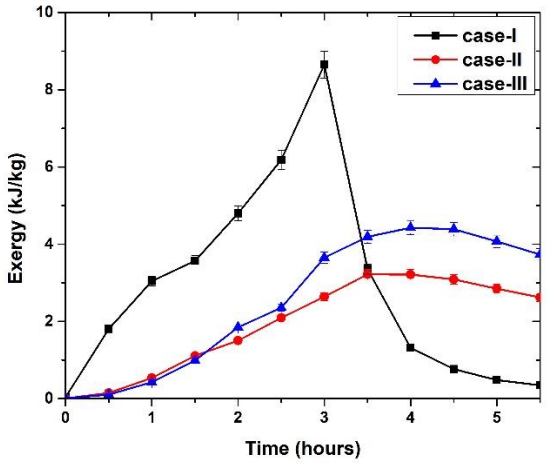

Fig. 5.5 (b) Exergy of the hot air just below the PCM tray for three different cases

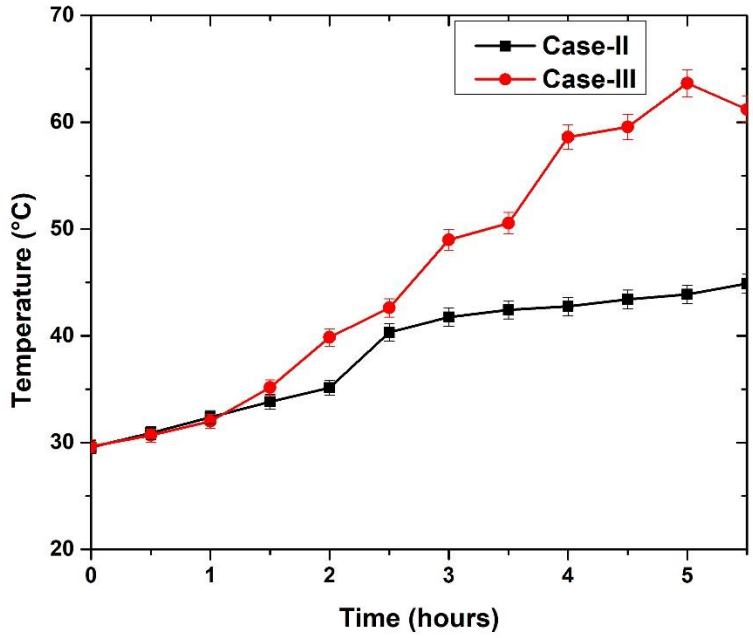

Fig. 5.6 Temperature in the PCM tray for case-II and case-III

Hence, case-III can be assumed as the best condition for the developed natural convection dryer. Figure 5.6 shows the temperature of the paraffin wax tray for case-II and case-III. During the study, the temperature in the paraffin wax tray was found to be higher and it retains for a longer period in the case-III. The temperature and exergy of the flue gas in the exhaust pipe are shown in Fig.

5.7. The maximum temperature of the flue gas during the biomass-burning was recorded as 294 °C and the maximum amount of exergy loss in the flue gas during the biomass burning period was found as 78.38 kJ/kg. From the result, it can be seen that, as biomass burning stops, the flue gas temperature and exergy decreases sharply.

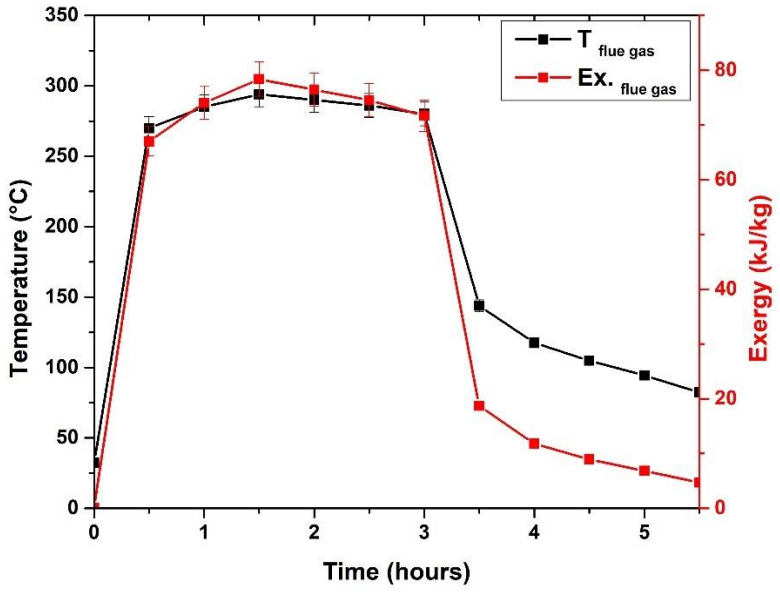

Fig. 5.7 Variations of temperature and exergy of flue gas in the exhaust pipe

5.4 Energy and exergy analysis of the modified biomass operated dryer

In this study, the energy and exergy analysis of the modified biomass-operated grain dryer has been performed for the paddy drying process. This study has been performed for three different cases viz. (i) without sensible storage medium in the rectangular chamber, (ii) with sensible storage medium (pebbles) in the chamber, and (iii) with sensible storage when exhaust valve is closed at the end of biomass burning. In all three different cases of studies, biomass was burnt at the rate of 2.5 kg/h for three hours and the experimental data were recorded at an interval of 30 minutes. Figures 5.8 (a) and (b) show the variations of temperature and exergy in the rectangular chamber just below the PCM tray for the three different cases. The maximum value of temperature in the rectangular chamber just below the PCM tray was recorded as 145.4 °C, 127.4 °C, and 124.5°C with a mean of 74.23 °C, 76.89 °C, and 82.33 °C for the case-I, case-II, and case-III, respectively. In the study, a relatively higher values of the temperature below the PCM tray were observed

during the biomass-burning period. The cause of higher temperature in the chamber is the generation of heat by the biomass burning which increases the temperature. When biomass burning stopped in the furnace, the temperature of the hot air decreased sharply.

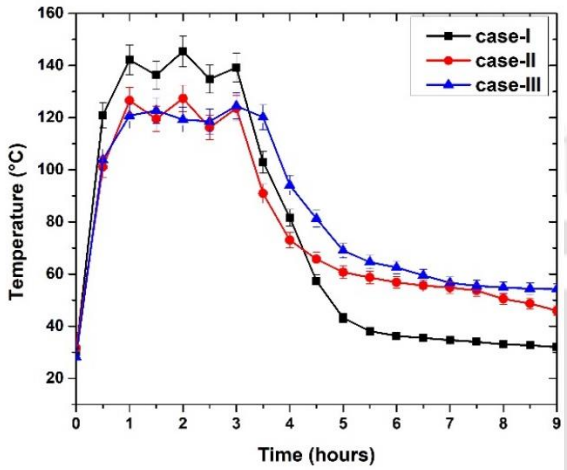

Fig. 5.8 (a) Variations of temperature just rectangular chamber below PCM tray

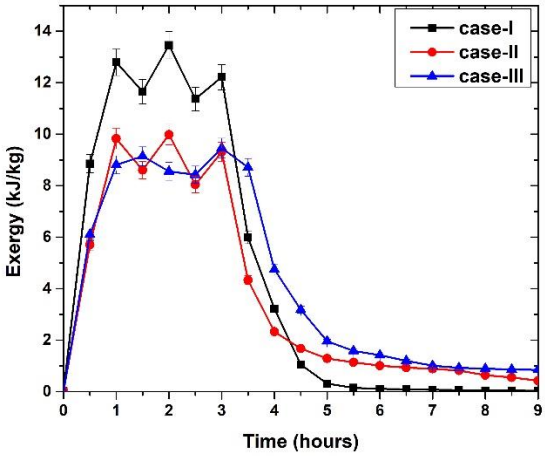

Fig. 5.8 (b) Exergy variations in the just below PCM tray

From the results, it was also observed that the air temperature after stopping the biomass burning in the furnace maintained higher for a longer period for the case-III. This indicates that the energy retaining capacity of the hot air is relatively higher in this case. From Fig. 5.8 (b), it was found that as biomass burning starts, the exergy gained by the hot air increases rapidly, and once the biomass burning stopped, the exergy in the rectangular chamber decreases. The exergy achieved by the hot air during the biomass burning was higher for case-I. However, the exergy retains by the air after stopping the biomass burning was relatively higher for the case-III while it was relatively lesser at the time of biomass burning. It extends the uniformity of energy in the drying process. Figures 5. 9 (a) and (b) show the variations of temperature and exergy in the PCM tray for the three different cases. The maximum temperature in the paraffin wax tray was obtained as 98.7 °C, 95.27 °C, and 92.15 °C for case-I, case-II, and case-III, respectively. From the figure, it can be seen that the PCM tray temperature is higher during the biomass-burning period in case-I but once biomass feeding in the furnace stops, the temperature decreased rapidly. While a higher value of the temperature in the PCM tray is maintained for a longer period in the case-III. From the results, it was also found

that the temperature of the PCM tray is relatively higher after the biomass burning for the case-III that means the temperature retains by the PCM is longer in this case.

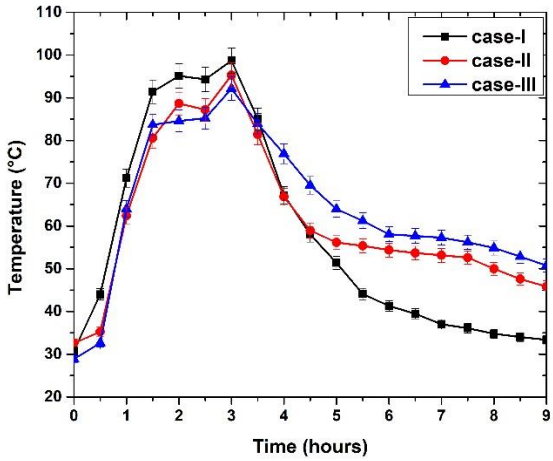

Fig. 5.9 (a) Variations of the temperature of the PCM tray with time

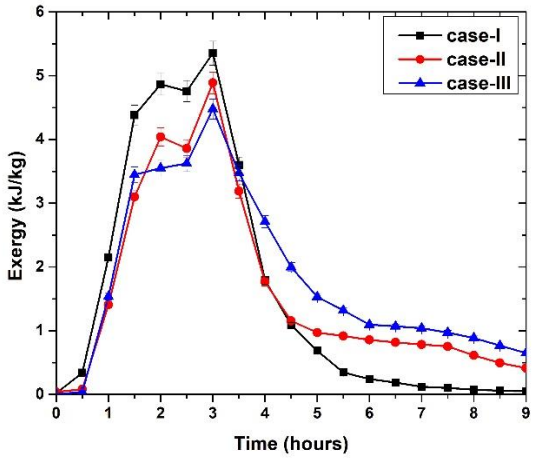

Fig. 5.9 (b) Exergy variations in the PCM tray

From Fig. 5.9 (b), it was found that the exergy achieved by the PCM tray is higher for the biomass burning period and it drops sharply when the biomass feeding stop. The average value of exergy achieved by the paraffin wax tray was recorded as 1.59 kJ/kg, 1.586 kJ/kg, and 1.798 kJ/kg for the case-I, case-II, and case- III, respectively. During the study, the average exergy achieved in case-III was higher as compared to the other cases of studies. From the result, it was seen that the paraffin wax tray retains a relatively higher value of exergy for a longer time in the case-III. Figures 5.10 (a) and (b) show the variations of air temperature and exergy in the drying chamber for case-I, case-II, and case-III. During the drying process, the highest value of air temperature in the drying chamber was achieved as 49 °C, 46.18 °C, and 48.2 °C with an average of 39.39 °C, 40.3 °C, and 43.45 °C for the case-I, case-II, and case-III, respectively. From the results, it was found that the temperature of air in the drying chamber in the case-III remains relatively higher for a longer period as compared to the other cases of studies. The temperature variations in the drying chamber during the paddy drying process were obtained in the range of 40–48.2 °C in case-III while a relatively wide range of temperature variations in the drying chamber was observed for case-I and case-II. The obtained range of temperature in the case-III is the most appropriate for the quality drying of paddy.

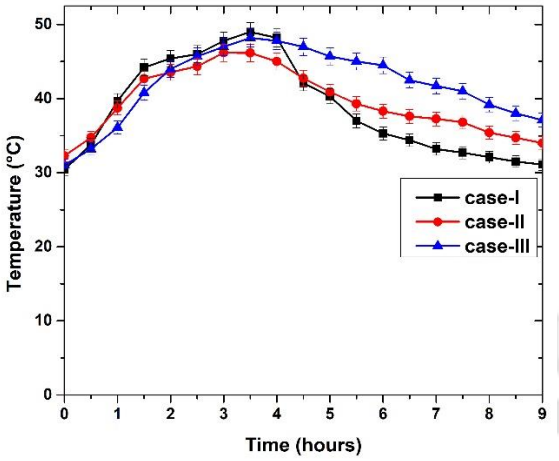

Fig. 5.10 (a) Variations of air temperature with time in the drying chamber

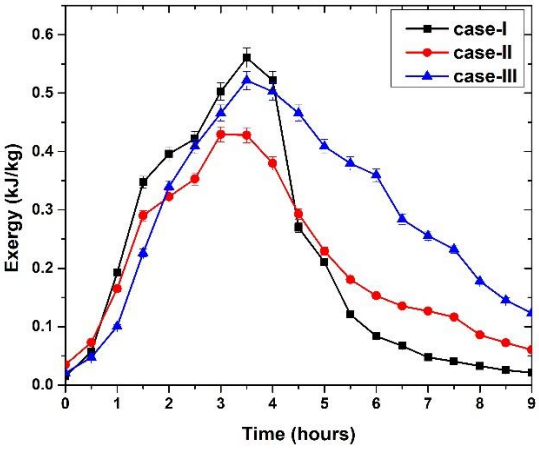

Fig. 5.10 (b) Exergy variations in the drying chamber with time

From Fig. 5.10 (b), it was found that as the biomass burning progresses, the exergy in the chamber increases and achieved a maximum value between 2.5 and 3.5 hours from the initiation of biomass burning after that its value decreases. From the results, it can be seen that the exergy in the drying chamber is relatively higher for a longer period in the case-III. Figures 5.11 (a) and (b) present the temperature and exergy of the flue gas in the exhaust pipe for the three different cases. The highest value of the flue gas temperature was recorded as 135.2 °C, 121.3 °C, and 122 °C with a mean of 69.16 °C, 68.47 °C, and 60.2 °C for the case-I, case-II, and case-III, respectively. In this study, a comparatively lesser value of the flue gas temperature was obtained in the case-III. This indicates that a relatively less amount of energy loss takes place in the flue gas through the exhaust pipe. Hence, the energy stored by the thermal storage medium in the rectangular chamber is higher in the case-III as compared to the other cases of studies. The maximum value of the flue gas temperature in the exhaust pipe was reported as 294 °C (Kumar et al., 2020). Hence, this study reduces the energy losses in the flue gas. From Fig. 11 (b), it was found that a significant amount of exergy loss was taking place in the flue gas during the biomass-burning period. It was also seen from the results that a relatively less amount of exergy loss in the flue gas takes place in the case-III. In the present study, a relatively lesser amount of exergy in the flue gas was recorded as compared to the flue gas exergy reported by Kumar et al., 2020.

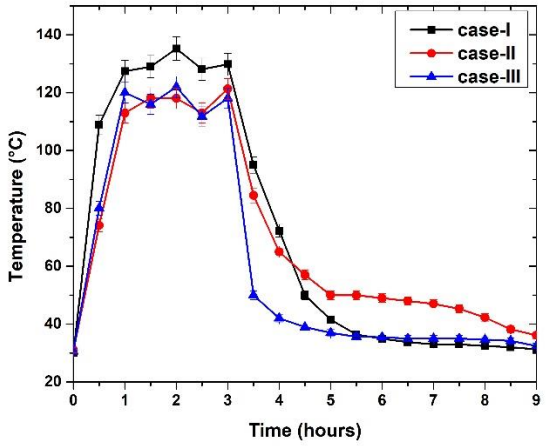

Fig. 5.11 (a) Variations of flue gas temperature with time in the exhaust pipe

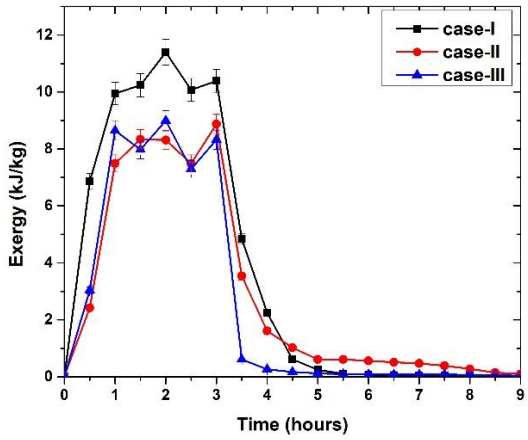

Fig. 5.11 (b) Variations of exergy loss in the flue gas with time

Figure 5.12 shows the exergy efficiency variations for the three different cases. From the figure, it can be seen that the value of exergy efficiency of the dryer is very less at the initial stage of the study. This is because, as biomass burning starts, the energy of the burnt biomass is stored by the thermal energy storage material. Once the thermal storage material stores energy, it supplies uniform heat in the drying chamber. As time progress, energy efficiency increases reach a maximum value and then decreases when the biomass burning stopped in the furnace. The average values of exergy efficiency were obtained as 0.95%, 0.95% and 1.6% for the case-I, case-II and case-III, respectively. From the results, it was found that the average exergy efficiency of the dryer for case-I and case-II are the same but case-II retains relatively higher values for a longer period after biomass burning stopped in the furnace. Hence, case-II extends the uniformity of the exergy utilization in the dryer as compared to case-I. During the study, a relatively higher value of average exergy efficiency was obtained in case-III as compared to case-I and case-II. Relatively higher values of exergy efficiency for a longer period after biomass burning stopped was in the case-III.

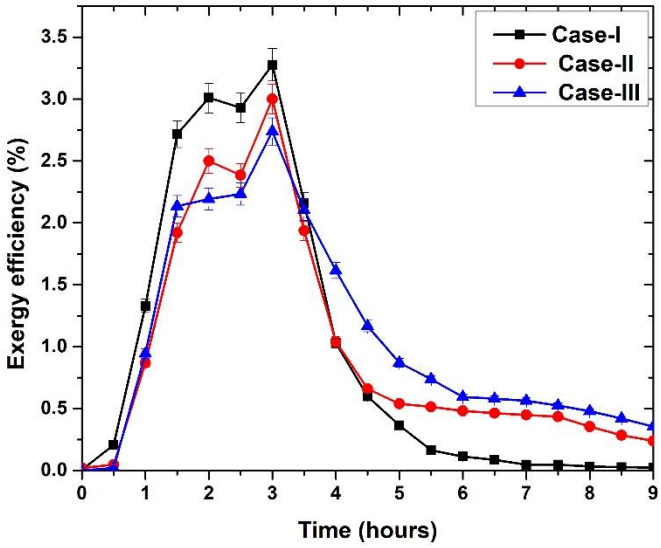

Fig. 5.12 Variations of exergy efficiency for the three different cases

5.5 Energy and exergy analysis of the solar air heater

5.5.1 Energy and exergy analysis of the flat plate solar air heater

This study was conducted from 7:30 h to 17:30 h in August 2019. The experimental data have been recorded at an interval of 30 minutes throughout the experiment. The solar intensity and temperature at the various points in the solar air heater (SAH) are shown in Fig. 5.13. During the study, solar radiation intensity was ranged from 120–924 W/m^2 with a mean of 649.57 W/m^2 and the ambient temperature ranged from 31.2–36.5 °C. The collector inlet and outlet air temperature were ranged from 31.3–41.2 °C and 38.7–77.4 °C, respectively. The collector plate temperature and the hot air temperature in the solar air heater were ranged from 58.3–121°C and 55–109.5 °C, respectively. From the figure, it was observed that the collector plate temperature and the hot air temperature are higher for the high solar intensity. The energy and exergy gained by the hot air at the collector outlet are shown in Fig. 5.14. The value of energy and exergy obtained at the collector outlet were recorded as 38.34–546.93 J/s and 3.14–52.94 J/s, respectively. In the study, it was found that the energy and exergy of the hot air at the collector outlet follow similar trends. The maximum value of the energy and exergy was recorded at 11:00 h and the lowest in the evening. From the figure, it was found that the energy and exergy achieved by the hot air are higher for the higher solar radiation intensity.

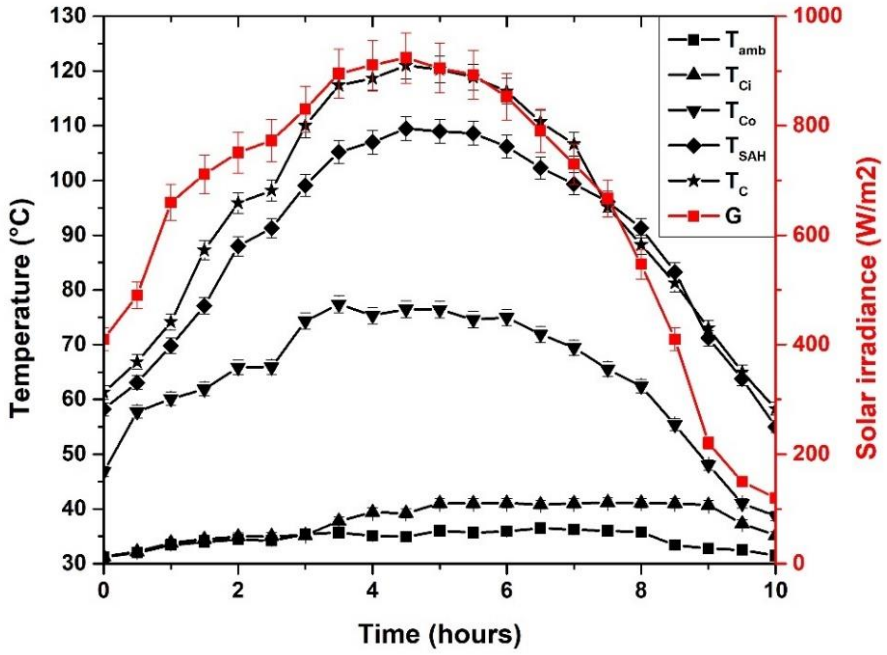

Fig. 5.13 Variations of temperature at the various points in the solar air heater and solar intensity

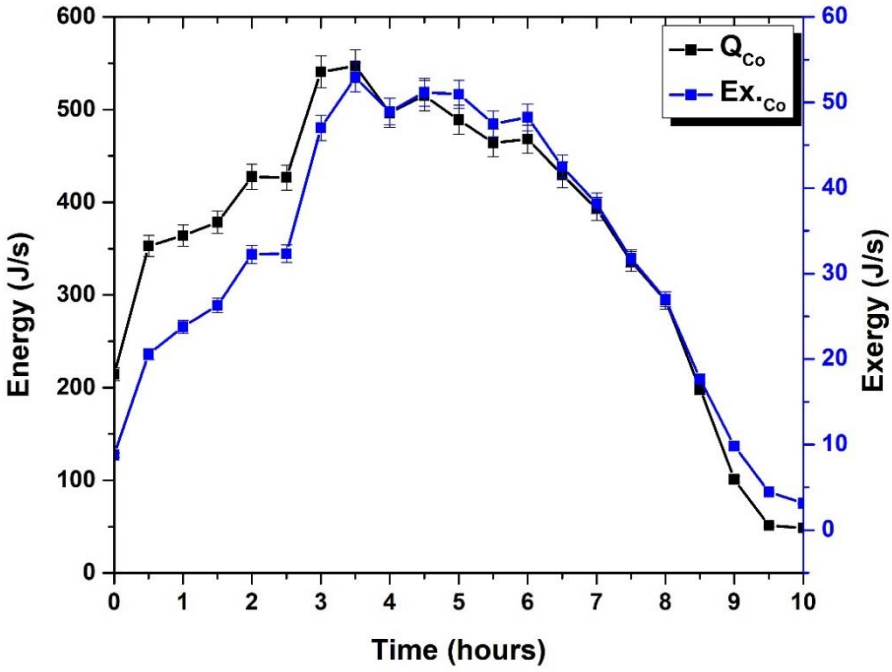

Fig. 5.14 Energy and exergy variations of the hot air at the collector outlet

The thermal and exergetic efficiency of the collector is shown in Fig. 5.15. The energy and exergy efficiency were varied in the range of 15.45–28% and 0.67–1.86% with an average of 19.2% and 1.43%, respectively. The average thermal efficiency of the SAH was reported as 15.31% (Sevik and Abuşka, 2020) and 22% (Vijayan et al., 2016). In this study, the maximum value of thermal efficiency was obtained at 16:30 h while the maximum exergetic efficiency at 11:00 h. In the study, a relatively higher value of exergy efficiency was obtained between 10:00 h and 15:00 h and while a relatively lower value of thermal efficiency was obtained during this period (when solar intensity is higher). Similar findings for the thermal and exergy efficiency were obtained by M. Abus, 2018.

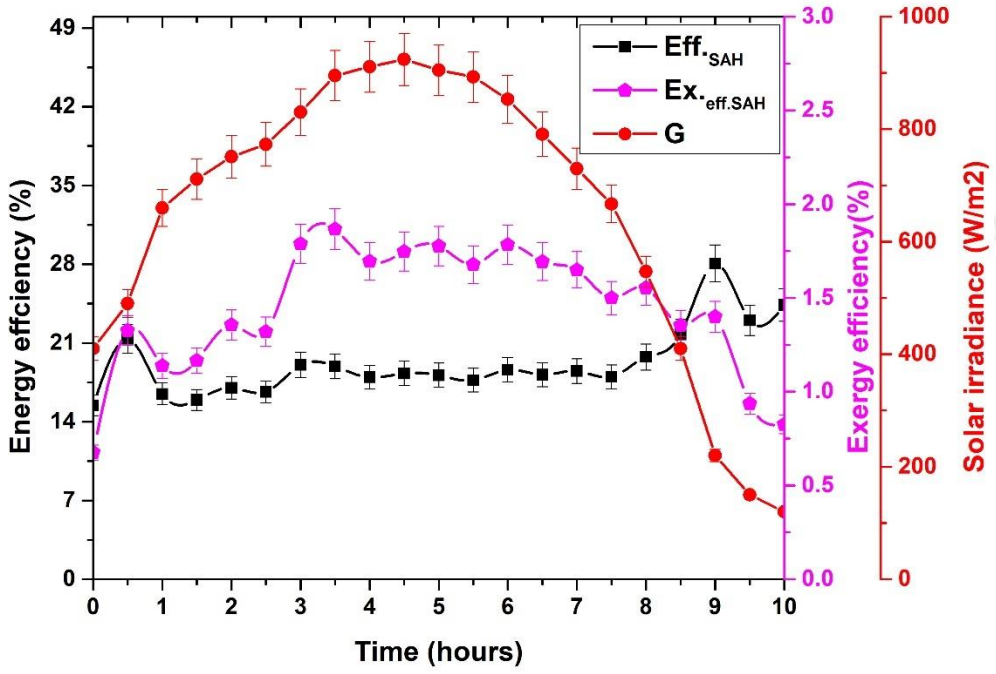

Fig. 5.15 Energy and exergy efficiency variations of the SAH

5.5.2 Energy and exergy analysis of the solar air heater with and without copper tubes attached collector

In this study, the performance of the SAH-1 (flat plate collector) and SAH-2 (flat plate collector with copper tubes) are compared by using the energy-exergy methodology. This study was performed to analyze whether attaching copper tubes to the collector plate enhances the performance of the SAH. This study was conducted between 9 AM and 2 PM. Figure 5.16 shows the collector outlet air temperature, ambient temperature, and solar intensity. The value of solar

intensity was recorded in the range of 728–975 W/m^2 with a mean of 884.18 W/m^2, the collector outlet temperature ranged from 61.8–73.1 °C and 66.2–78.8 °C with a mean of 69.9 °C and 74.28 °C for the SAH-1 and SAH-2, respectively. During the study, the ambient temperature was ranged from 32.7–35.7 °C. From the result, it was found that the collector outlet air temperature varied with variations of solar radiation intensity.

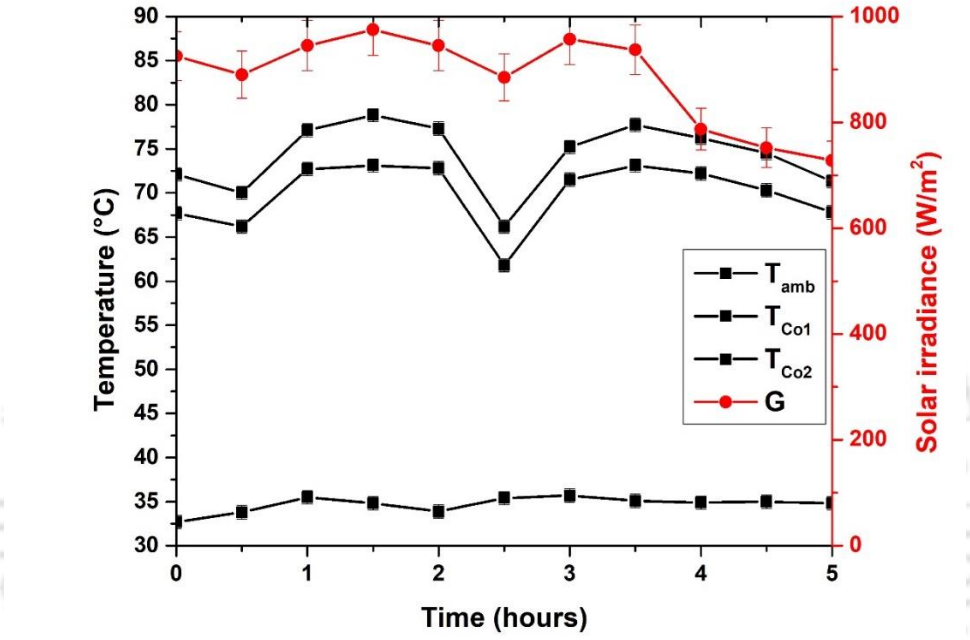

Fig. 5.16 Temperature and solar intensity variations of the SAH-1 and SAH-2

Figure 5.17 presents the exergy received and loss in the SAHs. The exergy received by the SAH was recorded in the range of 1.152–1.5432 kJ/s and the exergy losses ranged from 1.1367–1.5193 kJ/s and 1.1341–1.5134 kJ/s for the SAH-1 and SAH-2, respectively. From the figure, it was seen that a relatively more amount of exergy loss takes place through the SAH-1 as compared to SAH-2. The thermal efficiency and exergy efficiency variations of the SAHs are shown in Figs. 5.18 (a) and (b). The thermal efficiency of the SAH-1 and SAH-2 were ranged from 12.45–17.53% and 14.53–20.36% with an average of 16.32% and 18.3%, respectively. In this study, a higher thermal efficiency was obtained for the SAH-2 as compared to the SAH-1. From Fig. 5.18 (b), the exergetic efficiency of SAH-1 and SAH-2 were ranged from 0.95–1.53% and 1.2–1.939% with an average of 1.41% and 1.69%, respectively. The exergy efficiency for the two SAHs connected in series

was reported as 0.9% and 0.8% (Rabha and Muthukumar, 2017). The exergy efficiency of the roasting and the drying unit was reported as 1.58% and 0.44% (Sheikhshoaei et al., 2019), respectively. The improvement potential of the SAHs is shown in Fig 5.19. The value of improvement potential was varied in the range of 1.12–1.45 kJ/s and 1.116–1.44 kJ/s for the SAH-1 and SAH-2, respectively. The improvement potential of the SAH was reported in the range of 0.74–1.07 kJ/s (Fudholi et al., 2013) for the forced convection mode. In the study, the improvement potential and waste energy ratio obtained for the SAH-1 was relatively higher than that of the SAH-2. That means energy losses from the SAH-2 is relatively lesser than that of the SAH-1.

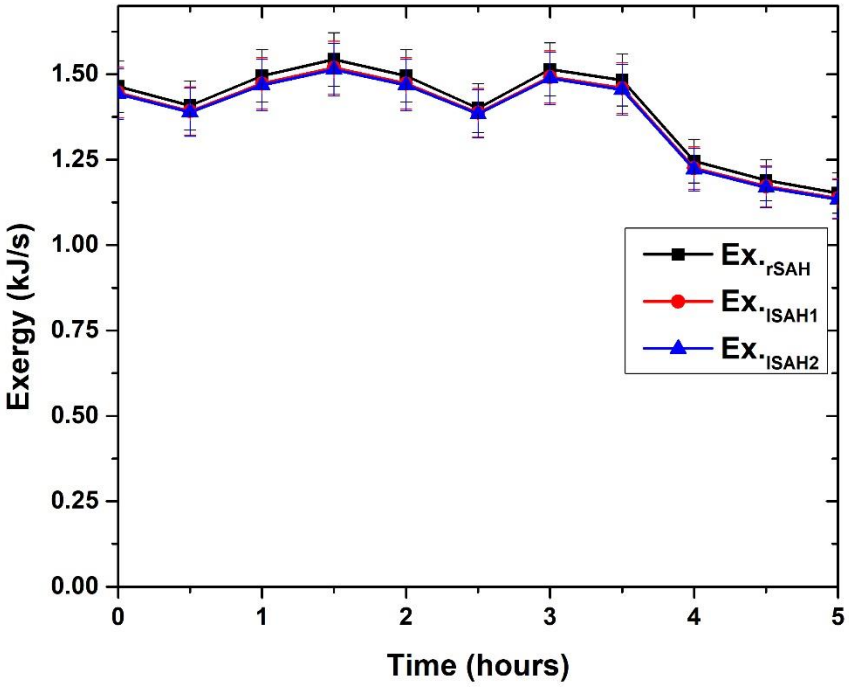

Fig. 5.17 Variations of exergy received and loss in the SAHs

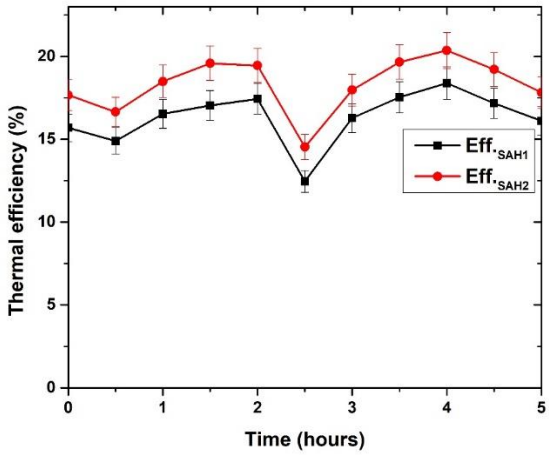

Fig. 5.18 (a) Thermal efficiency of the SAHs

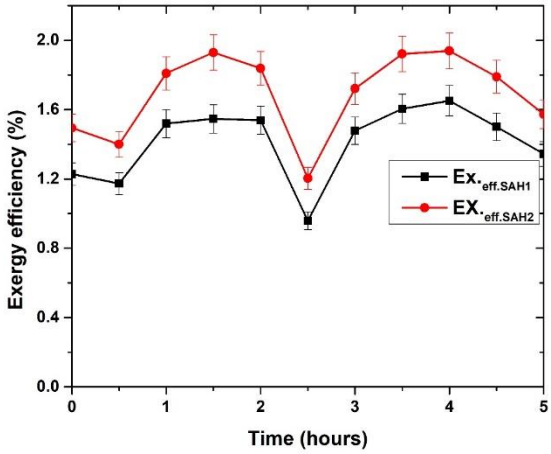

Fig. 5.18 (b) Exergetic efficiency variations of the SAHs

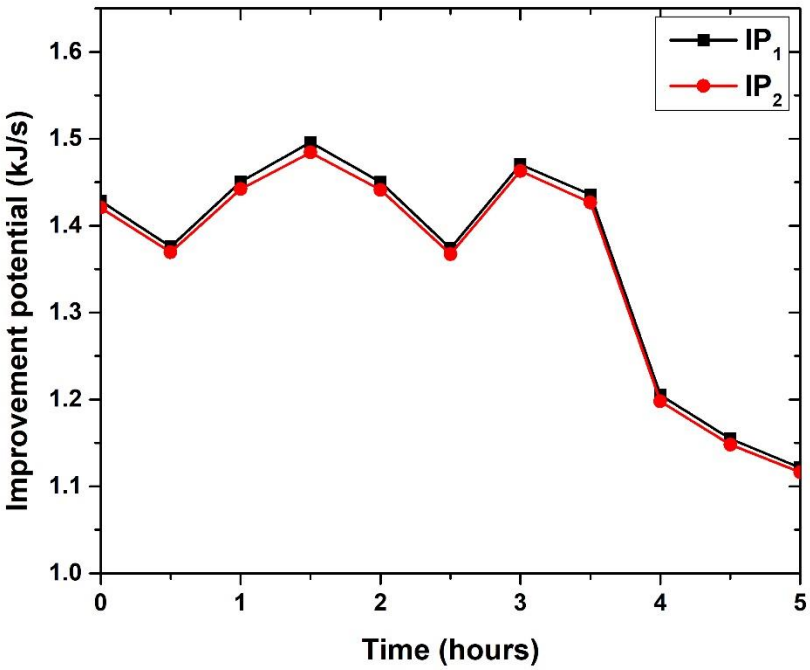

Fig. 5.19 Variations in improvement potential for the SAH-1 and SAH-2

Figures 5.20 (a) and (b) show the waste energy ratio and the sustainability index of the SAHs. The value of the waste energy ratio was found in the range of 0.983–0.99 and 0.9806–0.9879 for the SAH-1 and SAH-2, respectively. During the study, the sustainability index value was recorded in

the range of 1.00095–1.00454 and 1.0012–1.00193 for the SAH-1 and SAH-2, respectively. In this study, relatively higher values of the sustainability index and lower values of the waste energy ratio were obtained for the SAH-2. Hence, the performance of the SAH-2 is better than that of the SAH-1.

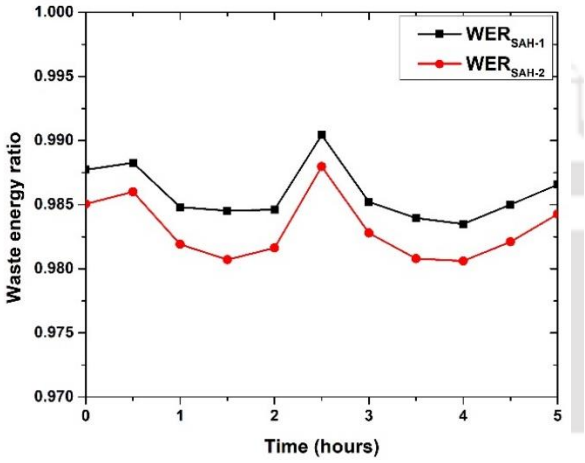

Fig. 5.20 (a) Variations of waste energy ratio for the SAH-1 and SAH-2

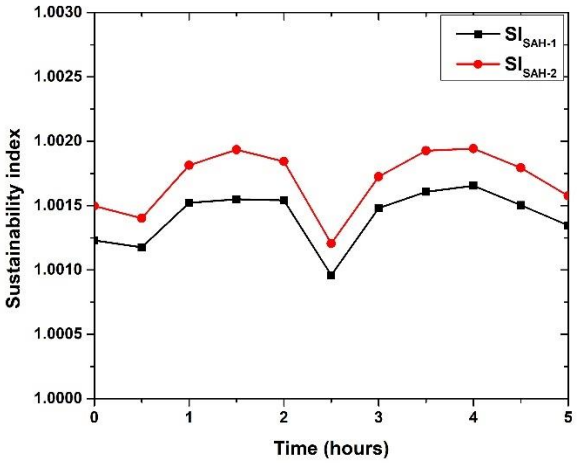

Fig. 5.20 (b) Variations of sustainability index for the SAH-1 and SAH-2

5.6 Energy and exergy analysis of the natural convection solar dryer

5.6.1 Climatic variation and drying curve

The variations in ambient temperature and solar intensity during the study are shown in Fig. 5.21 (a) and the temperature at the various points in the dryer is shown in Fig. 5.21 (b). The solar intensity during the drying process was ranged from 715–987 W/m^2 with a mean of 882.45 W/m^2. In the study, higher values of solar intensity were observed between 10:30 h and 11:00 h. The temperature of ambient air was varied between 33.7 °C and 36.2 °C with a mean of 35.4 °C. During the 5 hours of experimentation, the drying air temperature variations at the inlet and outlet of the SAH were found in the range of 34.8–39.6 °C and 67.55–80.8 °C with an average of 37.58 °C and 75.8 °C, respectively. The drying chamber inlet and outlet air temperature were ranged from 64.8–77.6 °C and 37.1–44.2 °C with a mean of 73 °C and 41.45 °C, respectively. From the result, it can be seen that the temperature at the collector outlet and the drying chamber inlet vary with solar radiation intensity. From the figure, it was also observed that the hot air temperature at the drying chamber outlet increases with time. The main cause to increase the drying chamber

outlet temperature is, as the drying progresses moisture content in the paddy decreases, which required less amount of energy. Hence, energy utilization in the drying chamber decreases with time. Figure 5.22 shows the moisture content of paddy with time. In this study, 12 kg of paddy having an initial moisture content of 33.5% (db) was loaded on the drying tray and it reduced to the desired moisture content after 5 hours of the loading. It was observed from the drying curve that the slope of the curve decreases with time.

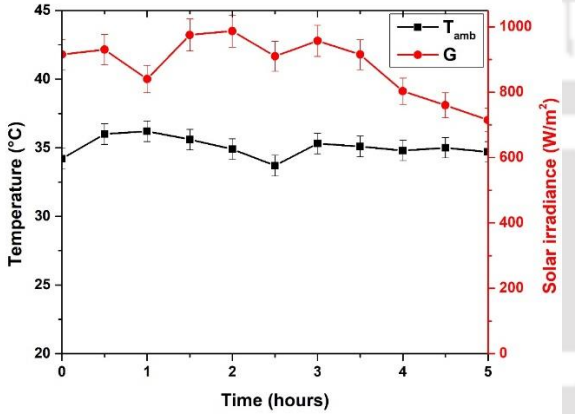

Fig. 5.21 (a) Variations of solar radiation intensity and ambient temperature

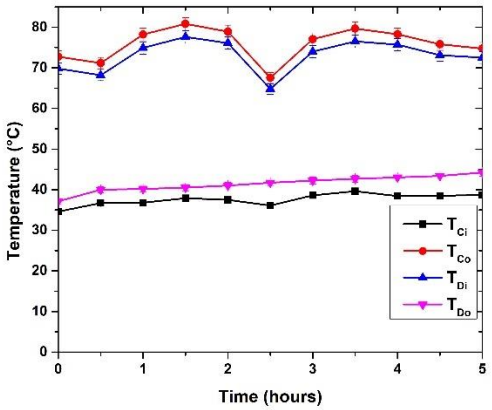

Fig. 5.21 (b) Variations in collector inlet and outlet, drying chamber inlet, and outlet temperatures

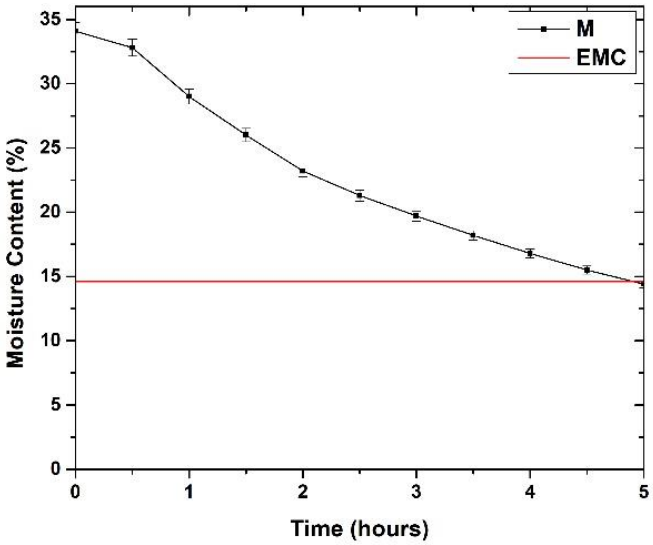

Fig. 5.22 Variations in the moisture content of the paddy

It indicates that the moisture removal rate decreases with time because as drying progresses inner moisture diffuse on the outer surface and evaporate. A similar trend of the drying curve for paddy drying was reported (Zare et al., 2006; Naghavi et al., 2010). A similar trend of decreasing slope of the drying curve was also reported (Bhardwaj et al., 2017) for the Valeriana jatamansi herb and (Karthikeyan and Murugavelh, 2018) for turmeric drying process.

5.6.2 Energy analysis of the natural convection solar dryer

The rate of energy received and loss in the SAHs is shown in Fig. 5.23. The rate of energy received by the SAH was ranged from 2.632–3.567 kJ/s with an average of 3.0849 kJ/s. The heat loss rate from the SAH was varied from 2.06–2.94 kJ/s with a mean of 2.52 kJ/s. From the result, it was observed that the energy received and loss rate by the SAH depend on the solar intensity. Figure 5.24 shows the heat gained by the air at the SAH inlet, SAH outlet, inlet of the drying chamber, heat utilized in the drying process, and the heat loss rate from the PVC pipe. The heat gained by the air at the outlet of SAH was in the range of 0.486–0.624 kJ/s with a mean of 0.564 kJ/s and at the inlet of the drying chamber varied between 0.444 kJ/s and 0.58 kJ/s with an average of 0.524 kJ/s. The energy utilized in the drying chamber ranged from 0.41–0.534 kJ/s and the energy loss rate in the PVC pipe varied between 3 J/s and 45.57 J/s with a mean of 39.73 J/s. From the result, it was found that the heat carried by air at the collector outlet, drying chamber inlet and the heat utilized in the chamber follows the same trend. The maximum heat gained by the air at the inlet of SAH was 62.15 J/s. From the result, it can be seen that the heat gained by the air at the inlet of SAH increases with time. Figure 5.25 shows the efficiency of SAH and the dryer system. The average thermal efficiency of SAH was achieved at 18.46%. Thermal efficiency of the SAH having flat plate collector was reported as 15.31% (Sevik and Abuşka, 2020). The efficiency of the dryer system was achieved between 10.49% and 17.66% with a mean of 14.55%. From the results, it can be seen that the thermal efficiency of the SAH and the dryer system varies with solar radiation intensity. The results show that the efficiency of the SAH and the dryer system was relatively higher at the later stage of the study even though solar radiation intensity was lower. This may be because of the energy stored by the SAH materials.

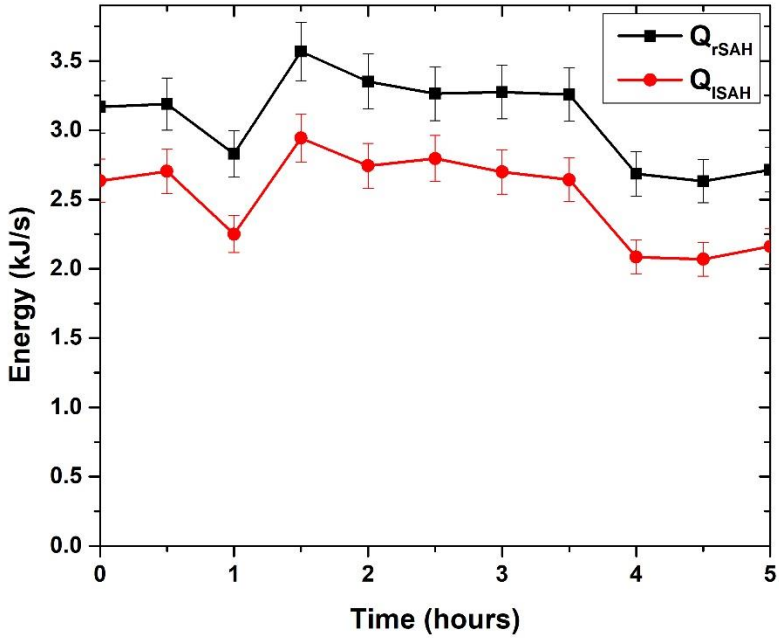

Fig. 5.23 Variations in energy received and loss rate in the SAH

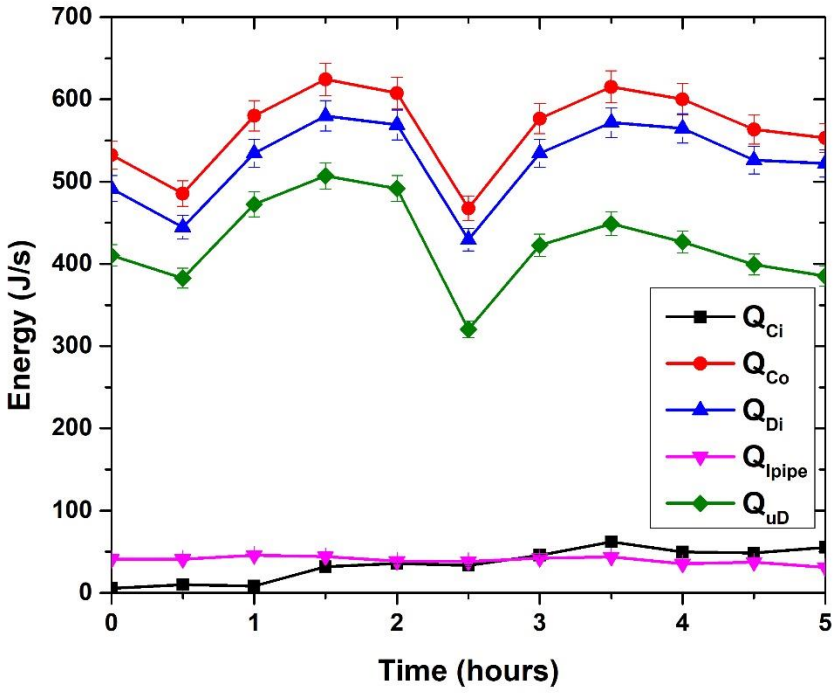

Fig. 5.24 Variations in the energy of air at different points

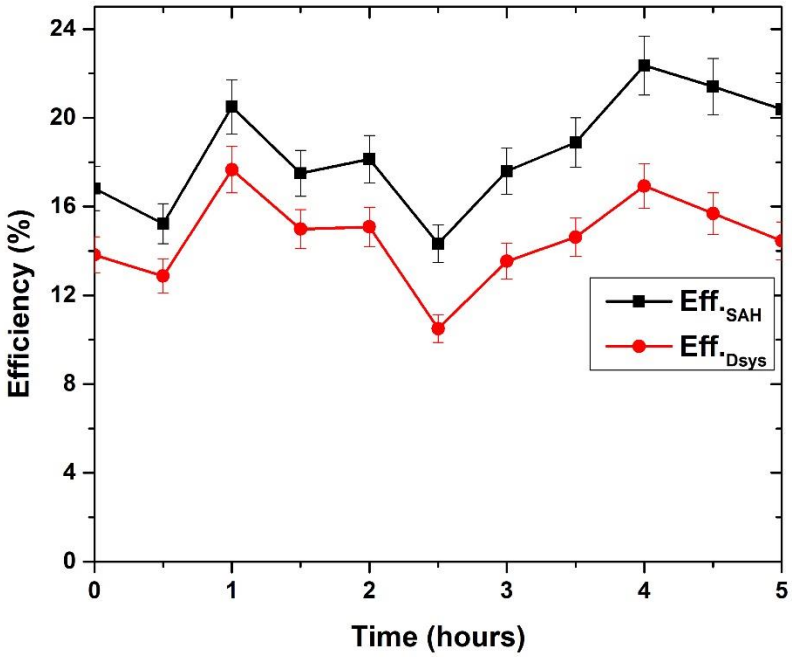

Fig. 5.25 Variations in the thermal efficiency of SAH and the dryer

5.6.3 Exergy analysis of the natural convection solar dryer

The second law analysis is a helpful tool to find the effectiveness of energy utilization in a thermodynamic system. Figure 5.26 shows the rate of exergy received and the loss in the SAHs. The maximum exergy received at the SAH was 3.294 kJ/s with an average of 2.841 kJ/s and the exergy loss from the SAH was recorded between 2.359 kJ/s and 3.237 kJ/s with an average of 2.791 kJ/s. The maximum amount of exergy received, and loss was found between 10:30 h and 11:00 h. From the result, it was found that the exergy loss and gain in the SAH vary with solar intensity. Figure 5.27 shows the changes in exergy at the collector outlet, drying chamber inlet, and the exergy utilized in the drying chamber. The maximum exergy of hot air at the drying chamber inlet and SAH outlet were obtained as 59.91 J/s and 53.34 J/s with a mean of 50.244 J/s and 44.79 J/s, respectively. The maximum amount of exergy utilized in the drying process was recorded as 50.099 J/s with a mean of 40.43 J/s. The main cause of changes in the exergy at the collector outlet and drying chamber inlet is the variation in the solar intensity. The cause of variations in exergy utilization in the drying chamber is due to the variation in the exergy of hot air at the inlet of the drying chamber.

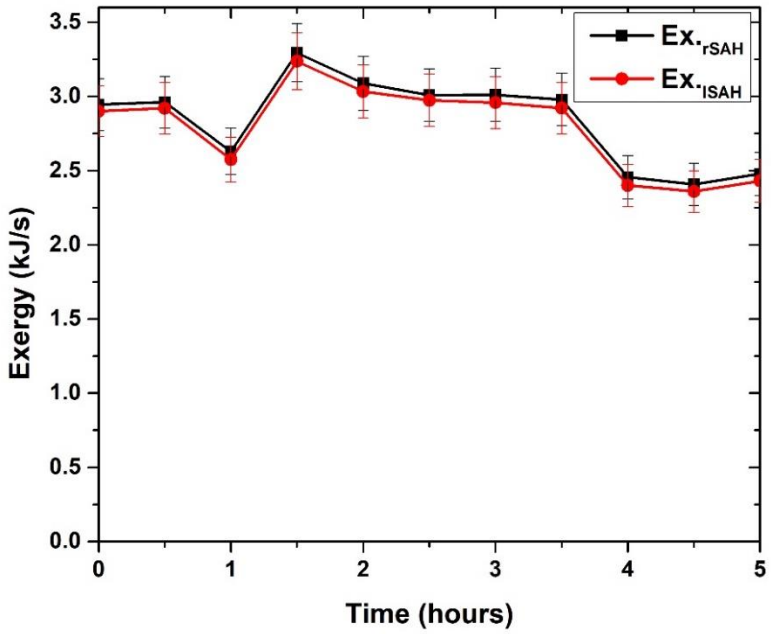

Fig. 5.26 Variations in exergy received and loss rate in the SAH

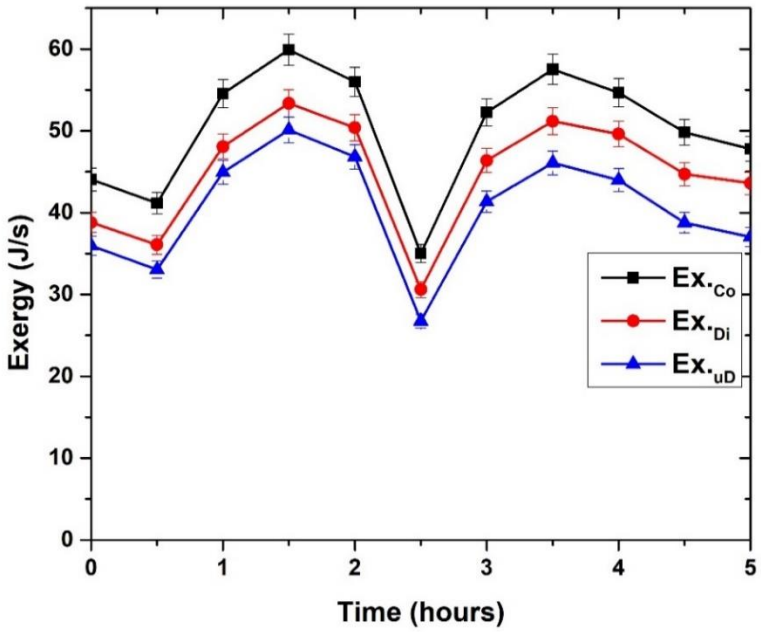

Fig. 5.27 Variations in exergy at collector outlet, drying chamber inlet, and exergy utilized in the drying chamber

The exergy gained by the air at the inlet of SAH and exergy loss in the pipe is shown in Fig. 5.28. The exergy of air at the inlet of SAH and exergy loss in the pipe were ranged from 1.35–3.63 J/s and 4.19–6.56 J/s with an average of 2.62 J/s and 4.45 J/s, respectively. From the result, it was found that the exergy gained by the air at the inlet of SAH and the exergy loss through the pipe varies randomly and it shows dependency on solar intensity. Figure 5.29 shows the second law efficiency of the SAH and the dryer system. The exergetic efficiency of the SAH and dryer system were obtained from 1.16–2.22% and 0.88–1.78% with an average of 1.78% and 1.43%, respectively. The exergy efficiency of a wood chips dryer was reported as 4.39% (Coskun et al., 2009). The exergy efficiency for the two SAHs connected in series was reported as 0.9% and 0.8% (Rabha and Muthukumar, 2017). The exergy efficiency of the roasting and the drying unit was reported as 1.58% and 0.44% (Sheikhshoaei et al., 2019), respectively. Figure 5.30 (a) shows the variations in the improvement potential. The improvement potential varied in the range of 2.62–5.59 J/s with an average of 3.9 J/s. A similar range of improvement potential variation from 0–17 J/s was reported by (Akpinar, 2010a) for the mint leaves drying process. Figure 5.30 (b) shows the sustainability index and waste energy ratio of the drying chamber. From the figure, a random variation in the sustainability index and waste energy ratio was observed.

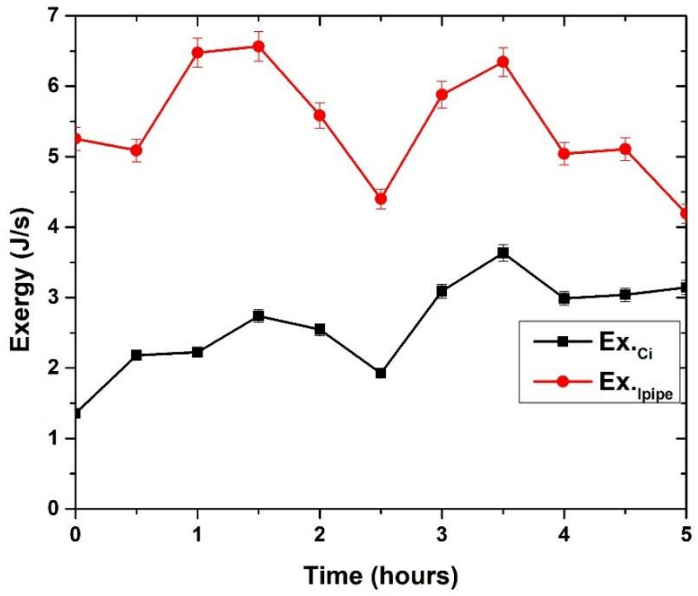

Fig. 5.28 Exergy of air at the inlet of SAH and exergy loss at the inlet to the drying chamber

The sustainability index varied in the range of 6.62–16.41 and the waste energy ratio varied from 6.09–15.1%. From the result, it was observed that the sustainability index follows the same trend as the exergy efficiency while the waste energy ratio shows the reverse trend of the exergy efficiency. The performance parameters of the present study are shown in Table 5.1.

Table 5.1 Performance of the natural convection solar dryer

Parameter and performance	Value
The initial mass of the product (kg)	12
The final mass of the product (kg)	9.35
Initial moisture content (%)	33.5
Final moisture content (%)	14.7
Drying time (hours)	5
SAH thermal efficiency (%)	18.46
Thermal efficiency of the dryer (%)	14.45
SAH exergy efficiency (%)	1.78
The overall exergetic efficiency of the dryer (%)	1.43

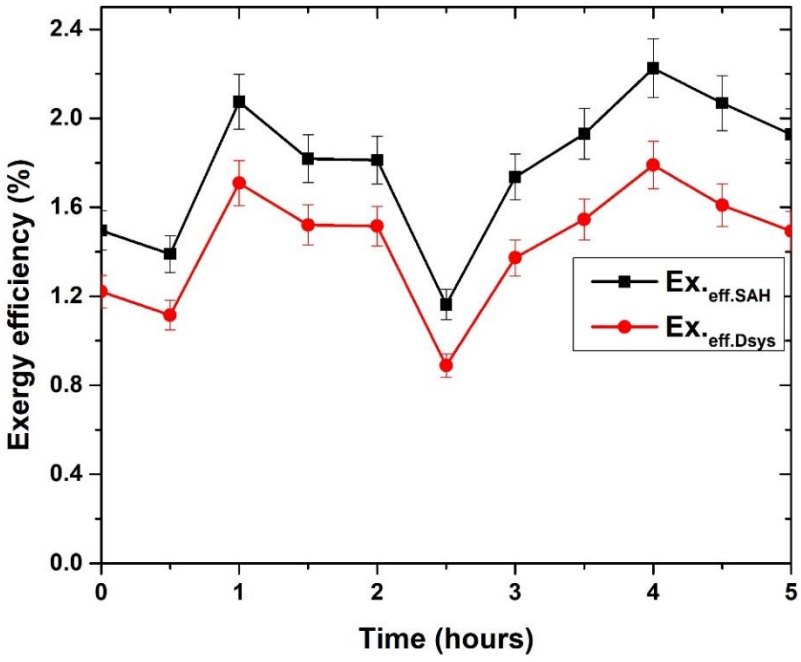

Fig. 5.29 Variations in exergy efficiency of SAH and the solar dryer

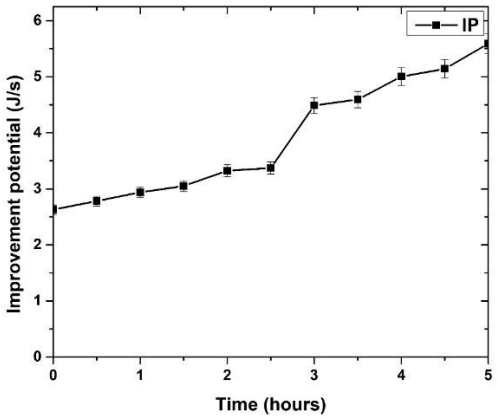

Fig. 5.30 (a) Variations in improvement potential rate with time

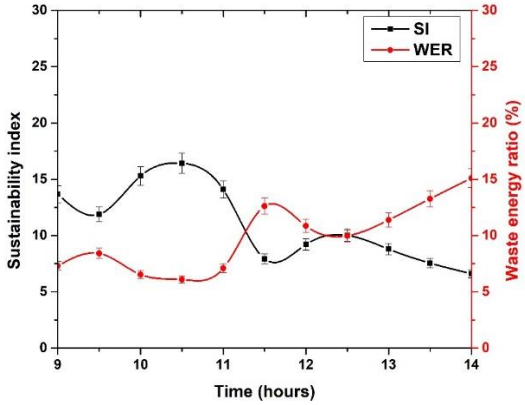

Fig. 5.30 (b) Variations in sustainability index and waste energy ratio

5.7 Energy and exergy analysis of the forced convection solar dryer

5.7.1 Performance analysis of SAH at varying air mass flowrate

This study was performed to utilize most of the solar energy received by the collector and it was optimized by varying air mass flow rates in the SAH. This study was conducted between 10:30 AM to 11:30 AM because solar irradiance variations was relatively low during this period. Figure 5.31 (a) presents the collector outlet air temperature with air flowrate. In this study, the collector outlet air temperature decreased from 80.55–68.7°C for the air mass flowrate variations of 0.0166–0.0582 kg/s. During the study, solar radiation intensity was varied in the range of 888–910 W/m^2. From the figure, it was observed that the collector outlet air temperature decreases with an increase in air mass flowrate. Similar results were reported (Akpinar and Koçyiĝit, 2010) where air achieved higher temperature at the lower airflow rate. Figure 5.31 (b) shows the heat gained by the air at the collector outlet, heat loss from the SAH, and efficiency of the SAH. From the results, it was observed that the maximum value of heat gained at the collector outlet and thermal efficiency of the SAH was obtained for the air mass flow rate of 0.05 kg/s. The lower value of the heat loss through the SAH was obtained at the air mass flow rate of 0.05 kg/s. The maximum value of the thermal efficiency was obtained at 62.8%. A similar result was reported (Akpinar and Koçyiĝit, 2010; Alta et al., 2010) where thermal efficiency of the SAH increases with air mass

flowrate. The maximum value of the collector thermal efficiency was reported 83.56% (Şevik et al., 2019b). The exergy at the collector outlet, exergy destruction in the SAH, and the exergetic efficiency of the SAH are presented in Fig. 5.31 (c). From the figure, it can be seen that the exergy at the collector outlet and the exergetic efficiency increases up to the air mass flow rate of 0.05 kg/s and then decreases. The exergy destruction decreases with air mass flow rate up to 0.05 kg/s and after that its value increases. The highest value of the exergetic efficiency and the lowest value of the exergy destruction were obtained at the air mass flow rate of 0.05 kg/s.

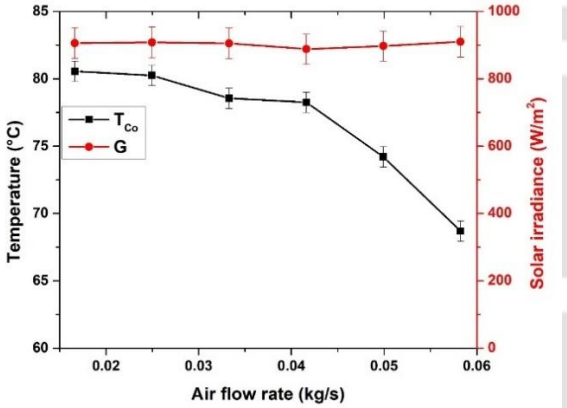

Fig. 5.31 (a) Variations in the collector outlet air temperature with air flowrate

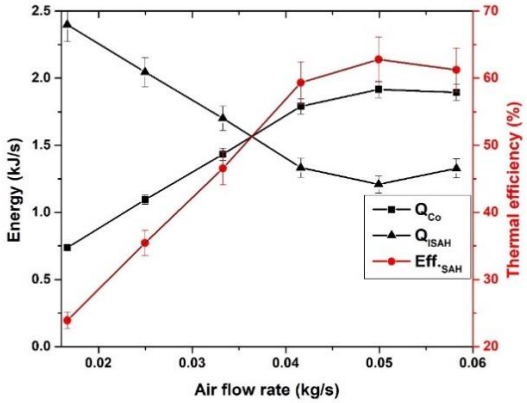

Fig. 5.31 (b) Variations in energy at collector outlet, energy loss, and efficiency of the SAH

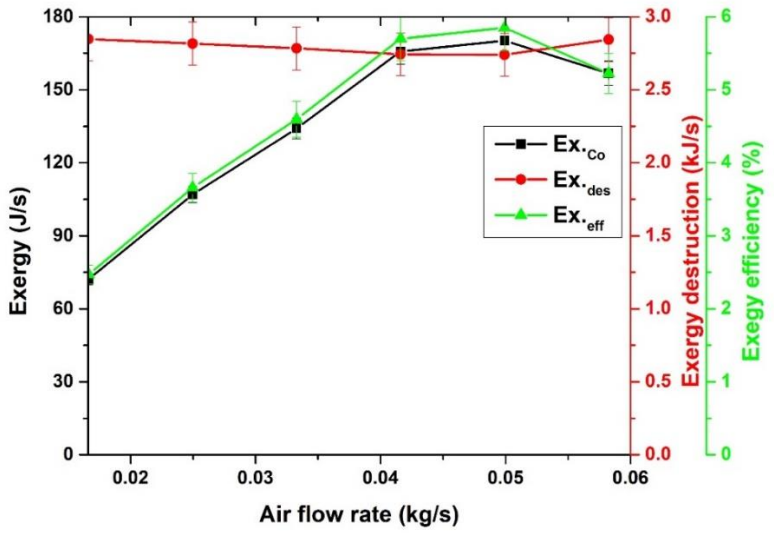

Fig. 5.31 (c) Variations in exergy at collector outlet, exergy destruction, and exergetic efficiency of the SAH

The maximum value of the exergetic efficiency of the SAH was recorded at 5.848%. The maximum exergy efficiency of the SAH was reported as 4.36% (Matheswaran et al., 2018) for the air mass flow rates of 0.035 kg/s.

5.7.2 Climatic variation and drying curve

This investigation was performed during October 2019 from 9:00 h to 13:00 h for the paddy drying process. During the study, all the experimental data were recorded at an interval of 30 minutes. The variations in solar irradiance, ambient temperature and the temperature at various points in the dryer is shown in Fig. 5.32 (a). The solar intensity during the drying process was ranged from 700–970 W/m^2 with a mean of 849.88 W/m^2. During the investigation, a higher value of solar intensity was observed between 10:30 h and 11:30 h. The ambient temperature varied between 32.6 °C and 36.7 °C with a mean of 34.63 °C. The air temperature variations at the inlet and outlet of the SAH were found in the range of 34.6–37.9 °C and 58.3–81.65 °C with an average of 36.15 °C and 72.51 °C, respectively. The drying chamber inlet and outlet air temperature were ranged from 56.7–79.4 °C and 34.8–47.6 °C with a mean of 70.7 °C and 42.51 °C, respectively. From the results, it can be seen that the temperature at the corresponding points in the dryer varies with solar radiation intensity.

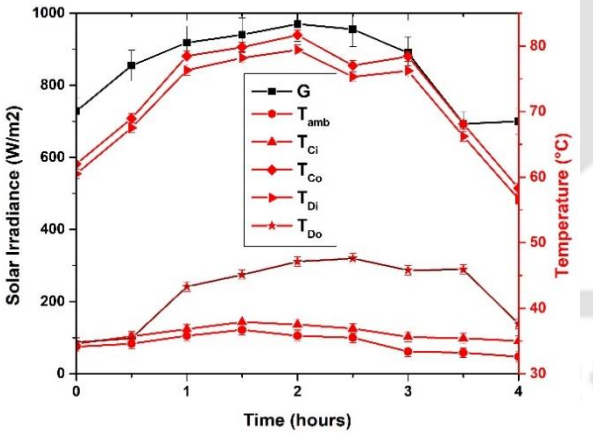

Fig. 5.32 (a) Variations in solar irradiance and temperature at the various points in the dryer

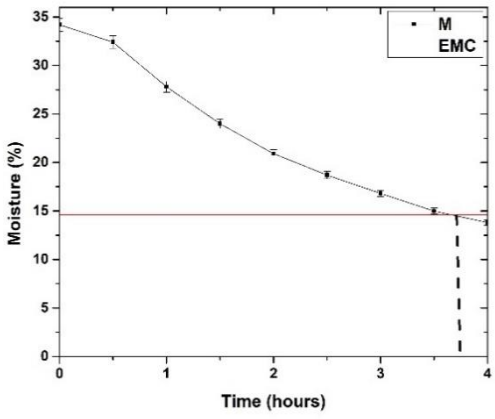

Fig. 5.32 (b) Variations in the moisture content of the paddy

Figure 5.32 (b) shows the moisture content variation of paddy with time. In this study, 12 kg of paddy having an initial moisture content of 34.2% (db) was loaded on the drying tray at 9 AM and

it reduced to 13.8% of moisture content after 4 hours of the loading. From the result, it was observed that the slope of the drying curve decreases with time. It indicates that the moisture removal rate from the paddy decreases with time. The main cause of the decreasing moisture removal rate is, at the start of the drying process surface moisture removal takes place. As time progresses, inner moisture removal takes place due to the diffusion process, it required time hence moisture removal rate decreases. A similar trend of the drying curve for paddy drying was reported by (Zare et al., 2006), (Naghavi et al., 2010). A decreasing slope of the drying curve was also reported by (Bhardwaj et al., 2017) for the Valeriana jatamansi herb, (Karthikeyan and Murugavelh, 2018) for turmeric, (El-Sebaii and Shalaby, 2012) for mint and (Rabha et al., 2017a) for the ghost chili pepper and ginger drying, respectively.

5.7.3 Energy analysis of the forced convection solar dryer

The energy at the various points in the dryer is shown in Figs. 5.33 (a) and (b). The rate of heat received by the SAH was ranged from 2.46–3.38 kJ/s with an average of 2.96 kJ/s and the rate of energy gained by the hot air at the collector outlet varied in the range of 1.29–2.3 kJ/s with a mean of 1.9 kJ/s. The heat loss rate from the SAH was varied from 0.709–1.233 kJ/s with a mean of 1.059 kJ/s. From the result, it was observed that the energy received by the collector, energy gained by the hot air, and the energy loss from the SAH depend on the solar intensity. As solar radiation intensity increases, energy at the corresponding points increases. The heat gained by the air at the collector inlet, drying chamber inlet, heat utilized in the drying process, heat loss from the PVC pipe, and the energy loss at the outlet of the drying chamber are shown in Fig. 5.33 (b). The heat gained by the hot air at the inlet of the drying chamber was varied between 1.26 kJ/s and 2.19 kJ/s with an average of 1.81 kJ/s and the energy utilized in the drying chamber ranged from 1.07–1.77 kJ/s. The energy loss rate in the PVC pipe and at the drying chamber outlet were varied from 73–132.28 J/s and 35.17–477.93 J/s with a mean of 91.47 J/s and 297.44 J/s, respectively. From the result, it was found that the heat carried by air at the drying chamber inlet and the heat utilized in the chamber follow the same trend. At the initial period of drying, the hot air energy utilization in the drying chamber was relatively high. That is because, at the start of the drying process, a relatively high amount of energy is required to heat the paddy and remove the moisture. From the figure, it can be seen that the heat carried by air at the drying chamber outlet increases with time. That is because as drying progresses, the water molecules in the paddy decrease hence

the heat utilized in the paddy drying process decreases with time. The maximum heat gained by the air at the collector inlet was 120.84 W with a mean of 62.7 W.

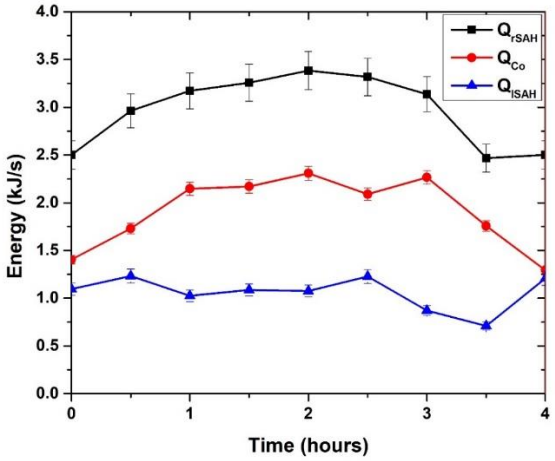

Fig. 5.33 (a) Variations in energy received, loss and at the outlet of the SAH

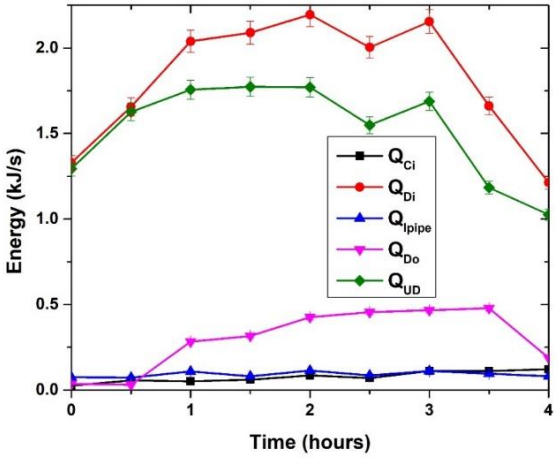

Fig. 5.33 (b) Variations in the energy of the drying air at various points in the dryer

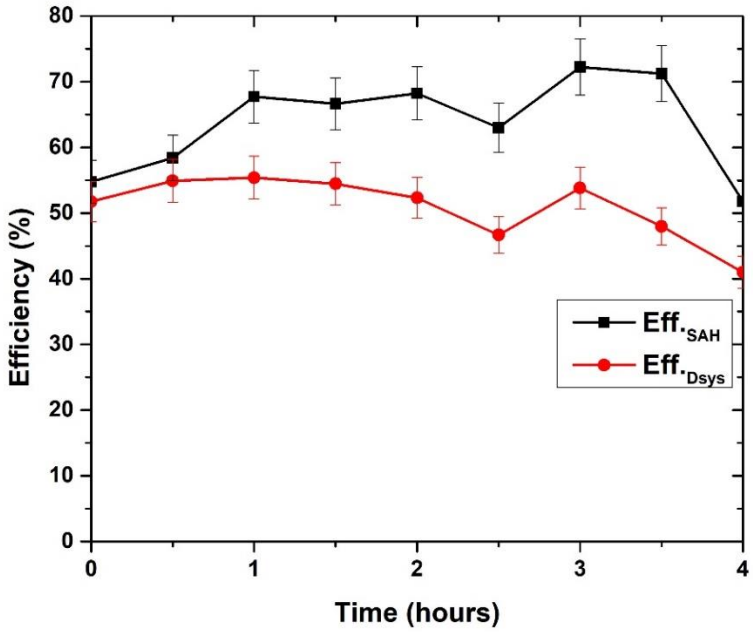

Fig. 5.34 Variations in the thermal efficiency of the SAH and the dryer system

Figure 5.34 shows the thermal efficiency of the SAH and the dryer system. The collector efficiency was obtained in the range of 51.54–72.23% with an average of 63.76%. The collector efficiency was reported in the range of 9–48% (Fudholi et al., 2015), an average thermal efficiency for SAH-1 was reported as 56.3% (Lakshmi et al., 2019) and the maximum value of the collector efficiency was reported as 88.66% (Şevik et al., 2019b). In the present study, SAH efficiency and the overall efficiency of the dryer system vary with solar radiation intensity. The thermal efficiency of the dryer system was recorded between 40.99% and 55.39% with a mean of 50.92%.

5.7.4 Exergy analysis of the forced convection solar dryer

The exergy received and the losses in the SAH are shown in Fig. 5.35 (a) and the exergy of hot air at various points in the dryer is shown in Fig. 5.35 (b). The maximum value of exergy received at the SAH was 3.079 kJ/s with an average of 2.697 kJ/s and the exergy loss from the SAH was recorded between 2.068 kJ/s and 2.854 kJ/s with an average of 2.534 kJ/s. The maximum amount of exergy received and loss was found between 10:30 h and 11:30 h. From the result, it was found that the exergy received and loss in the SAH vary with solar radiation intensity and follow a similar trend. The maximum exergy of hot air at the drying chamber inlet and SAH outlet were obtained as 207.79 J/s and 224.98 J/s with a mean of 151 J/s and 163.1 J/s, respectively. The maximum amount of exergy utilized in the drying process was recorded as 174.85 J/s with a mean of 129.4 J/s. The exergy of air at the inlet of SAH and exergy loss in the pipe were ranged from 4.94–9.98 J/s and 7.46–17.19 J/s with an average of 9 J/s and 12 J/s, respectively. The main cause of changes in the exergy at the collector outlet and drying chamber inlet is the variation in the solar intensity. The variations in exergy utilization in the drying chamber are due to the variation in the exergy of hot air at the inlet of the drying chamber. The exergy of air at the drying chamber outlet varied in the range of 5.21–34.54 J/s with an average of 21.67 J/s. The performance parameters of the present study are shown in Table 5.2.

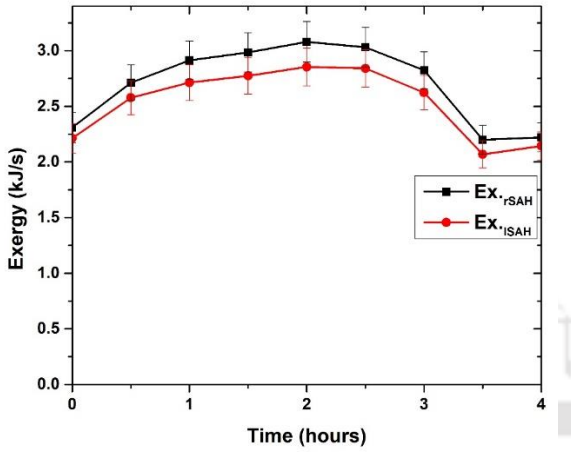

Fig. 5.35 (a) Variations in exergy received and loss in the SAH with time

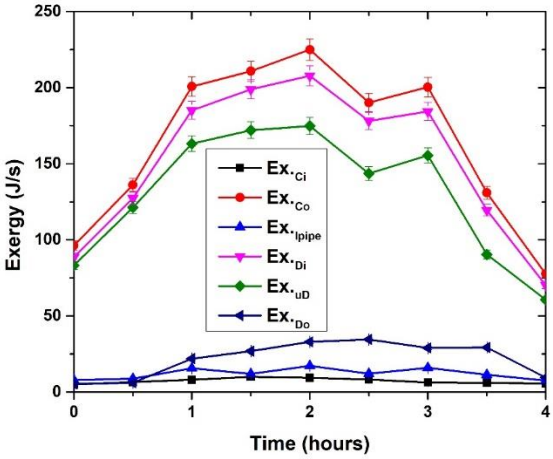

Fig. 5.35 (b) Variations in exergy at collector inlet and outlet, drying chamber inlet, outlet, and utilized exergy in the drying chamber

Table 5.2 Performance of the forced convection solar dryer

Parameters and performance	Value
Initial mass of the product (kg)	12
Final mass of the product (kg)	9.16
Initial moisture content (%)	34.2
Final moisture content (%)	13.8
Drying time (hours)	4
SAH thermal efficiency (%)	63.76
Energy efficiency of the solar dryer (%)	50.92
SAH exergy efficiency (%)	5.91
The exergetic efficiency of the solar dryer (%)	4.68

Figure 5.36 shows the second law efficiency of the SAH and the dryer system. The exergetic efficiency of the SAH and dryer system were obtained from 3.49–7.3% and 2.73–5.76% with an average of 5.91% and 4.68%, respectively. The exergy efficiency for the two SAHs connected in series was reported as 0.9% and 0.8% (Rabha and Muthukumar, 2017). The exergy efficiency of a wood chips dryer was reported as 4.39% (Coskun et al., 2009) and the exergy efficiency of the

roasting and the drying unit was reported as 1.58% and 0.44% (Sheikhshoaei et al., 2019), respectively.

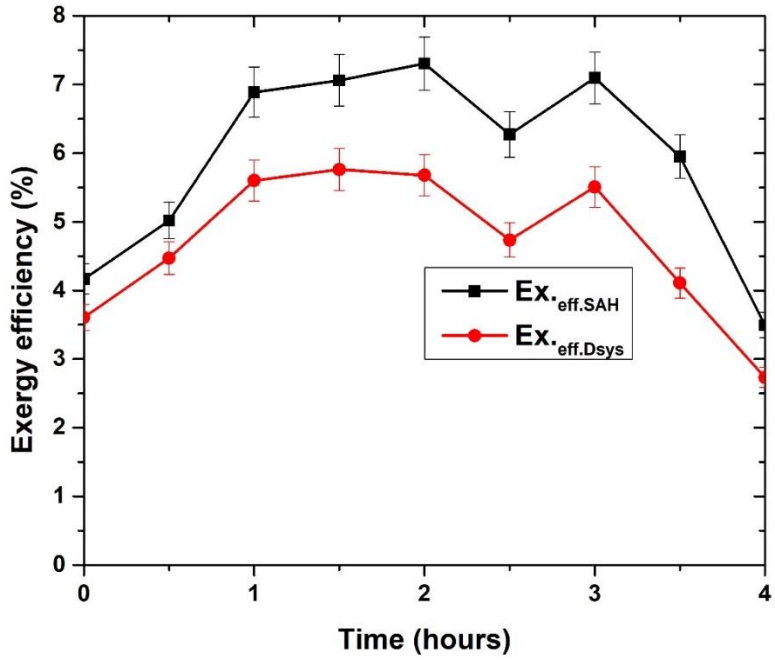

Fig. 5.36 Variations in exergy efficiency of SAH and the dryer system

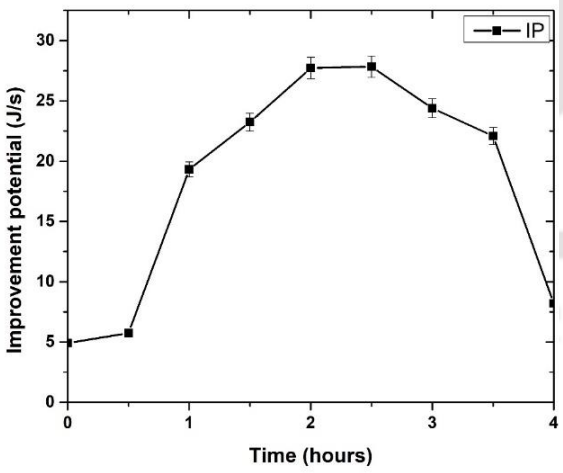

Fig. 5.37 (a) Variations in the improvement potential with time

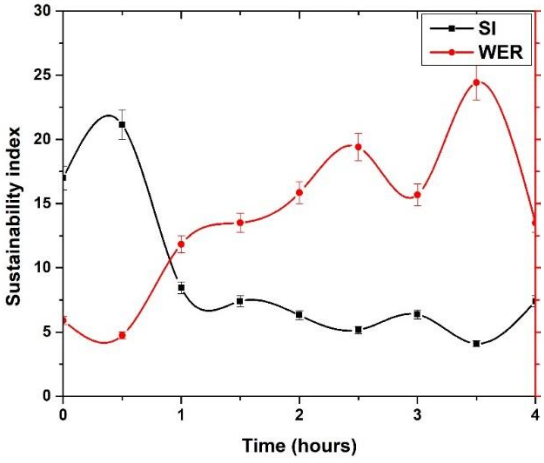

Fig. 5.37 (b) Variations in the sustainability index and waste energy ratio

The variations in improvement potential are presented in Fig. 5.37 (a). The improvement potential was varied in the range of 4.9–27.84 J/s with an average of 18.15 J/s. The improvement potential variations for the mint leaves drying process were reported in the range of 0–17 J/s (Akpinar, 2010a). The sustainability index and waste energy ratio of the drying chamber is shown in Fig. 5.37 (b). From the figure, it was found that the sustainability index and waste energy ratio varied randomly in the range of 4.09–21.14 and 4.73–24.43% with an average of 9.25 and 13.87%, respectively. From the result, it can be seen that the sustainability index follows the same trend as the exergy efficiency while the waste energy ratio shows the reverse trend.

5.8 Summary

In this chapter, energy and exergy analysis of the dryer have been performed. From the study, it was observed that the use of a sensible heat storage medium reduces the energy and exergy losses from the rectangular chamber of the biomass-operated dryer. In this study, Case-III (with sensible thermal storage medium and hot air from the rectangular chamber is not allowed to the drying tray) was considered as the best condition. In the modified dryer, case-III (with sensible thermal storage medium and the exhaust valve is closed at the end of biomass burning) was considered as the best drying condition. From the study, it was found that the energy losses in the flue gas are lower in the modified dryer. In the solar dryer, the average value of energy and exergy efficiency of the solar air heaters under natural convection mode was found to be 18.46% and 1.78%, respectively. The overall energy and exergy efficiency of the dryer were found as 14.45% and 1.43%, respectively. The maximum value of the energy and exergy efficiency of the solar air heaters under forced convection mode were obtained as 63.76% and 5.91%, respectively. The energy and exergy efficiency of the dryer were ranged from 40.99–55.39% and 2.73–5.76% with an average of 50.92% and 4.685%, respectively. In this study, the thermal efficiency of the forced convection solar dryer was found to be higher as compared to the natural convection solar dryer. The major conclusions of the thesis and the scope of future work are discussed in the next chapter.

Chapter 6

Conclusions and future works

6.1 Conclusions

The present investigation is attempted to analyze the performance of the biomass-operated grain dryer, solar dryer under natural and forced convection mode, and biomass-solar hybrid dryer. The drying characteristics of paddy in the biomass-operated dryer, solar dryer and solar-biomass hybrid dryer has been performed. The performance study of the dryer has also been carried out with the help of thermodynamic analysis. The performance of each component of the dryer is conducted with the help of energy-exergy methodology. The major findings of the study are presented in the following subsections.

6.1.1 Drying characteristics of paddy in the biomass-operated dryer

This study has been performed for three different cases viz. (i) without sensible thermal storage in the rectangular chamber, (ii) with sensible thermal storage in the rectangular chamber, and (iii) with sensible thermal storage and the exhaust valve was closed after biomass burning. The drying kinetics of paddy has been performed in the developed dryer. 12 kg paddy having initial moisture content of 33.1%, 33.2% and 33% has been dried to the final level of moisture content of 16.9%, 16.1% and 13.2% in 7.5 hours in the case-I, case-II and case-III, respectively. During the study, the products achieved the equilibrium moisture content (EMC) in about 5.5 hours only in the case-III. Hence, the performance of the dryer was analyzed for the different masses of paddy in the case-III and 12 kg inventory was found as most suitable for the dryer. The drying kinetics of 12 kg inventory has been studied. The values of the drying rate were ranged from 0.01–0.056 kg/kg h with an average of 0.032 kg/kg h. The drying curve of the paddy was fitted with 8 mathematical models. The best model was selected on the basis of lowest value of reduced chi-square (χ^2) and root mean square error (RMSE), and the highest value of the determination coefficient (R^2). The following important conclusions has been obtained in the present study.

- The faster drying of the product was obtained in the case-III. Hence, case-III is considered as the best for the paddy drying process.

- The maximum value of temperature in the drying chamber was recorded as 48.2 °C with an average of 43.45 °C in case-III (with sensible thermal storage and the exhaust valve was closed after biomass burning).
- The Wang and Singh model was found to be most suitable to describe the drying process of paddy in the dryer.
- The values of χ^2, RMSE and R^2 were obtained as 0.001079, 0.0328563, and 0.99964, respectively.

6.1.2 Drying characteristics of paddy in the natural convection solar dryer

In this study, the experiments were performed for three different inventories viz. 10 kg, 12 kg, and 14 kg, and the drying characteristics were analyzed. During the study, the inventories of masses 10 kg, 12 kg and 14 kg having moisture content of 33.4%, 34.1% and 33.9% has been successfully dried in 4.5 hours, 5 hours and 6 hours. In this dryer, 12 kg inventory was considered as the best for the drying process. Therefore, the drying kinetics of the 12 kg inventory has been analysed in the present study. The moisture evaporation rate and the drying rate values were varied in the range of 4–20.99 g/min and 0.022–0.076 kg/kg h, respectively. The average value of specific moisture extraction rate (SMER) was obtained as 0.152 kg/kWh. The drying curve of paddy was fitted with eight mathematical drying models. The following important conclusions have been obtained in the present study.

- The air temperature in the drying chamber during 12 kg paddy drying was ranged from 43.48–48.88 °C with a mean of 46.68 °C.
- It took five hours to achieve equilibrium moisture content (EMC). Hence, this amount of paddy can be dry two batches per day.
- The Verma model was found to be most suitable to describe the drying process of paddy in the dryer.
- The values of χ^2, RMSE and R^2 were obtained in the selected model as 0.00065 0.02175 and 0.99533, respectively.

6.1.3 Drying characteristics of paddy in the forced convection solar dryer

In this study, the experiments were performed for 12 kg, 16 kg, and 20 kg inventory, and the drying behaviors of paddy were analyzed. During the study, 12 kg, 16 kg and 20 kg inventory have been successfully dried in 3 hours 45 minutes, 4 hours 50 minutes, and 6 hours 50 minutes respectively. In this dryer, 16 kg inventory was considered as the most suitable for the drying of paddy. Therefore, the drying kinetics of the 16 kg inventory has been analysed in the present study. The value of moisture evaporation rate was recorded as 12.37 g/min. The drying rate and the specific moisture extraction rate were reported as 0.0398 (kg/kg h) and 0.22 kg/kWh, respectively. The drying curve of the paddy was fitted with eight mathematical drying models. The important conclusions from this study are as follows.

- The air temperature in the drying chamber was ranged from 38.96–56.36°C with an average of 51.41°C.
- The time needed to achieve the EMC of 16 kg paddy is 4 hours 50 minutes.
- In this study, the Page and the modified Page model was best fitted for the paddy drying process.
- The values of χ^2, RMSE and R^2 were achieved as 0.00036, 0.01907, and 0.99644, respectively.
- Forced convection solar dryer dries 12 kg product in 3 hours 45 minutes, while the natural convection solar dryer took 5 hours for the same amount of product.
- The forced convection mode dries the product faster as compared to the natural convection mode of solar dryer.
- Relatively wider range of temperature in the drying chamber was obtained in the forced convection mode.

6.1.4 Performance of the hybrid dryer

The air temperature in the drying chamber was ranged from 36.4–47.7 °C and 36.1–57.8 °C for the natural and forced convection mode of the solar-biomass hybrid dryer. This study found that the natural convection hybrid dryer could dry 48 kg of paddy per day while the forced convection hybrid dryer could dry 56 kg paddy. In the study, the amount of biomass burnt in the conical furnace under the natural and forced convection hybrid dryer during the night period was 12.5 kg. The important conclusions from this study are as follows.

- The wide range of temperature (36.1–57.8 °C) in the drying chamber was obtained in the forced convection hybrid dryer.
- The drying capacity of the forced convection hybrid dryer was found to be higher than that of the natural convection hybrid dryer.
- Coupling the solar air heaters to the biomass-operated dryer reduces biomass consumption by about 40%. Because the drying process is continued for about 10 hours/day using solar energy as an input source.

6.1.5 Energy and exergy analysis of the biomass-operated dryer

This study has been performed to enhance the performance of the biomass-operated dryer. The effect of the sensible heat storage medium in the rectangular chamber was studied. In the study, it was found that the sensible thermal storage reduces the energy losses in the dryer. It will reduce the energy consumption in the agricultural products drying process. Hence, enhances the performance of the dryer. The energy retaining capacity of the hot air in the dryer was higher in the case-III (when the sensible thermal storage is present in the rectangular chamber and the hot air is not allowed to the drying chamber), it provides the uniformity of temperature in the paraffin wax tray. The performance of the dryer has also been analyzed by utilizing the flue gas energy in the rectangular chamber below the PCM tray (modified biomass-operated dryer). The energy and exergy analysis of the modified dryer has been performed and observed that allowing the flue gas in the rectangular chamber reduces the energy losses in the flue gas through the exhaust pipe. The energy retaining capacity of the hot air in the drying chamber of the modified dryer was found to be higher for a longer period in the case-III (when the sensible thermal storage is present in the rectangular chamber and the exhaust valve is closed at the end of biomass burning). The major conclusions of this study are as follows.

- The use of sensible thermal storage medium reduces the energy losses from the rectangular chamber (brick wall) and retains heat for a longer time in the dryer.
- It reduces the exergy destruction in the rectangular chamber of the dryer. The energy loss in the flue gas was lower when the valve in the exhaust pipe was closed after biomass burning (case-III). Relatively higher temperature in the drying chamber was obtained in this case.

- The maximum value of the flue gas temperature for the case-III in the modified dryer was recorded as 122 °C while it was 294 °C for without modification.
- A significant amount of flue gas energy has been recovered in the modified biomass-operated dryer.
- The temperature in the rectangular chamber and the PCM tray of the modified dryer was found to be higher as compared to without modification.
- The exergy efficiency of the dryer was found to be higher for case-III.

6.1.6 Energy and exergy analysis of the natural convection solar dryer

Energy and exergy analysis of the natural convection solar dryer has been conducted for the paddy drying process. The energy efficiency of the solar air heater (SAH) and the dryer system was found in the range of 14.32–22.35% and 10.49–17.66%, with an average of 18.46% and 14.55%, respectively. The exergetic efficiency of the SAH and the dryer system were found in the range of 1.16–2.22% and 0.88–1.78%, respectively. The improvement potential, sustainability index, and waste energy ratio were ranged from 2.62–5.59 J/s, 6.62–16.41, and 6.09–15.1%, respectively. Followings are the major findings of the present study.

- Attaching the copper tubes to the collector plate enhances the performance of the solar air heater (SAH).
- The higher values of the energy and exergy efficiency of the SAH having copper tubes attached collector was obtained.
- The higher values of the sustainability index and the lower values of the waste energy ratio were obtained for the copper tubes attached collector.

6.1.7 Energy and exergy analysis of the forced convection solar dryer

This study has been conducted to enhance the performance of the developed solar air heater (SAH). The performance of the SAH was optimized by varying air flow rates. The energy and exergy analysis of the SAH has been performed for the airflow rate range of 0.0166–0.058 kg/s. In the study, the energy efficiency of the SAH and the dryer system were ranged from 51.54–67.7% and 40.99–55.39%, respectively. The SAH exergetic efficiency and the overall exergetic efficiency of the dryer were obtained in the range of 3.49–7.3% and 2.73–5.76%, respectively. The improvement potential, sustainability index, and waste energy ratio were ranged

from 4.9–27.84 J/s, 4.09–21.14, and 4.73–24.43%, respectively. The important observations of this study are as follows.

- The thermal efficiency of the solar air heater (SAH) increases with air flow rate, reaches a maximum value and then decreases.
- The optimum value of the energy and exergy efficiency of the SAH was obtained at the air flow rate of 0.05 kg/s.
- A significant increase in the thermal efficiency of the SAH under forced convection was obtained as compared to the natural convection mode, which leads to an increase in the energy efficiency of the forced convection solar dryer.
- The performance of the forced convection solar dryer was found to be higher as compared to the natural convection solar dryer.

6.2 Major findings from the thesis

- A significant amount of thermal energy carried by the flue gas is recovered in the modified biomass-operated dryer. A narrow temparature range is obtained in the drying chamber. It is highly recommendable for the drying of temperature sensitive products.
- Due to low range of temperature in the drying chamber, natural convection solar-biomass hybrid dryer is recommendable for the temperature sensitive products.
- The forced convection solar-biomass hybrid dryer is recommendable for the faster drying of the products.

6.3 Scope of future work

- Simulation and scale-up study can be performed to optimize the performance of the dryers. This study will optimize the experimental setup for varrying amount of agricultural products.
- Study can be carried out to improve the performance of the solar dryer by using thermal energy storage (TES) medium in the SAH. The use of TES will control the energy in the SAH and it will also reduce the losses of energy especially in the natural convection mode.
- The performance enhancement study may be done more effectively by recovering waste heat from the flue gas in case of biomass-based dryer.

References

Abuşka, M., Şevik, S., Kayapunar, A., 2019. Comparative energy and exergy performance investigation of forced convection solar air collectors with cherry stone/powder. Renewable Energy 143, 34–46. https://doi.org/10.1016/j.renene.2019.04.149

Afzali, F., Darvishi, H., Behroozi-Khazaei, N., 2019. Optimizing exergetic performance of a continuous conveyor infrared-hot air dryer with air recycling system. Applied Thermal Engineering 154, 358–367. https://doi.org/10.1016/j.applthermaleng.2019.03.096

Aghbashlo, M., Kianmehr, M.H., Arabhosseini, A., 2009. Performance analysis of drying of carrot slices in a semi-industrial continuous band dryer. Journal of Food Engineering 91, 99–108. https://doi.org/10.1016/j.jfoodeng.2008.08.020

Akbulut, A., Durmuş, A., 2010. Energy and exergy analyses of thin layer drying of mulberry in a forced solar dryer. Energy 35, 1754–1763. https://doi.org/10.1016/j.energy.2009.12.028

Akpinar, E., Midilli, A., Bicer, Y., 2003. Single layer drying behaviour of potato slices in a convective cyclone dryer and mathematical modeling. Energy Conversion and Management 44, 1689–1705. https://doi.org/10.1016/S0196-8904(02)00171-1

Akpinar, E.K., 2010. Drying of mint leaves in a solar dryer and under open sun: Modelling, performance analyses. Energy Conversion and Management 51, 2407–2418. https://doi.org/10.1016/j.enconman.2010.05.005

Akpinar, E.K., 2005. Energy and exergy aanalyses of drying of eggplant slices in a cyclone type dryer. Journal of Mechanical Science and Technology 19, 692–703. https://doi.org/10.1007/BF02916191

Akpinar, E.K., 2004. Energy and exergy analyses of drying of red pepper slices in a convective type dryer. International Communications in Heat and Mass Transfer. https://doi.org/10.1016/j.icheatmasstransfer.2004.08.014

Akpinar, E.K., Koçyiĝit, F., 2010. Energy and exergy analysis of a new flat-plate solar air heater having different obstacles on absorber plates. Applied Energy 87, 3438–3450. https://doi.org/10.1016/j.apenergy.2010.05.017

Al Siyabi, I., Khanna, S., Mallick, T., Sundaram, S., 2019. An experimental and numerical study on the effect of inclination angle of phase change materials thermal energy storage system. Journal of Energy Storage 23, 57–68. https://doi.org/10.1016/j.est.2019.03.010

Alta, D., Bilgili, E., Ertekin, C., Yaldiz, O., 2010. Experimental investigation of three different

solar air heaters : Energy and exergy analyses. Applied Energy 87, 2953–2973. https://doi.org/10.1016/j.apenergy.2010.04.016

Arun, K.R., Kunal, G., Srinivas, M., Kumar, C.S.S., Mohanraj, M., Jayaraj, S., 2020. Drying of untreated Musa nendra and Momordica charantia in a forced convection solar cabinet dryer with thermal storage. Energy 192, 116697. https://doi.org/10.1016/j.energy.2019.116697

Ashaolu, M.O., Akinbiyi, J.O., 2015. Effects of chips sizes on thin layer drying characteristics of some plantain varieties (Dwarf cavendish and Musa sapientum) 6, 18–27.

Asiru, W.B., Raji, A.O., Igbeka, J.C., Elemo, G.N., 2013. Mathematical Modelling of Thin Layer Dried Cashew Kernels. Nigerian Food Journal 31, 106–112. https://doi.org/10.1016/s0189-7241(15)30083-7

Aydin, D., Ezenwali, S.E., Alibar, M.Y., Chen, X., 2019. Novel modular mixed-mode dryer for enhanced solar energy utilization in agricultural crop drying applications. Energy Sources, Part A: Recovery, Utilization and Environmental Effects 00, 1–17. https://doi.org/10.1080/15567036.2019.1663306

Ayensu, A., 1997. Dehydration of food crops using a solar dryer with convective heat flow. Solar Energy 59, 121–126. https://doi.org/10.1016/S0038-092X(96)00130-2

Bal, S., Ojha, T.P., 1975. Determination of biological maturity and effect of harvesting and drying conditions on milling quality of paddy. Journal of Agricultural Engineering Research 20, 353–361. https://doi.org/10.1016/0021-8634(75)90072-4

Baniasadi, E., Ranjbar, S., Boostanipour, O., 2017. Experimental investigation of the performance of a mixed-mode solar dryer with thermal energy storage. Renewable Energy 112, 143–150. https://doi.org/10.1016/j.renene.2017.05.043

Behnaz, R., Reddy, B. V., Rosen, M.A., 2016. Thermodynamic analysis and the design of sensible thermal energy storages. International journal of energy research 41, 39–48. https://doi.org/10.1002/er.3587

Belessiotis, V., Delyannis, E., 2011. Solar drying. Solar Energy 85, 1665–1691. https://doi.org/10.1016/j.solener.2009.10.001

Bena, B., Fuller, R.J., 2002. Natural convection solar dryer with biomass back-up heater. Solar Energy 72, 75–83. https://doi.org/10.1016/S0038-092X(01)00095-0

Bhardwaj, A.K., Chauhan, R., Kumar, R., Sethi, M., Rana, A., 2017. Experimental investigation of an indirect solar dryer integrated with phase change material for drying valeriana jatamansi

(medicinal herb). Case Studies in Thermal Engineering 10, 302–314. https://doi.org/10.1016/j.csite.2017.07.009

Bhaskaran Anangapal, H., 2014. Energy and exergy analysis of fuels. International Journal of Energy Sector Management 8, 330–340. https://doi.org/10.1108/ijesm-04-2013-0012

Borah, P.P., Nayak, P.K., 2013. Quality Characteristics of Dried Jahajibanana Chips after Deep Fat Frying. International Journal of Agriculture and Food Science Technology 4, 2249–3050.

Bosomtwe, A., Danso, J.K., Osekre, E.A., Opit, G.P., Mbata, G., Armstrong, P., Arthur, F.H., Campbell, J., Manu, N., McNeill, S.G., Akowuah, J.O., 2019. Effectiveness of the solar biomass hybrid dryer for drying and disinfestation of maize. Journal of Stored Products Research 83, 66–72. https://doi.org/10.1016/j.jspr.2019.05.011

Caliskan, H., Dincer, I., Hepbasli, A., 2012a. Energy and exergy analyses of combined thermochemical and sensible thermal energy storage systems for building heating applications. Energy & Buildings 48, 103–111. https://doi.org/10.1016/j.enbuild.2012.01.017

Celma, A.R., Cuadros, F., 2009. Energy and exergy analyses of OMW solar drying process. Renewable Energy 34, 660–666. https://doi.org/10.1016/j.renene.2008.05.019

Chakraverty, A., Das, S.K., 1992. Development of a two directional air flow paddy dryer coupled with an integrated array of solar air heating modules. Energy Conversion and Management 33, 183–190. https://doi.org/ISSN 0196-8904/92

Chauhan, P.S., Kumar, A., Nuntadusit, C., Banout, J., 2018a. Thermal modeling and drying kinetics of bitter gourd flakes drying in modified greenhouse dryer. Renewable Energy 118, 799–813. https://doi.org/10.1016/j.renene.2017.11.069

Chauhan, P.S., Kumar, A., Nuntadusit, C., Mishra, S.S., 2018b. Drying Kinetics, Quality Assessment, and Economic Analysis of Bitter Gourd Flakes Drying Inside Forced Convection Greenhouse Dryer. Journal of Solar Energy Engineering, Transactions of the ASME 140, 1–10. https://doi.org/10.1115/1.4039891

Chavan, B.R., Yakupitiyage, A., Kumar, S., 2008. Mathematical modeling of drying characteristics of Indian mackerel (Rastrilliger kangurta) in solar-biomass hybrid cabinet dryer. Drying Technology 26, 1552–1562. https://doi.org/10.1080/07373930802466872

Chen, C., Wu, P.C., 2001. Thin-layer drying model for rough rice with high moisture content. Journal of Agricultural and Engineering Research 80, 45–52. https://doi.org/10.1006/jaer.2000.0677

Chowdhury, M.M.I., Bala, B.K., Haque, M.A., 2011. Energy and exergy analysis of the solar drying of jackfruit leather. Biosystems Engineering 110, 222–229. https://doi.org/10.1016/j.biosystemseng.2011.08.011

Chukwunonye, C.D., Nnaemeka, N.R., Chijioke, O.V., Obiora, N.C., 2016. Thin Layer Drying Modelling for Some Selected Nigerian Produce : A Review Thin Layer Drying Modelling for Some Selected Nigerian Produce : A Review.

Coskun, C., Bayraktar, M., Oktay, Z., Dincer, I., 2009. Energy and exergy analyses of an industrial wood chips drying process. International Journal of Low-Carbon Technologies 4, 224–229. https://doi.org/10.1093/ijlct/ctp024

Dagde, K.K., Nmegbu, C.G.J., 2014. Mathematical Modeling of a Tray Dryer for the Drying of Potato Chips Using Hot Air Medium. International Journal of Advancements in Research & Technology 3, 104–107. https://doi.org/10.13140/2.1.3257.1522

Darvishi, H., 2012. Energy consumption and mathematical modeling of microwave drying of potato slices. Agricultural Engineering International: CIGR Journal 14, 94–102.

Daş, M., Alıç, E., Kavak Akpinar, E., 2020. Numerical and experimental analysis of heat and mass transfer in the drying process of the solar drying system. Engineering Science and Technology, an International Journal. https://doi.org/10.1016/j.jestch.2020.10.003

Diamante, L.M., Munro, P.A., 1993. Mathematical modelling of the thin layer solar drying of sweet potato slices. Solar Energy 51, 271–276. https://doi.org/10.1016/0038-092X(93)90122-5

Dincer, I., Sahin, A.Z., 2004. A new model for thermodynamic analysis of a drying process. International Journal of Heat and Mass Transfer. https://doi.org/10.1016/j.ijheatmasstransfer.2003.08.013

Duffie, J.A., Beckman, W.A., 2013. Wiley: Solar Engineering of Thermal Processes, 4th Edition - John A. Duffie, William A. Beckman.

Ekka, J.P., Bala, K., Muthukumar, P., Kanaujiya, D.K., 2020. Performance analysis of a forced convection mixed mode horizontal solar cabinet dryer for drying of black ginger (Kaempferia parviflora) using two successive air mass flow rates. Renewable Energy 152, 55–66. https://doi.org/10.1016/j.renene.2020.01.035

El-Sebaii, A.A., Shalaby, S.M., 2012. Solar drying of agricultural products: A review. Renewable and Sustainable Energy Reviews 16, 37–43. https://doi.org/10.1016/j.rser.2011.07.134

Erbay, Z., Icier, F., 2010. A review of thin layer drying of foods: Theory, modeling, and experimental results. Critical Reviews in Food Science and Nutrition 50, 441–464. https://doi.org/10.1080/10408390802437063

Evangelisti, L., Guattari, C., Gori, P., Bianchi, F., 2017. Heat transfer study of external convective and radiative coefficients for building applications. Energy and Buildings 151, 429–438. https://doi.org/10.1016/j.enbuild.2017.07.004

Fakoor Pakdaman, M., Lashkari, A., Basirat Tabrizi, H., Hosseini, R., 2011. Performance evaluation of a natural-convection solar air-heater with a rectangular-finned absorber plate. Energy Conversion and Management 52, 1215–1225. https://doi.org/10.1016/j.enconman.2010.09.017

Farias, R.P., Santiago, D.C., Holanda, P.R.H., Lima, A.G.B., 2004. Drying of Grains in Conveyor Dryer and Cross Flow: a Numerical Solution Using Finite-Volume Method. Revista Brasileira de Produtos Agroindustriais 6, 1–16. https://doi.org/10.15871/1517-8595/rbpa.v6n1p1-16

Folayan, J.A., Osuolale, F.N., Anawe, P.A.L., 2018. Data on exergy and exergy analyses of drying process of onion in a batch dryer. Data in Brief 21, 1784–1793. https://doi.org/10.1016/j.dib.2018.10.132

Fudholi, A., Musthafa, M.F., Ridwan, A., Yendra, R., Desvina, A.P., Rahmadeni, R., Suyono, T., Sopian, K., 2019. Energy and exergy analysis of air based photovoltaic thermal (PVT) collector: a review. International Journal of Electrical and Computer Engineering (IJECE) 9, 109. https://doi.org/10.11591/ijece.v9i1.pp109-117

Fudholi, A., Sopian, K., Alghoul, M.A., Ruslan, M.H., Othman, M.Y., 2015. Performances and improvement potential of solar drying system for palm oil fronds. Renewable Energy 78, 561–565. https://doi.org/10.1016/j.renene.2015.01.050

Fudholi, A., Sopian, K., Othman, M.Y., Ruslan, M.H., Bakhtyar, B., 2013. Energy analysis and improvement potential of finned double-pass solar collector. Energy Conversion and Management 75, 234–240. https://doi.org/10.1016/j.enconman.2013.06.021

Gautam, A., Saini, R.P., 2020. A review on technical, applications and economic aspect of packed bed solar thermal energy storage system. Journal of Energy Storage 27, 101046. https://doi.org/10.1016/j.est.2019.101046

Ghandoor, A. Al, Hinti, I. Al, Akash, B., Nada, E.A., 2008. Analysis of energy and exergy use in

the Jordanian urban residential sector. International Journal of Exergy 5, 413. https://doi.org/10.1504/ijex.2008.019113

Ghorbani, B., Mehrpooya, M., 2020. Concentrated solar energy system and cold thermal energy storage (process development and energy analysis). Sustainable Energy Technologies and Assessments 37, 100607. https://doi.org/10.1016/j.seta.2019.100607

Goswami, D.Y., Vijayaraghavan, S., Lu, S., Tamm, G., 2004. New and emerging developments in solar energy 76, 33–43. https://doi.org/10.1016/S0038-092X(03)00103-8

Goyalde, N.A., Melo, E.D.C., Rocha, R.P., 2009. Mathematical modeling of the drying kinetics of sugarcane Sugarcane crop is most important economically , socially and environmentally . Brazil is the largest sugarcane producer in the world . With the objective of contributing towards precision agricultu. Revista Brasileira de Produtos Agroindustriais. 11, 117–121.

Gudiño-Ayala, D., Calderón-Topete, Á., 2014. Pineapple drying using a new solar hybrid dryer. Energy Procedia 57, 1642–1650. https://doi.org/10.1016/j.egypro.2014.10.155

Guerraiche, D., Bougriou, C., Guerraiche, K., Valenzuela, L., Driss, Z., 2020. Experimental and numerical study of a solar collector using phase change material as heat storage. Journal of Energy Storage 27, 101133. https://doi.org/10.1016/j.est.2019.101133

Gupta, M.K., Kaushik, S.C., 2008. Exergetic performance evaluation and parametric studies of solar air heater. Energy 33, 1691–1702. https://doi.org/10.1016/j.energy.2008.05.010

Huirem, B., Shakya, R., 2015. Thin layer drying kinetics of kiwifruits (var. Monty). International Journal of Science, Engineering and Technology Research 4, 1736–1746.

Jabeen, R., Aijaz, T., Gul, K., 2015. Drying kinetics of potato using a self-designed cabinet dryer. Cogent Food & Agriculture 1, 1–5. https://doi.org/10.1080/23311932.2015.1036485

Jafari, H., Kalantari, D., Azadbakht, M., 2018. Energy consumption and qualitative evaluation of a continuous band microwave dryer for rice paddy drying. Energy 142, 647–654. https://doi.org/10.1016/j.energy.2017.10.065

Jafari, H., Kalantari, D., Azadbakht, M., 2017. Semi-industrial continuous band microwave dryer for energy and exergy analyses , mathematical modeling of paddy drying and it ' s qualitative study. Energy 138, 1016–1029. https://doi.org/10.1016/j.energy.2017.07.111

Jafarkazemi, F., Ahmadifard, E., 2013. Energetic and exergetic evaluation of flat plate solar collectors. Renewable Energy 56, 55–63. https://doi.org/10.1016/j.renene.2012.10.031

Jain, D., Tewari, P., 2015. Performance of indirect through pass natural convective solar crop dryer

with phase change thermal energy storage. Renewable Energy 80, 244–250. https://doi.org/10.1016/j.renene.2015.02.012

Jain, D., Tiwari, G.N., 2004. Effect of greenhouse on crop drying under natural and forced convection II. Thermal modeling and experimental validation, Jain, Energy Conversion and Management, 2004.pdf.

Jittanit, W., Saeteaw, N., Charoenchaisri, A., 2010. Industrial paddy drying and energy saving options. Journal of Stored Products Research 46, 209–213. https://doi.org/10.1016/j.jspr.2010.04.005

Jun, Xing, Xin, L., , Yang, W., L., Ping, J., Hui, L., 2016. Changes in moisture effective diffusivity and glass transition temperature of paddy during drying. Computers and Electronics in Agriculture 128, 112–119. https://doi.org/10.1016/j.compag.2016.08.025

Kalapala, L., Devanuri, J.K., 2018. Influence of operational and design parameters on the performance of a PCM based heat exchanger for thermal energy storage – A review. Journal of Energy Storage 20, 497–519. https://doi.org/10.1016/j.est.2018.10.024

Kalidasan, B., Pandey, A.K., Shahabuddin, S., Samykano, M., Thirugnanasambandam, M., 2020. Phase change materials integrated solar thermal energy systems : Global trends and current practices in experimental approaches. Journal of Energy Storage 27, 101118. https://doi.org/10.1016/j.est.2019.101118

Karathanos, V.T., 1999. Determination of water content of dried fruits by drying kinetics. Journal of Food Engineering 39, 337–344. https://doi.org/10.1016/S0260-8774(98)00132-0

Karthikeyan, A.K., Murugavelh, S., 2018. Thin layer drying kinetics and exergy analysis of turmeric (Curcuma longa) in a mixed mode forced convection solar tunnel dryer. Renewable Energy 128, 305–312. https://doi.org/10.1016/j.renene.2018.05.061

Khanlari, A., Sözen, A., Şirin, C., Tuncer, A.D., Gungor, A., 2020. Performance enhancement of a greenhouse dryer: Analysis of a cost-effective alternative solar air heater. Journal of Cleaner Production 251. https://doi.org/10.1016/j.jclepro.2019.119672

Kumar, A., Gupta, A.K., 2006. Two stage drying of high moisture paddy with intervening rest period. Energy Conversion and Management 47, 3069–3083. https://doi.org/10.1016/j.enconman.2006.03.008

Kumar, A., Tiwari, G.N., 2007. Effect of mass on convective mass transfer coefficient during open sun and greenhouse drying of onion flakes. Journal of Food Engineering 79, 1337–1350. https://doi.org/10.1016/j.jfoodeng.2006.04.026

Kumar, A., Tiwari, G.N., 2006. Effect of shape and size on convective mass transfer coefficient during greenhouse drying (GHD) of Jaggery. Journal of Food Engineering 73, 121–134. https://doi.org/10.1016/j.jfoodeng.2005.01.011

Kumar, D., Mahanta, P., Kalita, P., 2020. Energy and exergy analysis of a natural convection dryer with and without sensible heat storage medium. Journal of Energy Storage 29. https://doi.org/10.1016/j.est.2020.101481

Lakshmi, D.V.N., Muthukumar, P., Layek, A., Kumar, P., 2019. Performance analyses of mixed mode forced convection solar dryer for drying of stevia leaves. Solar Energy 188, 507–518. https://doi.org/10.1016/j.solener.2019.06.009

Li, X., Cao, Z., Wei, Z., Feng, Q., Wang, J., 2011. Equilibrium moisture content and sorption isosteric heats of five wheat varieties in China. Journal of Stored Products Research 47, 39–47. https://doi.org/10.1016/j.jspr.2010.10.001

Li, X., Zhang, Yufeng, Fang, L., Jin, Z., Zhang, Yan, Yu, X., Ma, X., Deng, N., Wu, Z., 2019. Energy, exergy, economic, and environmental analysis of an integrated system of high-temperature heat pump and gas separation unit. Energy Conversion and Management 198, 111911. https://doi.org/10.1016/j.enconman.2019.111911

Liu, Z.L., Bai, J.W., Wang, S.X., Meng, J.S., Wang, H., Yu, X.L., Gao, Z.J., Xiao, H.W., 2019. Prediction of energy and exergy of mushroom slices drying in hot air impingement dryer by artificial neural network. Drying Technology 0, 1–12. https://doi.org/10.1080/07373937.2019.1607873

Matheswaran, M.M., Arjunan, T. V, Somasundaram, D., 2018. Analytical investigation of solar air heater with jet impingement using energy and exergy analysis. Solar Energy 161, 25–37. https://doi.org/10.1016/j.solener.2017.12.036

Midilli, Adnan, Kucuk, H., 2003. Mathematical modeling of thin layer drying of pistachio by using solar energy. Energy Conversion and Management 44, 1111–1122. https://doi.org/10.1016/S0196-8904(02)00099-7

Midilli, A., Kucuk, H., 2003. Energy and exergy analyses of solar drying process of pistachio. Energy 28, 539–556. https://doi.org/10.1016/S0360-5442(02)00158-5

Minaei, S., Chenarbon, H.A., Motevali, A., Hosseini, A.A., 2017. Energy consumption, thermal utilization efficiency and hypericin content in drying leaves of St John's Wort (Hypericum Perforatum). Journal of Energy in Southern Africa 25, 27–35. https://doi.org/10.17159/2413-

3051/2014/v25i3a2655

Mohapatra, S.S., Lakshmi, D.V.N., Mahanta, P., 2013. Performance Evaluation of Natural Convection Grain Dryer using Phase Change Material for Quality Drying of Paddy. International Journal of Agriculture and Food Science Technology. 4, 523–530. https://doi.org/ISSN 2249-3050

Mondal, M.H.T., Hossain, M.A., Sheikh, M.A.M., Md. Akhtaruzzaman, Sarker, M.S.H., 2020. Energetic and exergetic investigation of a mixed flow dryer: A case study of maize grain drying. Drying Technology 0, 1–15. https://doi.org/10.1080/07373937.2019.1709077

Murugavelh, S., Anand, B., Midhun Prasad, K., Nagarajan, R., Azariah Pravin Kumar, S., 2019. Exergy analysis and kinetic study of tomato waste drying in a mixed mode solar tunnel dryer. Energy Sources, Part A: Recovery, Utilization and Environmental Effects 00, 1–17. https://doi.org/10.1080/15567036.2019.1679289

Muthayya, S., Sugimoto, J.D., Montgomery, S., Maberly, G.F., 2014. An overview of global rice production, supply, trade, and consumption. Annals of the New York Academy of Sciences 1324, 7–14. https://doi.org/10.1111/nyas.12540

Nag, P K., 2013. Basic and Applied Thermodynamics, Second Edi. ed. McGra Hill Education (India) Private Limited, New Delhi.

Naghavi, Z., Moheb, A., Ziaei-rad, S., 2010. Numerical simulation of rough rice drying in a deep-bed dryer using non-equilibrium model. Energy Conversion and Management 51, 258–264. https://doi.org/10.1016/j.enconman.2009.09.019

Ndukwu, M.C., Bennamoun, L., Abam, F.I., Eke, A.B., Ukoha, D., 2017. Energy and exergy analysis of a solar dryer integrated with sodium sulfate decahydrate and sodium chloride as thermal storage medium. Renewable Energy 113, 1182–1192. https://doi.org/10.1016/j.renene.2017.06.097

Ondier, G.O., Siebenmorgen, T.J., Mauromoustakos, A., 2010. Low-temperature, low-relative humidity drying of rough rice. Journal of Food Engineering 100, 545–550. https://doi.org/10.1016/j.jfoodeng.2010.05.004

P K Nag, 2014. Heat and Mass Transfer, Third Edit. ed. McGraw Hill Education (India) Private Limited, New Delhi.

Panchariya, P.C., Popovic, D., Sharma, A.L., 2002. Thin-layer modelling of black tea drying process. Journal of Food Engineering 52, 349–357. https://doi.org/10.1016/S0260-8774(01)00126-1

Pangavhane, D.R., Sawhney, R.L., Sarsavadia, P.N., 2002. Design, development and performance testing of a new natural convection solar dryer. Energy 27, 579–590. https://doi.org/10.1016/S0360-5442(02)00005-1

Prachayawarakorn, S., Poomsa-ad, N., Soponronnarit, S., 2005. Quality maintenance and economy with high-temperature paddy-drying processes. Journal of Stored Products Research 41, 333–351. https://doi.org/10.1016/j.jspr.2004.05.001

Prasad, J., Vijay, V.K., 2005. Experimental studies on drying of Zingiber officinale, Curcuma longa l. and Tinospora cordifolia in solar-biomass hybrid drier. Renewable Energy 30, 2097–2109. https://doi.org/10.1016/j.renene.2005.02.007

Rabha, D.K., Muthukumar, P., 2017. Performance studies on a forced convection solar dryer integrated with a paraffin wax – based latent heat storage system. Solar Energy 149, 214–226. https://doi.org/10.1016/j.solener.2017.04.012

Rabha, D.K., Muthukumar, P., Somayaji, C., 2017a. Energy and exergy analyses of the solar drying processes of ghost chilli pepper and ginger. Renewable Energy 105, 764–773. https://doi.org/10.1016/j.renene.2017.01.007

Rabha, D.K., Muthukumar, P., Somayaji, C., 2017b. Experimental investigation of thin layer drying kinetics of ghost chilli pepper (Capsicum Chinense Jacq.) dried in a forced convection solar tunnel dryer. Renewable Energy 105, 583–589. https://doi.org/10.1016/j.renene.2016.12.091

Rafiee, S., 2009. Mathematical Modeling of Kinetics of Thin-layer Drying of Apple (var. Golab). Agricultural Engineering International: CIGR Journal 0.

Rosen, M.A., Dincer, I., 2003. Exergy-cost-energy-mass analysis of thermal systems and processes. Energy Conversion and Management 44, 1633–1651. https://doi.org/10.1016/S0196-8904(02)00179-6

Saidur, R., Boroumandjazi, G., Mekhlif, S., Jameel, M., 2012. Exergy analysis of solar energy applications. Renewable and Sustainable Energy Reviews 16, 350–356. https://doi.org/10.1016/j.rser.2011.07.162

Sallam, Y.I., Aly, M.H., Nassar, A.F., Mohamed, E.A., 2015. Solar drying of whole mint plant under natural and forced convection. Journal of Advanced Research 6, 171–178. https://doi.org/10.1016/j.jare.2013.12.001

Sami, S., Etesami, N., Rahimi, A., 2011. Energy and exergy analysis of an indirect solar cabinet dryer based on mathematical modeling results. Energy 36, 2847–2855.

https://doi.org/10.1016/j.energy.2011.02.027

Sekyere, C.K.K., Forson, F.K., Adam, F.W., 2016. Experimental investigation of the drying characteristics of a mixed mode natural convection solar crop dryer with back up heater. Renewable Energy 92, 532–542. https://doi.org/10.1016/j.renene.2016.02.020

Şevik, S., Aktaş, M., Dolgun, E.C., Arslan, E., Tuncer, A.D., 2019a. Performance analysis of solar and solar-infrared dryer of mint and apple slices using energy-exergy methodology. Solar Energy 180, 537–549. https://doi.org/10.1016/j.solener.2019.01.049

Şevik, S., Aktaş, M., Dolgun, E.C., Arslan, E., Tuncer, A.D., 2019b. Performance analysis of solar and solar-infrared dryer of mint and apple slices using energy-exergy methodology. Solar Energy 180, 537–549. https://doi.org/10.1016/j.solener.2019.01.049

Siebenmorgen, T.J., Qin, G., Jia, C., 2005. Influence of drying on rice fissure formation rates and mechanical strength distributions 48, 1835–1842. https://doi.org/ISSN 0001−2351

Şevik, S., Abuşka, M., 2020. Enhancing the thermal performance of a solar air heater by using single-pass semi-flexible foil ducts. Applied Thermal Engineering 179, 115746. https://doi.org/10.1016/j.applthermaleng.2020.115746

Sheikhshoaei, H., Dowlati, M., Aghbashlo, M., Rosen, M.A., 2019. Exergy analysis of a pistachio roasting system. Drying Technology 0, 1–19. https://doi.org/10.1080/07373937.2019.1649276

Shreelavaniya, R., Kamaraj, S., Subramanian, S., Pangayarselvi, R., Murali, S., Bharani, A., 2021. Experimental investigations on drying kinetics, modeling, and quality analysis of small cardamom (Elettaria cardamomum) dried in the solar-biomass hybrid dryer. Solar Energy 227, 635–644. https://doi.org/10.1016/j.solener.2021.09.016

Singh, F., Katiyar, V.K., Singh, B.P., 2014. Mathematical Modeling to Study Drying Characteristic of Apple and Potato. https://doi.org/10.15242/iicbe.c914067

Singh, S., 2020. Thermohydraulic performance of double pass solar thermal collector with inline, staggered and hybrid fin configurations. Journal of Energy Storage 27, 101080. https://doi.org/10.1016/j.est.2019.101080

Singh, S., Dhiman, P., 2016. Exergoeconomic analysis of recyclic packed bed solar air heater-sustained air heating system for buildings. Journal of Energy Storage 5, 33–47. https://doi.org/10.1016/j.est.2015.11.008

Singh, S., Dhruw, L., Chander, S., 2019. Experimental investigation of a double pass converging finned wire mesh packed bed solar air heater. Journal of Energy Storage 21, 713–723.

https://doi.org/10.1016/j.est.2019.01.003

Sitorus, A., Novrinaldi, Putra, S.A., Cebro, I.S., Bulan, R., 2021. Modelling drying kinetics of paddy in swirling fluidized bed dryer. Case Studies in Thermal Engineering 28, 101572. https://doi.org/10.1016/j.csite.2021.101572

Swami, V.M., Autee, A.T., T R, A., 2018. Experimental analysis of solar fish dryer using phase change material. Journal of Energy Storage 20, 310–315. https://doi.org/10.1016/j.est.2018.09.016

Syahrul, S., Dincer, I., Hamdullahpur, F., 2003. Thermodynamic modeling of fluidized bed drying of moist particles. International Journal of Thermal Sciences 42(7), 691–701. https://doi.org/10.1016/S1290-0729(03)00035-8

Tavakolipour, H., Zirjani, L., 2014. Banana Chips Production by Hot Air and Microwave Dehydration Methods : A Comparative Study 21, 1828–1836. https://doi.org/10.5829/idosi.mejsr.2014.21.10.21753

Tiwari, G.N., Das, T., Chen, C.R., Barnwal, P., 2009. Energy and exergy analyses of greenhouse fish drying. International Journal of Exergy 6, 620–636. https://doi.org/10.1504/IJEX.2009.027493

Tiwari, G.N., Das, T., Sarkar, B., 2006. Experimental Study of Greenhouse Prawn Drying under Natural Convection. CIGR E-Journal VIII, 1–9. https://doi.org/10.1289/ehp.0901582

Toğrul, I.T., Pehlivan, D., 2004. Modelling of thin layer drying kinetics of some fruits under open-air sun drying process. Journal of Food Engineering 65, 413–425. https://doi.org/10.1016/j.jfoodeng.2004.02.001

Torki Harchegani, M., Moheb, A., Sadeghi, M., Tohidi, M., Naghavi, Z., 2012. Experimental study of deep-bed drying kinetics of rough rice. Agricultural Engineering International: CIGR Journal 14, 195–202.

Tyagi, S.K., Wang, S., Singhal, M.K., Kaushik, S.C., Park, S.R., 2007. Exergy analysis and parametric study of concentrating type solar collectors. International Journal of Thermal Sciences 46, 1304–1310. https://doi.org/10.1016/j.ijthermalsci.2006.11.010

Tyagi, V. V, Pandey, A.K., Kaushik, S.C., Tyagi, S.K., 2012. Thermal performance evaluation of a solar air heater with and without thermal energy storage An experimental study. Journal of Thermal Analysis and Calorimetry 107(3), 1345–1352. https://doi.org/10.1007/s10973-011-1617-3

Utari, F.D., Yasintasia, C., Ratridewi, M., A'yuni, D.Q., Kumoro, A.C., Djaeni, M., Asiah, N., 2022. Evaluation of Paddy Drying with Vertical Screw Conveyor Dryer (VSCD) at Different Air Velocities and Temperatures. Chemical Engineering and Processing - Process Intensification 174, 108881. https://doi.org/10.1016/j.cep.2022.108881

Utlu, Z., Hepbasli, A., Turan, M., 2011. Performance analysis and assessment of an industrial dryer in ceramic production. Drying Technology 29, 1792–1813. https://doi.org/10.1080/07373937.2011.602921

Vasquez, R., Demirkaya, G., Goswami, D.Y., Stefanakos, E., Rahman, M.M., 2011. Heat transfer analysis of parabolic trough solar receiver. Applied Energy 88, 5097–5110. https://doi.org/10.1016/j.apenergy.2011.07.012

Vijayan, S., Arjunan, T.V., Kumar, A., 2020. Exergo-environmental analysis of an indirect forced convection solar dryer for drying bitter gourd slices. Renewable Energy 146, 2210–2223. https://doi.org/10.1016/j.renene.2019.08.066

Vijayan, S., Arjunan, T. V., Kumar, A., 2016. Mathematical modeling and performance analysis of thin layer drying of bitter gourd in sensible storage based indirect solar dryer. Innovative Food Science and Emerging Technologies 36, 59–67. https://doi.org/10.1016/j.ifset.2016.05.014

Wincy, W.B., Edwin, M., Sekhar, S.J., 2022. Optimization of process parameters to implement biomass gasifier for drying high moisture paddy in reversible flatbed dryer. Energy 249, 123771. https://doi.org/10.1016/j.energy.2022.123771

Yaldiz, O., Ertekin, C., Uzun, H.I., 2001. Mathematical modeling of thin layer solar drying of sultana grapes. Energy 26, 457–465. https://doi.org/10.1016/S0360-5442(01)00018-4

Yaldýz, O., Ertekýn, C., 2001. Thin layer solar drying of some vegetables. Drying Technology 19, 583–597. https://doi.org/10.1081/DRT-100103936

Yilmaz, F., 2019. Energy, exergy and economic analyses of a novel hybrid ocean thermal energy conversion system for clean power production. Energy Conversion and Management 196, 557–566. https://doi.org/10.1016/j.enconman.2019.06.028

Zaman, M.A., Bala, B.K., 2001. Thin layer solar drying of rough rice. Journal of Food Eng. 47(4), 295-301 https://doi.org/10.1016/S0260-8774(00)00133-3

Zare, D., Chen, G., 2009. Evaluation of a simulation model in predicting the drying parameters for deep-bed paddy drying 68, 78–87. https://doi.org/10.1016/j.compag.2009.04.007

Zare, D., Minaei, S., Mohamad Zadeh, M., H.Khoshtaghaza, M., 2006. Computer simulation of rough rice drying in a batch dryer. Energy Conversion and Management 47, 3241–3254. https://doi.org/10.1016/j.enconman.2006.02.021

Zarein, M., Banakar, A., Khafajeh, H., 2013. Mathematical Modeling , Energy Consumption and Thin Layer Drying Kinetics of Carrot Slices Under Microwave Oven 2057–2063.

Zuhur, S., Ceylan, İ., 2019. Energy , Exergy and Enviroeconomic (3E) analysis of concentrated PV and thermal system in the winter application. Energy Reports 5, 262–270. https://doi.org/10.1016/j.egyr.2019.02.003

Zvolinschi, A., Johannessen, E., Kjelstrup, S., 2006. The second-law optimal operation of a paper drying machine. Chemical Engineering Science 61, 3653–3662. https://doi.org/10.1016/j.ces.2005.12.030

Appendices

Appendix-I

Experimental Uncertainty

Uncertainty in the experimental results can be evaluated as in Eq. (I.1) (Daş et al., 2020). In Eq. (I.1), "*x*" represents uncertainty properties and W represents uncertainty value. In this study, the uncertainty analysis calculated for various measurements is shown in Table I.1.

$$W_x = \left[(x_1)^2 + (x_2)^2 + \ldots\ldots\ldots + (x_n)^2 \right]^{\frac{1}{2}} \quad \text{(I.1)}$$

Table I.1 Measurement Uncertainty

Parameters	**Relative uncertainty (%)**
Laser Beam Temperature Gun	±1.5
Pyranometer	±5
Thermocouples	±0.75
Moisture meter	±0.5
Anemometer	±3
Thermal efficiency of the SAH	±5.97
The exergy efficiency of the SAH	±5.92
The efficiency of the Dryer	±6.02
The exergetic efficiency of the Dryer	±5.97

Appendix-II

Experimental data

Table II.1 Experimental data for 12 kg paddy drying in the modified biomass-operated grain dryer for the case-III

Time (h)	Drying chamber temperature (°C)	Moisture Content (%)
0	40.8	33
0.5	44	31.7
1	45.7	29.3
1.5	47	26.5
2	48.2	24.2
2.5	47.8	22
3	47	20.2
3.5	45.7	18.6
4	45	17.2
4.5	44.5	16
5	42.5	15
5.5	41.7	14.3
6	41	13.8

Table II.2 Experimental data for 12 kg paddy drying under natural convection solar dryer

Time (h)	Drying chamber temperature (°C)	Moisture Content (%)	Solar Irradiance (W/m^2)
0	46.8	34.4	930
0.5	43.48	33.5	935
1	45.25	29	830
1.5	46.26	26.1	1040
2	45.48	23	975
2.5	43.31	21.6	950
3	46.61	19.8	950
3.5	48.88	18	940
4	48	16.7	775
4.5	48.41	15.8	760
5	48.08	14.5	782

Table II.3 Experimental data for 16 kg paddy drying under forced convection solar dryer

Time (h)	Drying chamber temperature (°C)	Moisture Content (%)	Solar Irradiance (W/m^2)
0	42.92	34.1	755
0.5	47.18	32.6	886
1	50.38	28.4	800
1.5	51.94	25.5	922
2	54.34	23.3	924
2.5	55.82	21	920
3	56.38	19.3	857
3.5	56.8	17.7	796
4	56.4	16.4	728
4.5	55.72	15.1	715
5	51.04	14.2	676

List of publications

JOURNALS

1. **Kumar, D.,** Mahanta, P., Kalita, P., 2020. Energy and exergy analysis of a natural convection dryer with and without sensible heat storage medium. Journal of Energy Storage 29. https://doi.org/10.1016/j.est.2020.101481.
2. **Kumar, D.,** Mahanta, P., Kalita, P., 2021. Performance analysis of a solar air heater modified with zig-zag shaped copper tubes using energy-exergy methodology. Sustainable Energy Technologies and Assessments 46, 101222. https://doi.org/10.1016/j.seta.2021.101222.
3. **Kumar, D**., Mahanta, P., Kalita, P., 2022. Performance analysis of a novel biomass-fired grain dryer integrated with thermal storage medium. Biosystems Engineering 216, 65–78. https://doi.org/10.1016/j.biosystemseng.2022.02.001.
4. **Kumar, D.,** Mahanta, P., Kalita, P., 2022. Materials Today : Proceedings Performance analysis of natural convection biomass operated grain dryer coupled with latent heat storage medium. Materials Today: Proceedings. https://doi.org/10.1016/j.matpr.2021.12.045.
5. **Kumar, D.,** Mahanta, P., Kalita, P., 2022. Energy and exergy analysis of a forced convection solar dryer coupled with biomass operated dryer having thermal energy storage medium. Energy Sources, part A: Recovery, Utilization, and Environmental Effects (Communicated).
6. **Kumar, D**., Mahanta, P., Kalita, P., 2022. Performance analysis of a newly developed natural convection solar dryer for paddy drying process. Biosystems Engineering (Communicated).
7. **Kumar, D.,** Mahanta, P., Kalita, P., 2022. Reduction in energy and exergy losses in a biomass-fired grain dryer using a sensible thermal storage medium. Material Today: proceedings (Communicated).

BOOK CHAPTERS

1. **Kumar, D.,** Mahanta, P., Kalita, P., 2019. Thermodynamic analysis of a natural convection dryer, in: Yengkhom Disco Singh, Helen Soibam, P.H. and B.N.H. (Ed.), Post Harvest Technology and Value Addition. The Dean, College of Hoticulture & Forestry, Central

Agricultural University, Pasighat-791102, Arunachal Pradesh., pp. 156–61. https://doi.org/ISBN 978-93-5396-087-2.

2. **Kumar, D.,** Mahanta, P., Kalita, P., 2019. Natural Convection Grain Dryer, Energy storage Systems: An Introduction, NOVA SCIENCE PUBLISHERS, INC. https://doi.org/ISBN: 978-1-53618-910-0.
3. **Kumar, D.,** Mahanta, P., Kalita, P., 2019. Chapter Title: Exergy analysis of a natural convection grain dryer. Chapter ID 68703, Book Title: Energy storage Systems: An Introduction, NOVA SCIENCE PUBLISHERS, INC. https://doi.org/ISBN: 978-1-53618-910-0.

CONFERENCES

1. **Kumar, D.,** Mahanta, P., Kalita, P., 2020. Non-dimensional numbers analysis of a natural convection grain dryer with and without sensible energy storage. Third International Conference on Recent Trends in Multidisciplinary Research. 26th-27th December 2020, Maldives.
2. **Kumar, D.,** Mahanta, P., Kalita, P., 2021. Non-dimensional numbers analysis of a Grain dryer. International Conference on Science Engineering and Technology. 27th-28th January 2021, Singapore.
3. **Kumar, D.,** Mahanta, P., Kalita, P., 2021. Performance analysis of natural convection biomass operated grain dryer coupled with the latent heat storage medium. International Conference on Novel Materials for Biomedical, Energy, Environment, Sensing and other applications. 11th-13th March 2021, NIT Trichy, India.
4. **Kumar, D.,** Mahanta, P., Kalita, P., 2022. Reduction in energy and exergy losses in a biomass-fired grain dryer using a sensible thermal storage medium. Material Tech 2022, Online Second International Conference on Materials and Technologies. 27th-29th January 2022, NIT Raipur, India.